POLITECNICO
MILANO 1863

School of Civil, Environmental and Land Management Engineering
Master of Science in Civil Engineering

Impact of Italian ground motion models in seismic hazard assessment: case studies in near-source region and volcanic context

Advisor:

Prof. Roberto PAOLUCCI

Co-advisors:

Dott.ssa Sara SGOBBA
Prof.ssa Manuela VANINI

Candidate:

Arianna CIPRIANO
ID 927282

Academic Year 2021-22

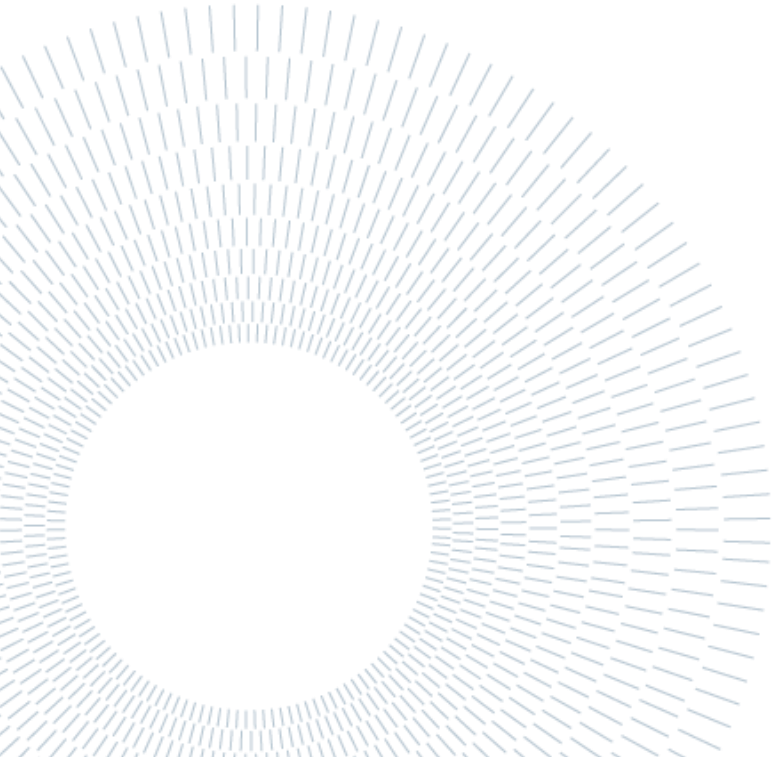

Abstract

Probabilistic seismic hazard analysis (PSHA) (Cornell 1968) is currently the standard approach adopted worldwide for hazard assessment within design building codes, such as in Italy (NTC18). Key ingredients of the PSHA are the ground motion models (GMMs) that provide the median predictions and corresponding uncertainty of the shaking parameters. Although GMMs are widely calibrated worldwide due to the growing number of recorded data, they are still poorly constrained in near-source conditions or volcanic regions. However, recent studies have underlined the importance of correctly quantifying these effects in the hazard estimates, as design seismic actions can often be exceeded, for example in the epicentral area for moderate to high magnitude earthquakes.

This thesis aims to investigate the impact, within a probabilistic seismic hazard calculation, of new Italian GMMs specifically calibrated for shallow crustal earthquakes and for volcanic areas, or adjusted with empirical factors, to account for the global effects of near-source ground motion.

In the analyses, particular attention is also given to assessing the variability associated with the models used as well as to the impact on hazard estimates of the vertical ground motion component, which can be significantly larger than its horizontal counterpart in the near-source region at short periods.

Special care was devoted as well to the used of a specific volcanic model and to its impact in the PSHA, to consider peculiar characteristics of ground motion in areas mainly affected by shallow volcanic events, such as in Sicily.

The main findings of this work have shown that significant differences may arise in UHS when different GMMs are used, depending on the distance and the vibration periods at play, while the type of modelling of the uncertainties of the GMMs had limited influence. A limited influence was shown as well for the way the vertical component was modelled inside the PSHA. The impact of the near source correction factors of the GMMs was proved to be meaningful for certain scenarios and periods ranges. For volcanic areas, the use of a specific GMM provided to have limited influence on the seismic hazard, due to the dominance of the tectonic seismicity of the adjacent source zones, particularly at short periods.

Key-words: probabilistic seismic hazard analysis (PSHA), Italian hazard model, ground motion model (GMM), near-source, vertical component, volcanic model, R-CRISIS.

Abstract

L'analisi probabilistica della pericolosità sismica (PSHA) (Cornell 1968) è attualmente l'approccio standard adottato in tutto il mondo per la valutazione della pericolosità all'interno dei codici di progettazione degli edifici, come in Italia (NTC18). I principali ingredienti della PSHA sono i modelli di moto del suolo che forniscono le previsioni mediane e la corrispondente incertezza dei parametri di scuotimento. Sebbene i GMM siano ampiamente calibrati in tutto il mondo, grazie al crescente numero di dati registrati, sono ancora scarsamente vincolati in condizioni prossime alla sorgente o in regioni vulcaniche. Tuttavia, studi recenti hanno sottolineato l'importanza di quantificare correttamente questi effetti nelle stime di pericolosità, poiché le azioni sismiche di progetto possono spesso essere superate, come ad esempio avviene in area epicentrale per terremoti di magnitudo medio elevati.

Questa tesi si propone di indagare l'impatto, all'interno di un calcolo probabilistico della pericolosità sismica, di nuovi GMM italiani specificamente calibrati per i terremoti di crosta superficiale o regolati con fattori empirici, per tenere conto degli effetti globali di campo vicino del moto del suolo.

Nelle analisi, particolare attenzione è stata data anche alla valutazione della variabilità associata ai modelli utilizzati e all'impatto sulle stime di pericolosità della componente verticale del moto del suolo, che può essere significativamente più grande della sua controparte orizzontale in campo vicino, a corti periodi.

Particolare interesse è stato dedicato anche all'utilizzo di uno specifico modello vulcanico e al suo impatto nella PSHA, per considerare le caratteristiche peculiari del moto del suolo in aree interessate da eventi vulcanici poco profondi, come in Sicilia.

I principali risultati di questo lavoro hanno mostrato che possono emergere differenze significative nell'UHS quando vengono utilizzati diversi GMM, a seconda della distanza e dei periodi di vibrazione in gioco, mentre il tipo di modellazione delle incertezze dei GMM ha avuto un'influenza limitata. Un'influenza limitata è stata evidenziata anche per il modo in cui la componente verticale è stata modellata all'interno del PSHA. L'impatto dei fattori di correzione delle sorgenti vicine dei GMM si è dimostrato significativo per alcuni scenari e periodi. Per le aree vulcaniche, l'uso di uno specifico GMM ha dimostrato di avere un'influenza limitata sulla pericolosità sismica, a causa della dominanza della sismicità tettonica delle zone sorgente adiacenti, in particolare a brevi periodi strutturali.

Parole chiave: analisi di pericolosità sismica, modello di pericolosità italiano, modello dello scuotimento al suolo, campo vicino, componente verticale, modello vulcanico, R-CRISIS.

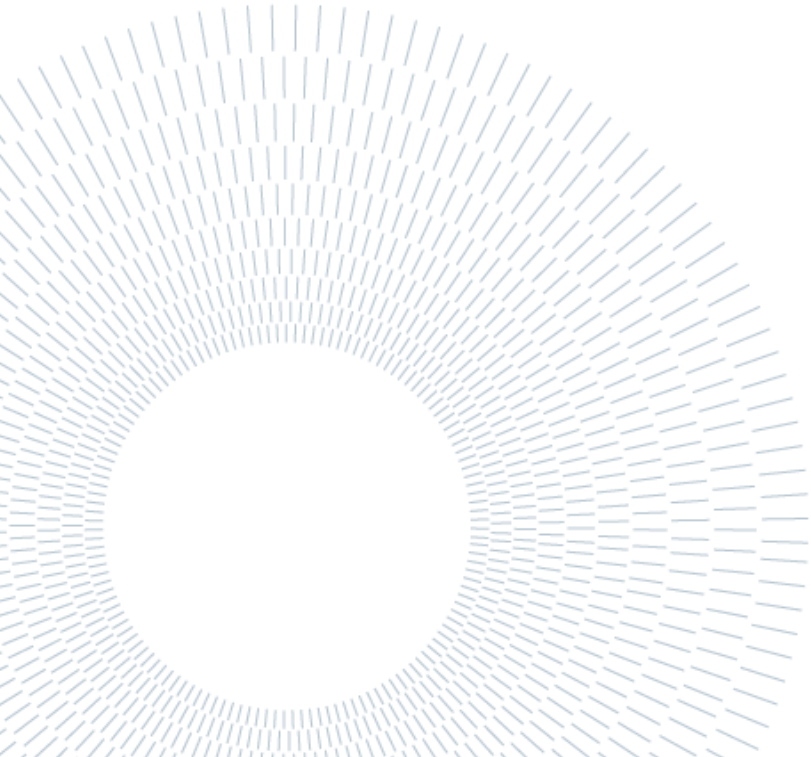

Contents

Introduction

The Seismic Hazard Analysis (SHA) aims to estimate both the amplitude and frequency of occurrence of earthquake ground motion expected at a site, with the goal of defining seismic actions for the design and evaluation of structures, which must be able to withstand a given level of ground shaking while maintaining a desired level of performance.

There are different approaches commonly used to the seismic hazard assessment: the Deterministic SHA (DSHA) approaches usually explore one or few controlling events, as the maximum credible earthquake or the earthquakes that may cause a predefined level of damage or malfunction, generated by one or more specific seismic sources [1]; while the Probabilistic SHA (PSHA) integrates over all possible earthquake ground motions at a site to develop a composite representation of the spectral amplitudes and hazards (annual frequencies of exceedance) [2].

In SHA, the expected median level of ground shaking and its associated uncertainty are evaluated through the Ground Motion Models (GMMs). The GMMs are calibrated by regression on empirical or simulated ground-motion intensity measures against a set of predictor variables such as earthquake magnitude, source-to-site distance, and local soil conditions. The accuracy of the predicted ground-motion amplitude is a fundamental issue for both the probabilistic and deterministic approaches, especially when the analysed site and the seismic source are very close to one another [1]. In such a case, the ground-motion median and standard deviation evaluated from any GMM are usually poorly constrained, due to the general lack of strong-motion records in near-source conditions.

In Italy, the seismic hazard model is based on a PSHA approach and results, in terms of the Uniform Hazard Spectra (UHS), used to define the seismic design actions of the Italian building code (NTC-18). The UHS is defined as the result of the combined possible magnitudes, distances, and ground motion amplitudes, evaluated for a given annual rate of exceedance probability. The actual reference seismic hazard map of Italy was elaborated in the MPS04 project [3], where the ZS9 area source model served as an input for PSHA (NTC-18) [4].

A new seismic hazard model for Italy, "Modello di Pericolosità Sismica 2019 -MPS19" [5] has been recently proposed by the Seismic Hazard Centre (Centro di Pericolosità Sismica, CPS) of the Istituto Nazionale di Geofisica e Vulcanologia (INGV). This model is constituted by a suite of Ground Motion Models (GMMs) [6] that are based on updated and new data acquired in the last decades after the release of the seismic

hazard model of 2004-2006 (MPS04; [3]). MPS19 describes in a probabilistic way the forecast of a variety of ground motion intensity measures (IM; such as PGA and other quantities) on the Italian territory [5], and considers only declustered seismicity, referenced on rock soil (i.e., in accordance to the Italian and European seismic norms the rock category corresponds to the NTC08/EC8 site category A, flat topography and $V_{S,30} > 800$ m/s) [5].

The GMMs currently implemented in the Italian seismic hazard models however do not explicitly take into account the specific effect of near-sources (directivity, higher vertical components, impulsive motion, hanging-wall/footwall effects, etc. [7]); moreover new and updated GMMs have been made available after the publication of MPS19 also with reference to the volcanic zones; but none of these new models have been assessed in terms of PSHA. The importance to evaluate the impact of new GMMs on the hazard estimates, has been also highlighted by recent studies carried out in the Italian context, which have revealed the need of a right quantification of shaking predictions in building codes, particularly due to near-source effects. In this respect, it has been demonstrated that elastic design spectral ordinates can be often exceeded in epicentral areas, for moderate-to-high earthquakes [8]. Indeed, the investigation of near-source effects is a well-known research issue, particularly motivated by the need to constrain GMMs near the epicentre and to define design spectra, based on PSHA.

In this context, specific GMMs for the Italian context corrected for global near-source effects [7], have been developed in the framework of the research program Dipartimento della Protezione Civile (DPC)-ReLUIS Agreement 2019–2021 - WP18, which led to the creation of (Near-Source Strong motion - NESS [1]), a near-source seismic datasets of accelerometer recordings.

Within this project framework, the calibration of empirical correction factors was also performed based on the modelling of the residuals of NESS observations with respect to the Italian reference GMM [6]. This thesis, among the framework of that project, aims to investigate the effect of adopting such corrected GMMs on uniform hazard spectra considering different locations on the national territory. To this aim, it has been adopted the new seismotectonic zoning "ZS16" proposed in the revised area-source seismogenic model (MA4; [4]), and included in the new MPS19 [5], to serve as an input for the PSHA. ZS16 considers new data available on the national territory for the study area, among which an historical earthquake catalogue (Catalogo Parametrico dei Terremoti Italiani CPTI15) [4] and it is based on the same seismotectonic knowledge used for designing ZS9 [9], reflecting the structural tectonic framework of Italy and composed of 50 area sources representing regions of spatially uniform occurrence of seismicity [10].

The analyses are implemented with the use of the ultimate version of the software CRISIS (R-CRISIS [11]).

In the thesis, the GMMs investigated include the recently calibrated model proposed by Lanzano et al. (ITA18; [6]) for Italy, adjusted to account for near-source conditions through empirical corrections, calculated from the residuals of a worldwide dataset.

The adopted corrections for hazard estimation does not aim to model each near-source peculiar phenomenon, such as directivity, pulse-like, and so on, although it incorporates all these effects in the model variability. In such cases, the correction enables to improve the predictive power of the attenuation model through a conservative increment that covers the global near-source effects observable in NESS2 [7].

The corrections factors considered are the ones proposed for the GMM ITA18 of Lanzano et al. [6], which was calibrated on the most up-to-date strong motion dataset for Italian crustal earthquakes. Since the dataset used to calibrate ITA18 model includes less than 7% of records at distances lower than 20 km, the "NESS" correction factor allows to improve its prediction of the median ground motion.

The ITA18 model is also compared in this work with the earlier model implemented by Bindi et al. [12] at the national scale (ITA10), which is characterized by a narrower dataset, with magnitudes lower than 6.9, with a weak magnitude scaling [6].

A particular care has been devoted in this work to the evaluation of the vertical ground motion component, which can be significantly larger than its horizontal counterpart, especially in the near-source region of earthquake and at short periods ($T < 0.3\ s$), with potential impact for short-period structures. In this work, two procedures were adopted to generate a vertical hazard spectrum. First, a vertical-to-horizontal model was used to scale the horizontal prediction of ground motion; second, the use of a specific GMM calibrated for vertical components was adopted. In both cases, the effects on the UHS spectra were analysed and compared. The ITA18-VH model of Ramadan et al. [13] was used in the first approach, while a new model ITA18-V, calibrated *ad-hoc* directly on the vertical component of the records of ITA18, was tested in the second approach.

The use of specific models for volcanic areas (LL19; [14]) has been tested in this work, to consider the effect of their impact in the results of a PSHA, as the consequence of a pronounced different nature of volcanic events (particularly the shallower with focal depth < 5 km) with respect to the tectonic earthquakes. Note that volcanic earthquakes have a strong impact in many Italian regions, being capable of producing severe ground accelerations; indeed, volcanic earthquakes have seriously endangered densely populated areas in Italy (e.g. Catania and surroundings, Campi Flegrei, Vesuvius in the past).

The thesis is organized as follows:

- **chapter 1** describes the adopted methodology for the evaluation of the PSHA, and the new seismic hazard map MPS19, relying on the earthquake catalogue CPTI15 and on the area source model ZS16 [4];
- **chapter 2** describes the ground motion models used in the PSHA of this work, for different case studies;
- **chapter 3** describes the main features of the software (R-CRISIS [11]);
- **chapter 4** shows and discusses the cases studies considered in the thesis: L'Aquila, Gemona del Friuli and Zafferana Etnea;
- the conclusions summarize the main findings on this work.

The site of L'Aquila was studied in terms of seismic hazard, to evaluate the impacts of the horizontal and the vertical GMMs ITA10 and ITA18, calibrated for shallow crustal earthquakes in the Italian active tectonic regions [6] and to assess the impact of the ground motion correction factors in near-source conditions (using the ITA18-NESS [7]).

Thereafter, the site of Gemona del Friuli (Friuli-Venezia Giulia), located in the epicentral area of the seismogenic source of the 1976 Friuli earthquake (Mw 6.4) was considered for the sole purpose of verifying the performance of the near source correction factors on the UHS, for a different style of faulting (mainly a reverse mechanism), for which more significant effects were expected, mainly over short periods, both for the horizontal and the vertical components.

Finally, the site of Zafferna Etnea was introduced to study the impacts of a volcanic GMM (the LL19 model [14]), with respect to an active shallow crustal one, on PSHA results.

1 Methods and data

1.1. Methodology

The Seismic Hazard Analysis (SHA) aims to estimate both the amplitude and frequency of occurrence of earthquake ground motion at a site, to rationally define seismic actions for design and assessment of structure, able to withstand a given level of ground shaking while maintaining a desired level of performance.

The SHA can follow two different approaches: the first is the Deterministic Seismic Hazard Analysis (DSHA) which aims to evaluate the expected ground shaking amplitude (i.e., worst case scenario), due to an earthquake of given magnitude, from a given fault that is likely to occur at any site of interest; the second approach is the Probabilistic Seismic Hazard Analysis (PSHA), which provides a quantitative estimation of the probability of exceedance of ground shaking amplitude at a site, due to whatever earthquake from whatever fault or areas source, within a reference time interval. More in detail, the PSHA aims to quantify the uncertainties related to the location, size and resulting shaking intensity of future earthquakes and combine them, with predictions of the potential shaking intensity [15].

The PSHA can be summarized according to Cornell [16] in four main steps (see Figure 1.1):

1. Definition of a seismogenic model, to characterize the source and contextualize the seismotectonic properties;
2. Definition of the seismicity of the area, defined by a frequency-magnitude relationship (e.g., Gutenberg-Richter [17]) which shows the activity rates at which earthquakes of magnitudes greater equal than a certain value are expected to occur;
3. Prediction of the resulting distribution of ground motion intensity as a function of earthquake magnitude, distance, etc. through a ground motion model based on the attenuation relation, Ground Motion Models (GMMs), carefully selected, depending on the region at study and on its seismotectonic characteristics;
4. Combination of uncertainties in earthquake size, location, and ground motion intensity, using a calculation known as the total probability theorem, and evaluation of exceedance probabilities for a given time period.

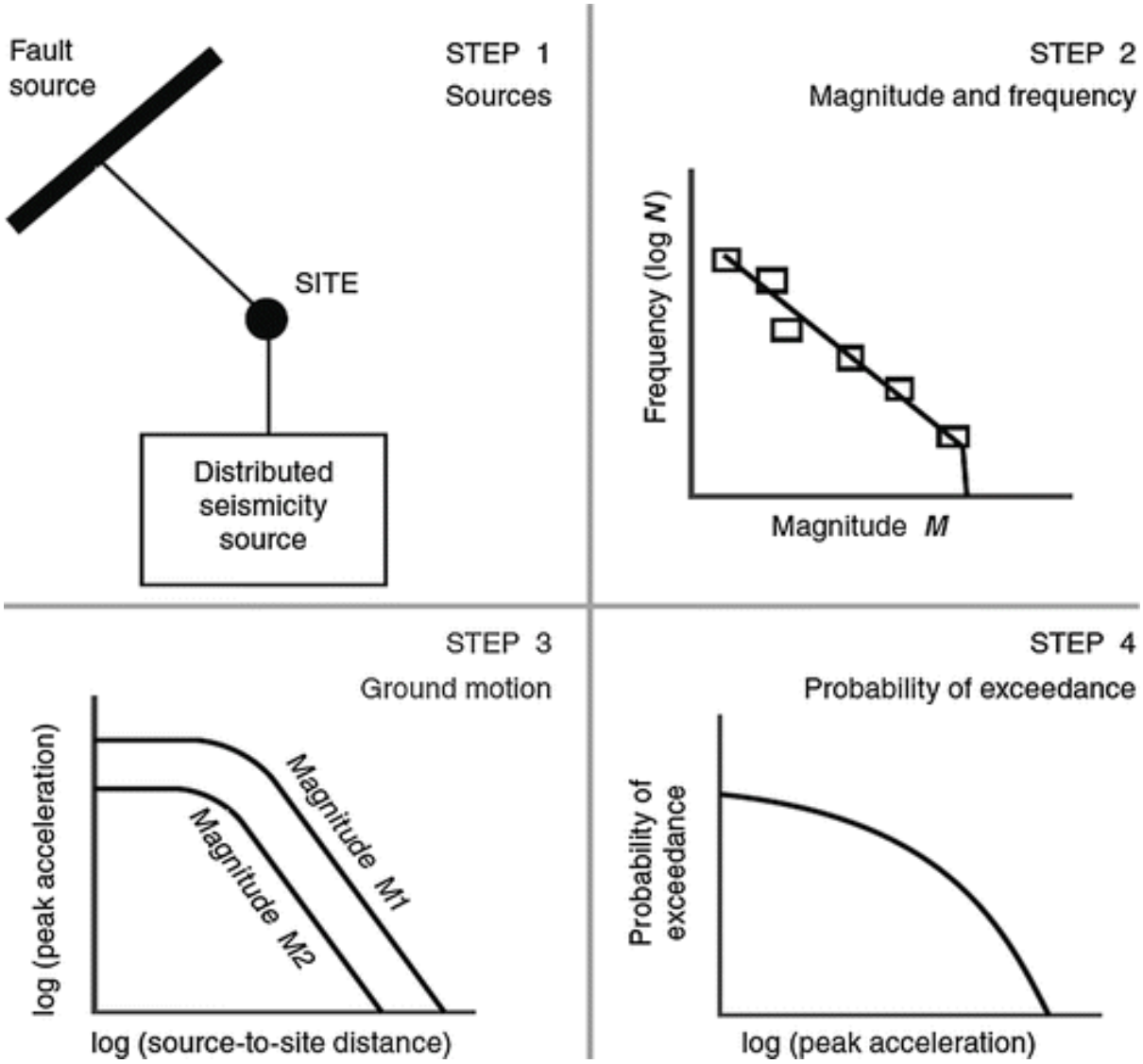

Figure 1.1 Schematic illustration of the basic four steps in probabilistic seismic hazard analysis.

The source can be described by faults, which are typically planar surface identified through observations of past earthquake locations and geological evidence, or if these are not identifiable, then earthquake sources may be described by areal regions in which earthquakes may occur anywhere [15].

Indeed, the area source models were introduced by Cornell [16] as the basic source model type to describe seismic activity within a given region, considered to have homogeneous seismic activity. The area sources are characterized by a single Gutenberg-Richter [17] recurrence law (with the same probability distribution of magnitude and the same annual rate of occurrence (i.e., Poisson model)) defined as follows:

$$\log \lambda_m = a - bM, \tag{1.1}$$

Where λ_m is the rate of earthquakes with magnitudes greater than M, and a and b are constants; the a and b constants are estimated using statistical analysis of historical observations. The a value indicates the overall rate of earthquakes in a region, and the b value indicates the relative importance of small to large magnitude earthquakes (typically b is approximately equal to 1) [15].

The next step is the selection of a ground motion model (GMM) to be used in the calculation of the probability distribution of ground motion intensity, as a function of many predictor variables such as the earthquake's magnitude, distance, faulting mechanism, the near-surface site conditions, the potential presence of directivity effects, etc. These models are generally developed using statistical regression on observations from large dataset of observed ground motion intensities and calibrated on strong motion records at a regional or worldwide scale. The functional form of a GMM is usually selected to reflect the mechanics of the ground motion process as closely as possible [15].

The ground motion model allows to compute the probability of exceeding an intensity level for a single source, for given magnitude and distance through the total probability theorem:

$$P(Y \geq y) = \int\int\int P(Y \geq y|r, m, \varepsilon) f_R(r) f_M(m) f_{\mathrm{E}}(\varepsilon) dr dm d\varepsilon, \qquad (1.2)$$

Where $P(Y \geq y|r, m, \varepsilon)$ is calculated using a ground motion model and the assumption on the distribution of its ground motion intensity; $f_M(m)$, $f_R(r)$ and $f_E(\varepsilon)$ are the probability density functions (PDFs) of magnitude, distance, and error. The integration operation adds up the conditional probabilities of exceedance associated with all possible magnitudes, distances, and error.

The probability of exceedance calculated through eq. (1.2) is combined with a model for the earthquake occurrence in time (such as the Poissonian one) so that the probabilities that, at a given site, for a given time interval, a given parameter Y of ground motion severity (e.g., PGA or any spectral ordinate) is going to be exceeded, are calculated. From these probabilities of exceedance, the Uniform Hazard Spectrum (UHS) are calculated, for fixed values of the return period. Note that the UHS does not represent the spectrum of any specific earthquake scenario, but it is the result of the combined contributions of all possible combinations of occurrence of earthquakes of given magnitude and distance, on different sources that contribute to the outcome of the PSHA.

In this work, the most recent version of software CRISIS (R-CRISIS [11]) has been used to perform the SH analyses.

1.2. The probabilistic seismic hazard model of Italy: from MPS04 to MPS19

The Seismic Hazard Centre (Centro di Pericolosità Sismica, CPS) of the Istituto Nazionale di Geofisica e Vulcanologia (INGV) recently produced a new seismic hazard model for Italy, called "Modello di Pericolosità Sismica 2019 -MPS19" [5]; the project was funded by the Italian Civil Protection Department. This model is constituted by a suite of Earthquake Rupture Forecasts (ERFs) [18] and Ground Motion Models (GMMs) [6] that are based on updated and new data acquired in the last decades after the release of the current reference Italian seismic hazard model in 2004-2006 (MPS04 project; [3]) on which the actual Italian Building Code (NTC-18) [4] is based.

MPS19 describes in a probabilistic way the forecast of a variety of ground motion intensity measures (IM; such as PGA and other quantities) on the Italian territory [5]. The ERF returns the long-term rate of all earthquakes throughout the region above a specified threshold, defined in MPS19 as $Mw \geq 4.5$, based on the observation that earthquakes with magnitude lower than 4.5 are generally unlikely to cause significant damage in Italy. The ERFs comprise various components, including faults, distributed seismicity, area sources, and geodetically derived tectonic strain, collectively reflecting over 15 years of raw data, analyses, and data-derived products on the onshore and offshore Italian territory and its conterminous areas [18].

The models cover the whole national territory and consider only declustered seismicity, referenced on rock soil (i.e., EC8 site category A, $V_{S,30} > 800$ m/s); the hazard is expressed in terms of mean horizontal peak ground acceleration (PGA), peak ground velocity (PGV), and peak ground displacement (PGD), spectral acceleration (SA), velocity, displacement, and macro seismic intensity [5].

It is based on 11 groups of earthquake rupture forecast inputs and, particularly, on 5 area-source seismogenic models, including the so-called "MA4" model (i.e., area-source model #4). The latter is the seismogenic model adopted in this PSHA of this work for the PSHA and consists of 20 seismicity models that consider epistemic uncertainty in the estimation of the completeness periods of the earthquake catalogue, of maximum magnitude values and of seismicity rates. A truncated Gutenberg-Richter frequency-magnitude distribution was considered to calculate the rates in 5 approaches: the first approach is the one taken into account for the development of the PSHA and estimates seismicity rates using earthquakes located in each source zone, while the other approaches firstly calculate the a and b values of the truncated Gutenberg-Richter relation for groups of zones considered tectonically homogenous, and successively partitions the values in different ways to the zones forming each group [4].

1.3. Earthquake catalogue

The boundaries and seismic parameters of the area sources have been recently specified in the new Italian Seismic Hazard Model (MPS19) [5], and are based on the collection and the analysis of several seismotectonic datasets. Among these datasets, the following have been used: the historical earthquake catalogue (Catalogo Parametrico dei Terremoti Italiani CPTI15, version 1.5 [19] [20]); an instrumental earthquake catalogue [21] [14]; the version 3.2.1 of the Database of Italian Seismogenic Sources (DISS 3.2.1 [22]; DISS Working Group 2018); a harmonized GPS velocity model for the Mediterranena area [23]; and other geological and geophysical data, available for specific regions and for the whole territory [4].

More in detail, CPTI15 v.1.5 lists 4389 earthquakes with moment magnitude $Mw \geq 4.0$, macroseismic intensity ≥ 5 occurred in the Italian and neighbouring areas in the period 1000-2014. The catalogue provides epicentral locations, while homogeneous moment magnitude estimates are derived from both macro-seismic and instrumental data. The catalogue takes advantage of the wealth of macro-seismic intensity data related to both historical and recent earthquakes collected in the Italian Macro-seismic Database DBMI15 (version 1.5 [19]).

For the definition of the earthquake catalogue, in MPS19, 3353 mainshocks were identified, according to the declustering procedure [24], corresponding to the 76% of the whole, unclustered catalogue of events [4].

Two independent sets of completeness time intervals for the CPTI15 catalogue were defined according to:

1. An historical approach [25];
2. A statistical method [26].

On one hand, the historical approach determines the complete intervals analyzing the local history of a set of sample localities, whose threshold and periods are assessed for the sample localities and then extrapolated to the area source they belong to and to others with similar history and seismotectonic features [25] [3]. On the other hand, the statistical completeness intervals [26] are assessed for the same macro-regions defined for the historical approach [4].

Moreover, the maximum magnitude definition of the area sources is based on the estimates provided in MPS19 [18]. The Italian source areas are divided into 18 tectonic domains and the earthquakes listed in CPTI15 are assigned to them, according to their location.

Two values of maximum magnitude are then assigned to each tectonic domain:

1. Mwmax1 that is the largest value between $Mwtect$ and $Mwobs + uncertainty$;
2. Mwmax2 that results by uniformly incrementing $Mwmax1$ by a cautionary value of 0.3 to account for epistemic uncertainties, except for the Etna volcanic domain where $Mwmax2$ is equal to $Mwmax1$.

Based on the average error of magnitude estimates for earthquakes occurring before and after 1980, a minimum value of uncertainty for the Mw evaluation of 0.3 and 0.2 is introduced for the historical and instrumental portion of the catalogue, respectively.

The PSHA implemented in this work refer to the rates computed for the ZS16 model, considering the statistical approach and the first value of the maximum magnitude (Mwmax1).

1.4. Seismic zonation: the area source model ZS16

The model "MA4" referred to in this work, is based on a seismotectonic zoning defined as "ZS16" (the actual update to ZS9 model) which has been used inside the software R-CRISIS to perform the analyses. ZS16 incorporates several different information for each defined area source:

- Geographical boundaries;
- Top and bottom depth of the seismogenic layer;
- Hypocentral distribution;
- Style of faulting;
- Activity rates.

As already mentioned, for each area source, 5 alternative frequency-magnitude distributions are computed, providing the annual rates of all earthquakes with $Mw \geq 4.5$ (the threshold magnitude adopted in MPS19 [5] [4]).

The definition of the boundaries of the area sources is based on the mapped active faults and on the combination of geological data with historical and instrumental seismicity, as well as with geophysical data, including geodetic strain field, maximum horizontal stress orientation and focal mechanism. The combination of all this information led to the definition of the geographical borders of the areas, the prevailing style of faulting, the upper and lower bounds of the characteristics seismogenic depth and the distribution of hypocentral depths [4]. Figure 1.2 [5] shows the expected style of faulting for each area source: full circles represent random seismic source and white circles represent 100% random while blue, red, and green circles correspond to reverse, normal and strike-slip random sources, respectively. Cumulative focal mechanisms colors follow the same criteria. Focal mechanisms with a grey background or circles with darker colors are the sources for deeper layers. Black

numbers are the percentages of contribution to the final source when their sum is the expected style of faulting [4].

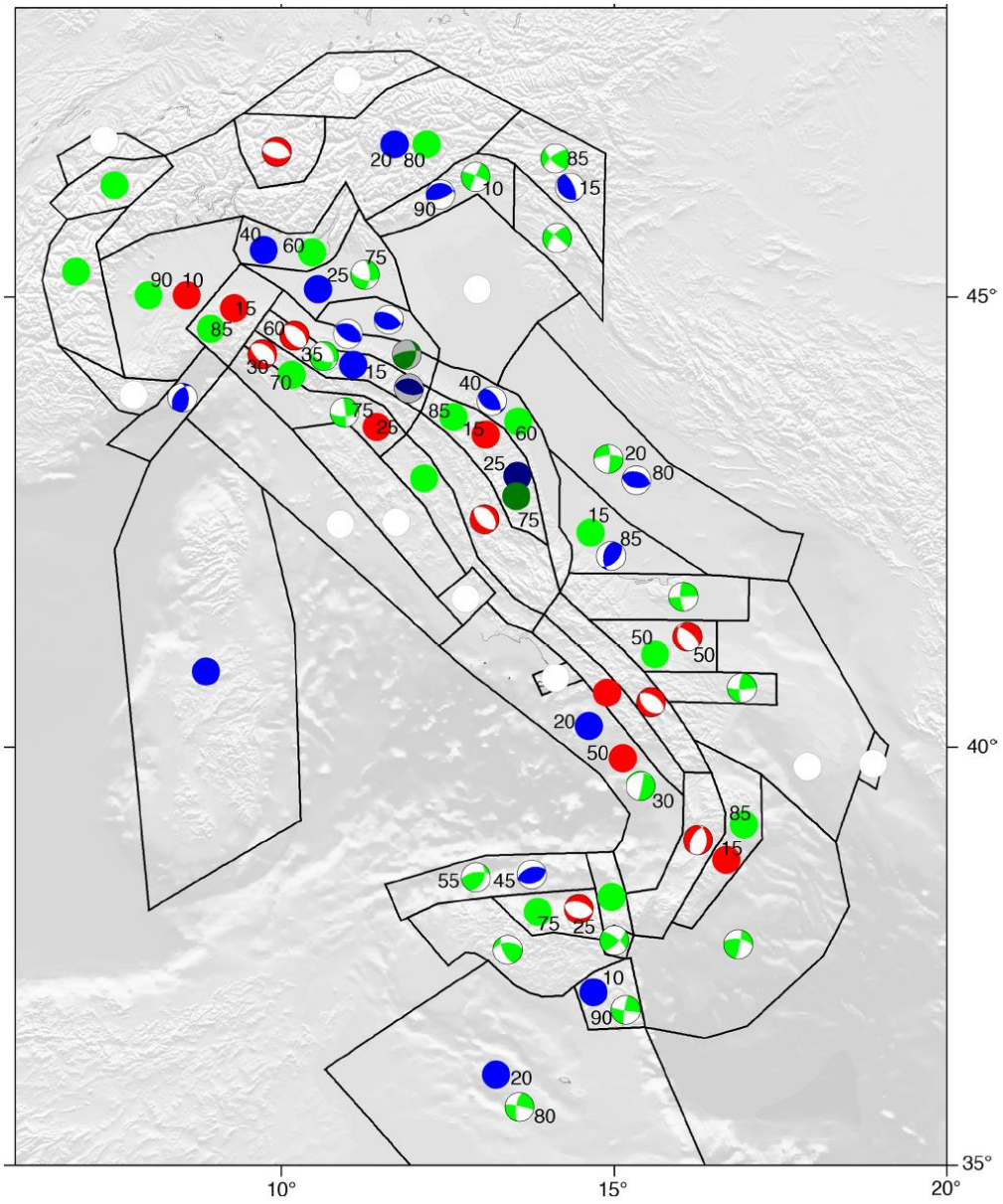

Figure 1.2 Expected style of faulting for each area source (modified from Pondrelli [10]).

The ZS16 model was built, starting from ZS9, adopting the following criteria:

1. start from the area source of the ZS9 model;
2. be consistent with the general background delineated by the geodynamic model proposed by Meletti et al. [27], i.e., an area source should contain a unique tectonic zone (active magma crustal, volcanic or subduction zone in the specific Italian case);
3. incorporate all recent advances in the understanding of the active tectonics of the territory and in the distribution of seismogenic sources modelled in the DISS

3.2.1 database and other active fault compilations at the national and regional scale;

4. incorporate information derived from the investigation of the most recent seismic sequences that struck Italy after the compilation of ZS9, namely L'Aquila 2009, Emilia 2012 and Amatrice-Norcia 2016 sequences;
5. be consistent with the CPTI15 earthquake catalogue;
6. define area source boundaries that primarily follow the surface projection of mapped active faults: an area source should not interrupt a normal or reverse fault system unless major differences are observed (changes in stress orientation and/or changes in crustal depth); strike-slip faults, boundaries should be parallel to the strike of the faults and the area source should contain the faults;
7. consider for the definition of the boundaries: the pattern of seismicity, focal mechanism, geodetic strain field, maximum horizontal stress Shmax orientation [28] and heat flow data;
8. account for the variation of the style-of-faulting and tectonic regime with depth, therefore multiple area sources can overlap on the volume domain;
9. cover the entire Italian territory, as required by MPS19.

These criteria were applied [5] to define the seismotectonic zoning, consisting of 48 active shallow crustal area sources and 2 area sources corresponding to the Campanian and Mt. Etna volcanic districts (i.e., area sources #31 and #49, respectively). A comparison between the two source zones models (i.e., ZS9 and ZS16) is shown in Figure 1.3, evidencing the different boundaries considered for each area source.

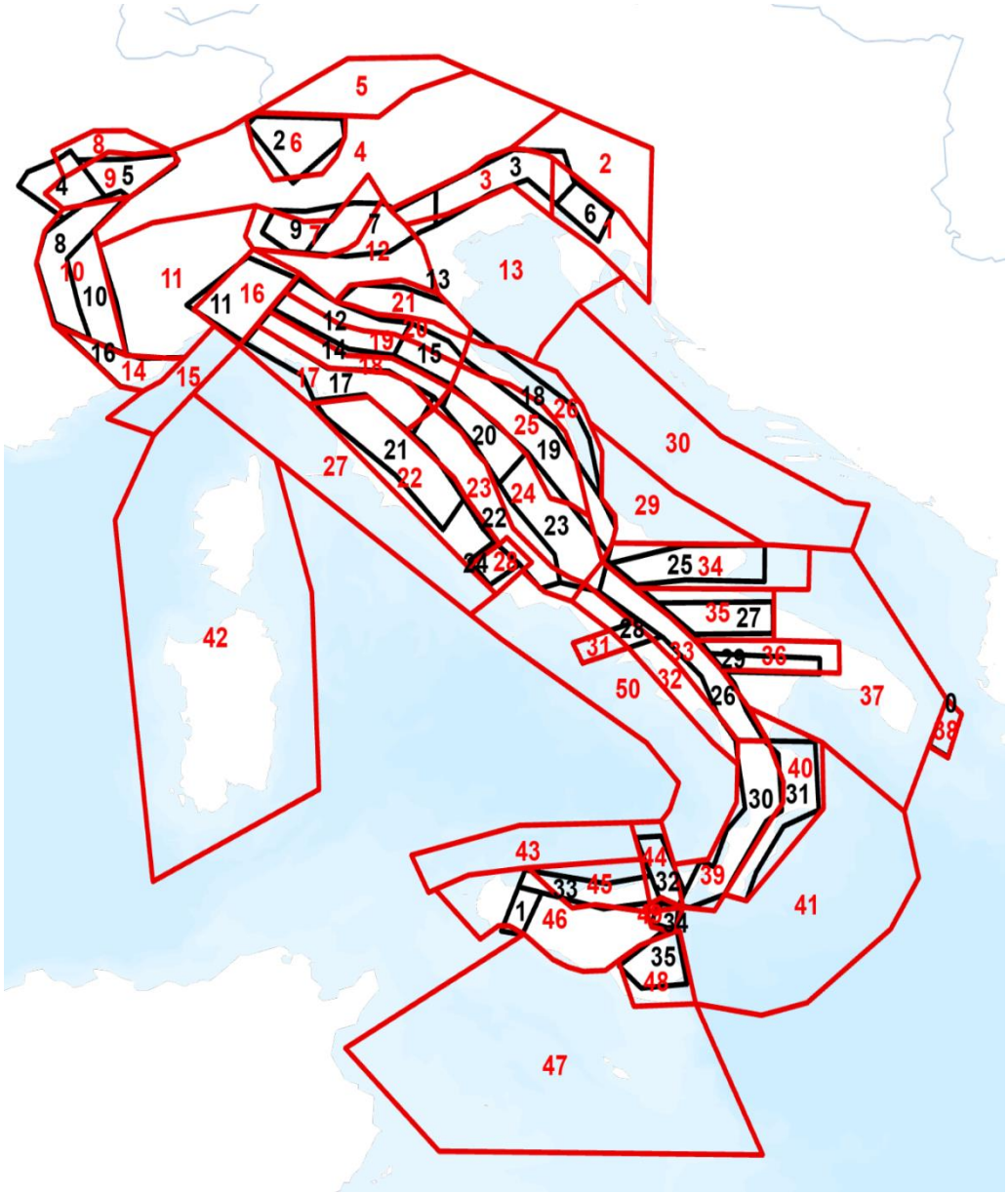

Figure 1.3 Comparison of ZS9 by Meletti et al. [9] and ZS16 by Visini et al. [18].

The seismogenic depths for each area source of ZS16 were estimated [5] using the instrumental catalogue [21], and the considered earthquakes were related to active crustal seismicity, based on the crustal models [29] [30]. In the Mt. Etna region, the earthquakes with hypocentral depth $< 10\ km$ were assigned to the volcanic domain (area source #49) and earthquakes with hypocentral depth $\geq 10\ km$ to the underlying active crustal area sources (#44, #45 and #46). Some criteria have been defined to parametrize the styles of faulting of expected earthquake ruptures and to evaluate their representativeness in each area source [4] [10].

The distribution of earthquake magnitudes was assumed to follows the Truncated Gutenberg-Richter (TruncGR) model, following the Pareto distribution with the probability density function truncated at both ends. Its cumulative density function related to the moment magnitude is:

$$\Lambda(M) = \Lambda_0 \frac{\exp(-\beta M_0) - \exp(-\beta M)}{\exp(-\beta M_0) - \exp(-\beta Mu)}, \quad (1.3)$$

Where $\Lambda(M)$ is the cumulative number of earthquakes per unit time equal to or larger than the magnitude threshold (M_0) and smaller than the maximum Mu. $\beta = 2.3b$ (the slope) and Λ_0 were derived from the declustered CPTI15 catalogue by adopting the completeness time intervals, the maximum magnitude values, and a maximum-likelihood [31] [4].

2 Ground motion models

The ground motion models (GMMs) establish probabilistic relations between earthquake characteristics, intensities, and distances at the computation sites; the intensities are regarded as random variables whose probability distribution is completely fixed by the GMM [11]. These relations are used in SH analyses to describe the distribution of ground motion in terms of a median and a logarithmic standard deviation, and their influence is very strong on the results of PSHA [32].

Several reviews of ground motion estimation studies have been made in the past and provide a good summary of the methods used, the results obtained, and the problems associated with such relations. Douglas et al. [33] reviews the procedures adopted in the past 30 years to derive equations for the estimation of ground motions using strong-motion records. He summarises over 120 studies that derived equations for the estimation of peak ground acceleration and over 80 studies for the estimation of response spectral ordinates [33].

The complete procedure that needs to be followed to derive ground motion estimation equations is first to get a set of records (recorded on analogue accelerographs) for analysis using strong-motion instruments, then the accelerograms are digitized to get the data into a form usable for numerical analysis. The digitized strong-motion records are processed to remove short- and long-period noise, which usually consists of fitting a zero baseline to the record and then applying a bandpass filter; a dependent variable (such as peak ground acceleration or spectral acceleration) is then selected and calculated from the strong-motion records and should be useful for seismic design and analysis [33].

More in detail, the derived equations are used in seismic hazard analysis, according to Cornell [16], to give estimates of the strong ground motion that could be expected at a site during a future earthquake and to quantify the rate of exceeding various ground-motion levels, given all possible earthquakes [33]. The investigation is done to study the effects of different new GMMs calibrated on specific dataset of shallow crustal tectonic and volcanic regimes. The assessment of the impact of recent GMMs on the seismic hazard is fundamental to define the corrective factors of the design spectrum, particularly in the near-source conditions.

The present work focuses on the impact, within the seismic hazard calculation, of new GMMs specifically calibrated for the Italian context for shallow crustal earthquakes [6], as well as on the empirically derived correction factors used to adjust the median

predictions of these GMMs to consider the effects of near source. This is a relevant topic from an engineering point of view because the general effect of the proximity to the seismogenic source is an increment on the seismic demand, which must be considered for engineering applications. However, the design norms do not consider specific near-source phenomena (directivity, higher vertical components, impulsive motion, hanging-wall/footwall effects, etc. [7]) but rather the average properties of the seismicity area of interest.

The ground motion effects in near-source conditions are quantified by the adoption of empirical corrections, calculated from the residuals of a worldwide dataset (Near-Source Strong motion - NESS [7]) with respect to the median prediction of a specific GMM of Italy. In particular, the corrections are assumed for the GMM proposed by Lanzano et al. (ITA18; [6]), calibrated on the most up-to-date strong motion dataset for Italian crustal earthquakes, and accounting for most recent seismic sequences (2012 Emilia, 2016-2017 Central Italy) with the largest events, to extend the maximum usable magnitude for PSHA calculations.

The correction NESS allows in general to improve the prediction of the median ground motion of the reference model (ITA18 is composed by less than 7% of records at distances lower than 20 km), leading to capture the global effects in conditions proximate to the source of the earthquake.

The ITA18 model is also compared with the earlier model implemented by Bindi et al. [12] at the national scale (ITA10; [12]), which is characterized by a narrower dataset to magnitudes lower than 6.9, with a weak magnitude scaling, and limited variation of periods up to 2 seconds [6].

A particular emphasis is also given to the evaluation of the vertical ground motion component, which can be significantly larger than its horizontal counterpart, especially in the near-source region of earthquake and at short periods ($T < 0.3\ s$), with potential impact for short-period structures. The model ITA18-VH is the ITA18 model with the spectral acceleration ratio between the vertical and the horizontal components (VH), exploited to scale the UHS of the horizontal component. The use of the ratio VH is the most used approach to generate a vertical hazard spectrum, compatible with the horizontal one. However, a new model ITA18-V, calibrated *ad-hoc* directly on the vertical component of the records of ITA18, is proposed to allow a direct comparison and a validation with the estimate of the vertical motion UHS-V obtained from the application of ITA18-VH model.

The introduction of a volcanic model (LL19; [14]) is the consequence of a pronounced different nature with respect to the tectonic activities, in fact the volcanic earthquakes have serious endangered densely populated areas (e.g., Catania and surroundings, Campi Flegrei, Vesuvius). The attention has been focused on the shallow volcanic events (focal depth < 5 km) because of their relevant importance in the evaluation of seismic hazard in Italy.

2.1. ITA10

A ground motion model was proposed by Bindi et al. [12] for Italy considering the strong motion ITACA database [34] (updated until 2009). The equation is derived for the geometrical mean of the horizontal components and the vertical, in terms of PGA, PGV and 5%-damped spectral acceleration at periods between 0.04 and 2 s [12].

The functional form is defined as:

$$\log_{10} Y = e_1 + F_D(R, M) + F_M(M) + F_S + F_{sof}, \tag{2.1}$$

Where e_1 is the constant term, $F_D(R, M)$, $F_M(M)$, F_S and F_{sof} represent the distance function, the magnitude scaling, the site amplification, and the style of faulting correction, respectively. M is the moment magnitude, R is the Joyner-Boore distance, or epicentral distance (in km), when the fault geometry is unknown (generally when $M < 5.5$).

The equation for the distance function is defined as:

$$F_D(R, M) = \left[c_1 + c_2\left(M - M_{ref}\right)\right] \log_{10}\left(\sqrt{R_{JB}^2 + h^2}/R_{ref}\right) - c_3\left(\sqrt{R_{JB}^2 + h^2} - R_{ref}\right), \tag{2.2}$$

While the magnitude function is:

$$F_M(M_w) = \begin{cases} b_1(M - M_h) + b_2(M - M_h)^2 & for\ M \le M_h \\ b_2(M - M_h) & otherwise \end{cases}, \tag{2.3}$$

Where M_{ref}, M_h, R_{ref} are coefficients to be determined through the analysis.

The functional form F_S in the equation (2.1) represents the site amplification and it is given by $F_S = s_j C_j$, for $j = 1, \dots, 5$, where s_j are the coefficients to be determined though the regression analysis, while C_j are dummy variables used to denote the five different EC8 site classes (A through E). The functional form $F_{Sof} = f_j E_j$, for $i = 1, \dots, 4$, where f_j are the coefficients to be determined during the analysis and E_j are dummy variables used to denote the different fault classes. The style of faulting considered are 4 types: normal (N), reverse (R), strike slip (SS) and unknown (U) [12].

Some variables are fixed after some trial regression performed by applying a random effect approach [35] [36] as: $R_{ref} = 1\ km$; $M_{ref} = 5$; $M_h = 6.75$; $b_3 = 0$.

ITA10 is characterized by several limitations because of the limited number of data available at the time it was calibrated (2009):

1. the magnitude range ($4.1 \le Mw \le 6.9$) limits the maximum usable magnitude to 6.9 for PSHA studies;

2. the longest period used for spectral ordinates predictions is 2 s because the ITA10 dataset contain a significant number of analog records (about half of dataset);
3. the distance metric is only that introduced by Joyner and Boore [37](R_{JB}) that is the shortest distance from a site to the surface projection of the rupture;
4. the site response is evaluated only for the Eurocode 8 (EC8) site categories.

In the following, some explicative scenarios are reported for the PGA from ITA10 model, assuming a Normal-Fault mechanism on the left, and a Strike-Slip mechanism on the right, referenced on rock site (EC8-A).

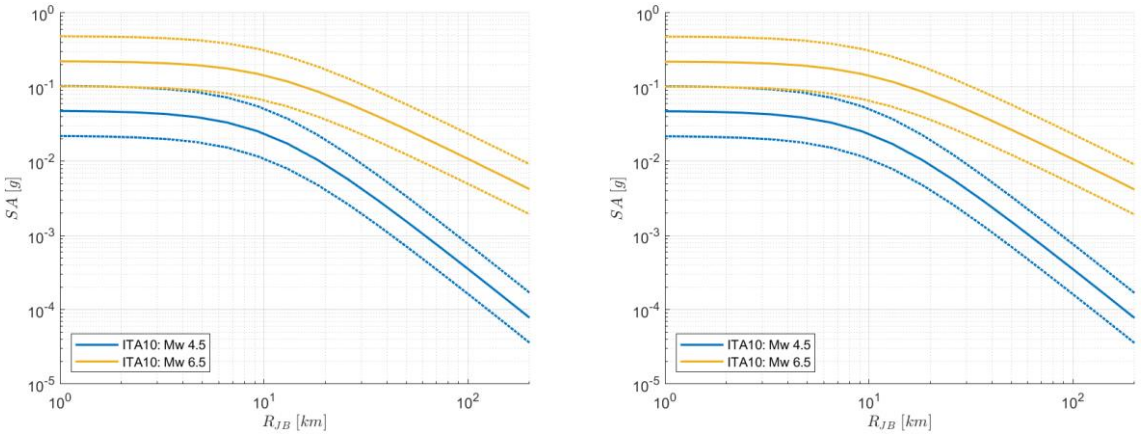

(a) Normal-Fault (b) Strike-Slip

Figure 2.1 Predictions of PGA from ITA10, for (a) NF and (b) SS mechanisms, rock site conditions (EC8-A), for different magnitude.

2.2. ITA10-V

This model has been derived for the vertical component of the previously mentioned ITA10 dataset [12] and has the same functional form, with different regression coefficients.

In the following, some explicative scenarios are reported for the PGA from ITA10-V model, assuming a Normal-Fault mechanism on the left, and a Strike-Slip mechanism on the right, referenced on rock site (EC8-A).

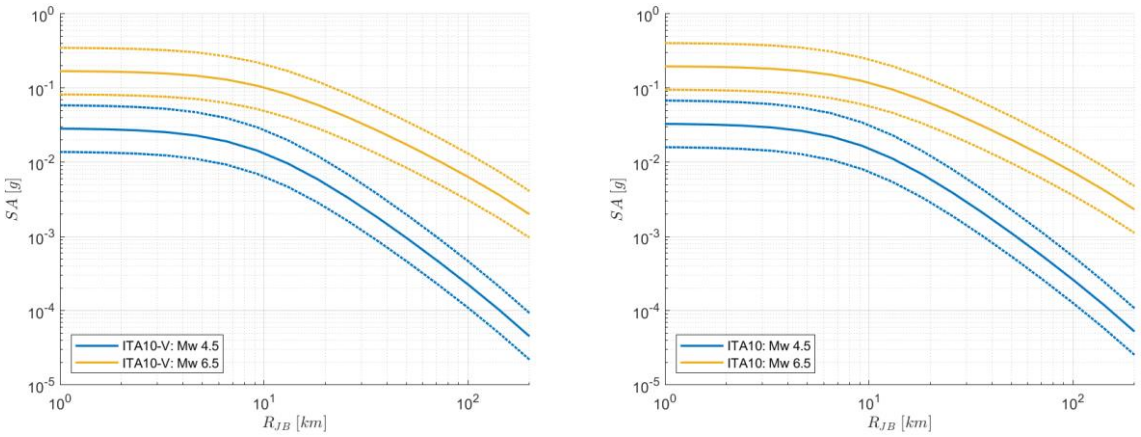

(a) Normal-Fault (b) Strike-Slip

Figure 2.2 Predictions of PGA from ITA10-V, for (a) NF and (b) SS mechanisms, rock site conditions (EC8-A), for different magnitude.

2.3. ITA18

A revised ground-motion prediction model for shallow crustal earthquakes (event depth < 30 km) is proposed by Lanzano et al. [6] to account for most recent seismic sequences (2012 Emilia, 2016-2017 Central Italy), and extend the dataset, implemented in Bindi et al. [12], to magnitudes larger than 6.9 to ensure robust magnitude scaling, with variation periods up to 10 [6].

The ground motion parameters are measured selecting the median of orientation independent amplitude (RotD50, obtained from the combination of the two horizontal components across all nonredundant azimuth [38]) instead of the geometric mean of the horizontal components of ground motion [12], and the rupture distance is considered in addition to the source-to-site metric Joyner-Boore distance (R_{JB}) [6].

More in detail, the ITA18 dataset is composed in the following manner:

- the records of 12 worldwide global events (3 Turkey, 2 Japan, 2 New Zealand, 2 California, 1 Iceland, 1 Iran and 1 Greece) in the magnitude range 6.1-8.0 have been added to increase the maximum usable magnitude with respect to ITA10;
- the selection of global earthquakes leads to extend the magnitude range of strike-slip (SS) and thrust (TF) mechanism that are less frequent in Italy;
- a small percentage of worldwide earthquake (8% of the total number of events), corresponding to the 14% of the dataset have been included to avoid oversampling of events that could be not representative of the regional attenuation or stress drop;

- a significant improvement of the records sampling in near-source conditions and in magnitude range 5.0-6.5 is the result of the calibration dataset about seven times larger with respect to ITA10;
- the near-source records in ITA18 consist of almost 300 records with distances lower than 10 km;
- the records used for ITA18 calibration are at least 2 times larger than ITA10 in each magnitude and distance bin.

Also, the strong-motion data selection is performed according to the following constraints:

- crustal conditions: earthquakes of active shallow (event depth < 30 km) crustal regions; different regimes are excluded (volcanic events or subduction events in the southern Tyrrhenian Sea);
- magnitude: moment magnitude range is from 3.5 to 8.0 in which the maximum magnitude for Italian events is 6.9 (1980 Irpinia earthquake);
- spatial distribution: not all the events with magnitudes less than 5.0 are included to avoid oversampling of small magnitudes; several aftershocks of major seismic sequence in Italy are disregarded to have, as much as possible, a homogeneous spatial distribution of events;
- event sampling: events having less than 10 records are excluded;
- distance: source-to-site distances lower than 200 km are included;
- components of ground motion: only records having three components (two horizontal and one vertical) are considered; the vertical component is also included for future studies on the same dataset;
- soil-structure interactions: only surface instruments with low or no interactions with nearby structure are included.

The quality and quantity of records are improved with the installation of new recording stations, the replacement of analog instruments, and the installation of temporary networks during the recent seismic sequences. As a result, the number of records per event is significantly larger, leading to more than 100 records, within 200 km for the most recent seismic sequences in Italy, and are uniformly and manually processed following the procedure of Paolucci et al. [39].

The model is calibrated for PGA and PGV and for 36 ordinates of acceleration response spectra (SA) at 5% damping in the 0.01 to 10 s period (T) range [6].

The simplicity of the functional form adopted by Bindi et al. [12] is maintained in the calibration of ITA18 GMM, with and improvement of the predictions in terms of median, epistemic uncertainty and aleatory variability [6].

$$\log_{10} Y = a + F_M(M_w, SoF) + F_D(M_w, R) + F_S(V_{S30}) + \varepsilon, \tag{2.4}$$

in which Y is the observed IM, a is the offset and ε is the error associated with the median prediction.

The source is modeled as two terms:

$$F_M(M_w) = \begin{cases} b_1(M_w - M_h) & where\ M_w \leq M_h \\ b_2(M_w - M_h) & where\ M_w > M_h \end{cases}, \tag{2.5}$$

$$F_M(SoF) = f_j SoF_j. \tag{2.6}$$

Different from Bindi et al. [12], a liner function has been adopted for $M_w \geq M_h$. The coefficients b_1 and b_2 control the magnitude scaling and the SoF coefficients fjs provide the correction for focal mechanism. The magnitude slope is set to be stepwise linear, and M_h is assumed as the period-dependent hinge magnitude. In equation (2.6) SoF_js are dummy variables, introduced to specify SS (j = 1), reverse TF (j = 2), and normal NF (j = 3) fault type, and f_j are the SoF coefficients (f_1 for S, f_2 for TF, and f_3 for NF). The regression is performed constraining to zero the coefficient of normal faulting (f_3 = 0) [6].

The path function has the form

$$F_D(M_w, R) = \left[c_1\left(M_w - M_{ref}\right) + c_2\right] \log_{10} R + c_3 R, \tag{2.7}$$

in which the first term is the magnitude dependent geometrical spreading and the second is the anelastic attenuation; M_{ref} is the reference magnitude, and $c_1 - c_3$ are the path coefficients. The coefficient for anelastic attenuation c_3 tends to assume positive values, even if very small, at intermediate and long periods, leading to an enhancement of the spectral amplitudes with respect to logarithmic decay. This is corrected by setting zero the value of c_3 in the regression, when c_3 is positive.

$R = \sqrt{R_i^2 + h_i^2}$, in which i can be either rup to indicate rupture distance, and JB indicates Joyner-Boore distance; h is the pseudo depth (km) and is estimated by regression.

Finally, the site term is function of V_{S30}:

$$F_S(V_{S30}) = k \log_{10}\left(\frac{V_0}{800}\right), \tag{2.8}$$

in which $V_0 = V_{S30}$ when $V_{S30} \geq 1500$ and $V_0 = 1500\ m/s$ otherwise. Different from ITA10, V_{S30} is selected as the variable representing the site amplification, because it is

more flexible than other proxies such as the EC8 site categories, being unrelated to a specific seismic code.

The values of hinge magnitude M_h, reference magnitude M_{ref} and the pseudo depth h are fixed and evaluated with a nonlinear regression as:

- M_h is assumed equal to 5.5 in the short periods and 6.3 in the long period range, similar to Boore et al. [40], regardless of the adopted distance metric;
- M_{ref} is dependent on distance metrics and spectral periods, in particular, at longer period, it assumes lower values, down to 4.0;
- h is dependent on the distance metric and assumes values in the range $3.3 - 7.2\ km$, which are generally lower with respect to Bindi [12].

The main difference with respect to ITA10 model is in median predictions at distance lower than 10 km and for strong events ($Mw > 6.5$); the total standard deviations are significantly lower at intermediate and long periods, with an average reduction of about 20% [6].

In the following, some explicative scenarios are reported for the PGA from ITA18 model, assuming a Normal-Fault mechanism on the left, and a Strike-Slip mechanism on the right, referenced on rock site (EC8-A).

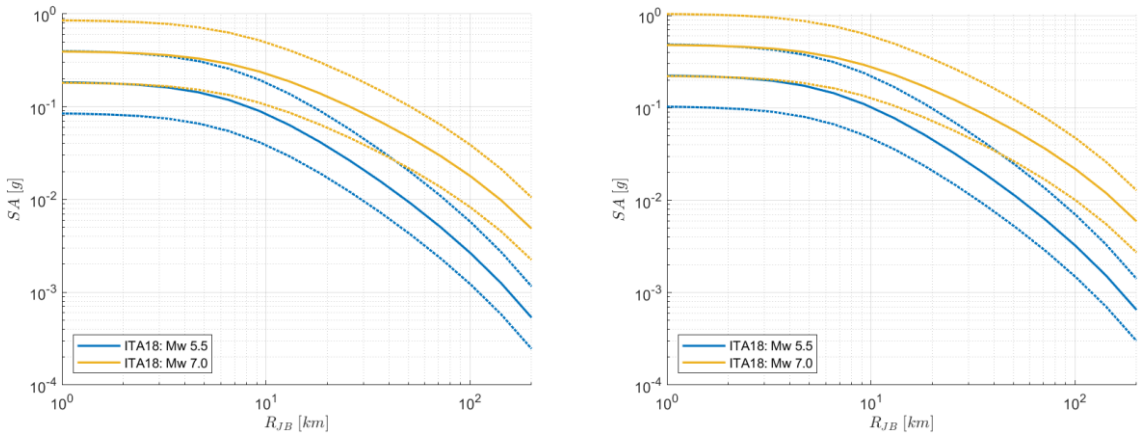

(a) Normal-Fault (b) Strike-Slip

Figure 2.3 Predictions of PGA from ITA18, for (a) NF and (b) SS mechanisms, rock site conditions (EC8-A), for different magnitude.

2.3.1. Homoscedastic ITA18

The distribution of ground motion is described in models both in terms of a median and a logarithmic standard deviation (σ), that may have a significant influence on the results of PSHA [32], particularly at long return periods. The truncation of the ground-motion distribution at a specified number of standard deviations above the median have proven unfeasible on statistical basis with current strong-motion datasets. The

most promising approach to reduce the overall impact of sigma on the results of PSHA is to find legitimate approaches to reduce the value of the standard deviation associated with ground-motion models (GMMs), as the partially nonergodic sigma procedure proposed by Al-Atik et al. [32].

Al-Atik et al. revisits the basics of ground-motion regression models and breaks down the residuals and the variability of the models into their respective components to provide a clear understanding of the uncertainty in seismic hazard studies [32]. The aleatory sigma can be reduced by the identification and the removal of the components of ground-motion variability at a single site that are repeatable rather than purely random, so that these may be quantified in the epistemic uncertainty by relaxing the ergodic assumption [6].

The total variability of the ground motion is usually decomposed into *between-events* variability ΔB (earthquake-to-earthquake) and *within-event* variability ΔW (record-to-record) which are zero-mean, independent, normally distributed random variables with standard deviations τ and ϕ, respectively [32].

The between-event residual (also called inter-event residual or event term), δBe is the average shift of the observed ground motion from an individual earthquake, e, from the population median predicted by the ground-motion model. It represents the average source effects (averaged over all azimuths) and reflects the influence of factors such as stress drop and variation of slip in space and time that are not captured by the inclusion of magnitude, style of faulting, and source depth [32].

Whereas the within-event residual (also called intra-event residual) δWes, is the misfit between an individual observation at station s from the earthquake-specific median prediction, also defined as the median prediction of the model plus the between-event term from earthquake e. It represents the azimuthal variations in source, path, and site effects reflecting the influence of those factors such as crustal heterogeneity, deeper geological structure, and near-surface layering that are not captured by a distance metric and a site-classification based on the averaged shear-wave velocity [32].

Here, the aleatory variability (σ) is assumed to be homoscedastic, independent of the variable of the predictive model and can be calculated as:

$$\sigma = \sqrt{\tau^2 + \phi_{S2S}^2 + \phi_0^2} \tag{2.9}$$

in which τ and ϕ_{S2S} represent between-event and site-to-site variability, and ϕ_0 is the standard deviation of the event- and site-corrected residuals [6].

2.3.2. Heteroscedastic ITA18

Also, the heteroscedastic model is built to account for the aleatory variability, as a function of moment magnitude and $V_{S,30}$.

Notice that some mistakes were found in the formulas reported by Lanzano et al. [6]; the magnitude-dependent model, selected for the event- and site-corrected variability (ϕ_0) has been corrected as:

$$\phi_0(M_w) = \begin{cases} \phi_{0,1} & where\ M_w \leq M_1 \\ \phi_{0,1} + (\phi_{0,2} - \phi_{0,1}) \dfrac{(M_w - M_1)}{(M_2 - M_1)} & where\ M_1 < M_w < M_2, \\ \phi_{0,2} & where\ M_w \geq M_2 \end{cases} \quad (2.10)$$

In which $\phi_{0,1}$ and $\phi_{0,2}$ represent the aleatory variability at small and large magnitudes, respectively, and M_1 and M_2 are the corner magnitudes, ranging from 4.5 to 5.5, and constant and equal to 6.0, respectively. At periods longer than 2 s, the dependance of ϕ_0 on magnitude is less clear, and the differences with respect to the homoscedastic models can be considered negligible.

Also, a model for ϕ_{S2S} is corrected as a function of $V_{S,30}$ as:

$$\phi_{S2S}(V_{S30}) = \begin{cases} \phi_{S2S,1} & V_{S30} \leq V_1 \\ \phi_{S2S,2} + (\phi_{S2S,1} - \phi_{S2S,2}) \left(\dfrac{\log_{10}(V_2/V_{S30})}{\log_{10}(V_2/V_1)} \right) & V_1 < V_{S30} < V_2, \\ \phi_{S2S,2} & V_{S30} \geq V_2 \end{cases} \quad (2.11)$$

In which the corner velocities are $V_1 = 250\, m/s$ and $V_2 = 400\, m/s$ at all IMs. The heteroscedastic model is not built for the component τ [6].

2.4. ITA18 VH

The vertical design spectra can be obtained by performing a hazard integration with a ground motion model specifically developed for the vertical response spectral ordinates (separately from those for the horizontal components) or by using a GMM for the VH response spectral acceleration ratios scaled by the horizontal component. The main limitation of the first approach is that disaggregation of hazard may lead to different earthquake scenarios controlling the horizontal and vertical spectral acceleration. For conservative reasons, the implementation of a vertical spectrum through empirical models for VH ratios is the most used approach; this although simplified, is effective for seismic design purposes and is validated with the direct approach in the framework of the present thesis reported in the following [13].

A vertical-to-horizontal (VH) ground motion model is proposed in Ramadan et al. [13], whose regression is based on the calibration performed on the ITA18 strong motion dataset, deeply described above. The proposed model uses a simple functional form

restricted to a limited number of predictor variables, namely, magnitude, source-to-site distance, focal mechanism, and site effects, and the variability associated with both VH, and V model is provided. The model is developed for VH ratios of SA, PGA and PGV for Italian shallow crustal earthquakes.

More in detail, the VH ratio is computed at each period, by dividing the vertical SA(T) by horizontal RotD50 component, defined as the median of the distribution of the SA, obtained from the combination of the two horizontal components across all nonredundant azimuths [13].

The function form adopted for the VH ITA18 median model is defined as follows:

$$\log_{10} Y = a + F_M(M_w, SoF) + F_D(M_w, R) + F_S(V_{S30}), \tag{2.12}$$

Where Y is the VH ratios for PGA, PGV and 36 ordinates of the 5% damping acceleration response spectra (SA) in the periods range $0.010 - 10s$. The functional form is consistent with the one adopted for the horizontal model of Lanzano et al. [6], apart from a minor modification regarding the source terms owing to the more limited dependence of VH on Mw (herein the magnitude scaling is controlled by a simple linear function, whereas Lanzano et al. [6] developed a stepwise linear function) [13]. The almost negligible dependence on Mw indicates that the source scaling of the horizontal component is very similar to that of the vertical component. For the final regression, the linear magnitude scaling terms is maintained because some sensitivity tests indicated a lower dispersion. Specifically, the source term consists of two terms:

$$F_M(SoF) = bM_w + f_j SoF_j. \tag{2.13}$$

Where coefficient b controls the source scaling and the coefficients f_j provide the correction for the Style of Faulting (SoF) of the event. The regression is performed constraining to zero the coefficient for normal faulting ($f_3 = 0$). The path term is defined as:

$$F_D(M_w, R) = \left[c_1\left(M - M_{ref}\right) + c_2\right] \log_{10} R, \tag{2.14}$$

where the first term is the magnitude-dependent geometrical spreading and the second is the distance attenuation, M_{ref} is the reference magnitude assumed to be constant to a value of 6.0, while c_1 and c_2 are the path coefficients. The distance is computed as $R = \sqrt{R_{JB}^2 + h^2}$, in which R_{JB} is substituted by R_{Rup} when using the model coefficients related to it, and h is the pseudo-depth, assumed to be constant for all periods with a value of 5 km. The value of $M_{Ref} = 6$ and $h = 5\ km$ were calibrated from a first stage non-liner regression.

Finally, the site term is defined as a function of the time-averaged shear wave velocity in the top 30 meters (V_{S30}):

$$F_S(V_{S30}) = k \log_{10}\left(\frac{V_0}{800}\right), \tag{2.15}$$

in which $V_0 = V_{S30}$ when $V_{S30} \geq 1500$ and $V_0 = 1500\, m/s$ otherwise. The function is linearly dependent on V_{S30}, consistently with ITA18 horizontal model. In particular, the non-linear site response term in horizontal GMM was neglected because there are insufficient records to robustly constrain these effects [13].

A linear ordinary least-squares mixed-effects regression method is used as suggested by Bates et al. [41] and is composed of fixed effects and random effects. The fixed effects are applied to evaluate the source b path c_1 and c_2 and is the term k coefficients and the random effects are applied to stations and events to perform the residual analysis and estimate the partially non-ergodic sigma [32] [13].

The total standard deviation σ_{VH} of the VH GMM is homoscedastic and is given by:

$$\sigma_{VH} = \sqrt{\tau_{VH}^2 + \psi_{VH}^2 + \phi_{VH}^2}. \tag{2.16}$$

Where τ_{VH}, ψ_{VH} and ϕ_{VH} are the standard deviation of the terms δB_e (between-event term), $\delta S2S_s$ (site-to-site term) and δW_{es} (site- and event- corrected term) respectively.

Furthermore, as the model is consistent with the ITA18 one, the vertical ground motion can be assessed by adding the logarithmic prediction of VH ITA18 ratio to the logarithmic prediction of horizontal SA from Lanzano et al. [6] as follows:

$$\log_{10} Y_V = \log_{10} Y_H + \log_{10} Y_{V,H}. \tag{2.17}$$

The standard deviations of the predicted vertical ground motion are computed from the error propagation of the various components of the standard deviation, considering the correlation between VH and H random variables under the assumption that they are log-normally distributed, as:

Between-event variability

$$\tau_V = \sqrt{\tau_H^2 + \tau_{VH}^2 + 2\varrho_{H,VH}^{\tau}\tau_H\tau_{VH}}. \tag{2.18}$$

Site-to-site variability

$$\psi_V = \sqrt{\psi_H^2 + \psi_{VH}^2 + 2\varrho_{H,VH}^{\psi}\psi_H\psi_{VH}}. \tag{2.19}$$

Event- and site-corrected variability (remaining variability)

$$\phi_V = \sqrt{\phi_H^2 + \phi_{VH}^2 + 2\varrho_{H,VH}^{\phi}\phi_H\phi_{VH}}. \tag{2.20}$$

Such that

$$\sigma_V = \sqrt{\tau_V^2 + \psi_V^2 + \phi_V^2}. \tag{2.21}$$

where H, V and VH belong to horizontal, vertical and vertical-to-horizontal components respectively; τ, ψ and ϕ are the various components of standard deviation; $\varrho_{H,VH}^{\tau}$, $\varrho_{H,VH}^{\psi}$ and $\varrho_{H,VH}^{\phi}$ are the correlation coefficients between H and VH components of δB_e, $\delta S2S_s$ and δW_{es}, respectively (provided in Supplement S1 of Ramadan et al. [13]).

In the following, some explicative scenarios are reported for the PGA from ITA18-V(VH) model, assuming a Normal-Fault mechanism on the left, and a Strike-Slip mechanism on the right, referenced on rock site (EC8-A).

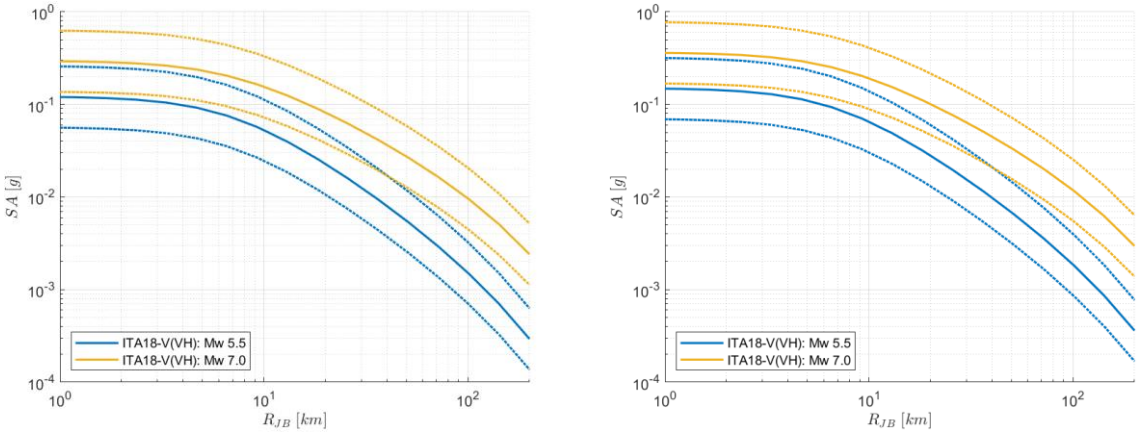

(a) Normal-Fault (b) Strike-Slip

Figure 2.4 Predictions of PGA from ITA18-V(VH), for (a) NF and (b) SS mechanisms, rock site conditions (EC8-A), for different magnitude.

2.5. ITA18-V

This model is not yet in the public domain, and it has been calibrated *ad-hoc* directly on the vertical records of the previously mentioned ITA18 dataset for the proposal of the present work by Ramadan F. of INGV (personal communication). This model constitutes an important validation of the vertical design spectra obtained by performing a hazard integration with the proposed ground motion model for the VH response spectral acceleration ratios scaled by the horizontal UHS. As a results, a comparison of the two approaches will be proposed for the implementation of the cases study.

The functional form is the same as the one proposed for the horizontal component, with the difference that the coefficients are now calibrated on the vertical direction and are reported in the table below.

Table 2.1 Coefficients of the predictive model for events (ITA18) in the vertical direction.

IMs	a	b_1	b_2	c_1	c_2
PGA	3.2473	0.2320	0.0629	0.2486	-1.4621
SA-T=0.01 s	3.2556	0.2313	0.0628	0.2487	-1.4636
SA-T=0.025 s	3.3689	0.1996	0.0542	0.2562	-1.4948
SA-T=0.04 s	3.6792	0.1442	0.0493	0.2666	-1.5582
SA-T=0.05 s	3.7622	0.1482	0.0590	0.2577	-1.5547
SA-T=0.07 s	3.7657	0.1867	0.0703	0.2373	-1.5224
SA-T=0.1 s	3.6607	0.2588	0.1123	0.2057	-1.4607
SA-T=0.15 s	3.4111	0.3412	0.1418	0.1768	-1.3528
SA-T=0.20 s	3.2201	0.3979	0.1641	0.1665	-1.3286
SA-T=0.25 s	3.1270	0.4337	0.1725	0.1652	-1.3290
SA-T=0.30 s	3.0451	0.4804	0.2007	0.1529	-1.3319
SA-T=0.35 s	2.9424	0.5138	0.2210	0.1453	-1.3459
SA-T=0.40 s	2.8782	0.5303	0.2223	0.1460	-1.3212
SA-T=0.45 s	2.8460	0.5525	0.2221	0.1442	-1.3159
SA-T=0.50 s	2.8527	0.5694	0.2203	0.1423	-1.3278
SA-T=0.60 s	2.7856	0.6056	0.2334	0.1406	-1.3353
SA-T=0.70 s	2.7677	0.6285	0.2354	0.1414	-1.3509
SA-T=0.75 s	2.7112	0.6324	0.2348	0.1469	-1.3500
SA-T=0.80 s	2.6852	0.6448	0.2450	0.1466	-1.3557
SA-T=0.90 s	2.6326	0.6767	0.2685	0.1436	-1.3710
SA-T=1.0 s	2.5593	0.7120	0.2976	0.1370	-1.3719
SA-T=1.2 s	2.4513	0.7446	0.3288	0.1378	-1.3888
SA-T=1.4 s	2.4047	0.7708	0.3425	0.1380	-1.3938
SA-T=1.6 s	2.3492	0.7996	0.3410	0.1428	-1.3752
SA-T=1.8 s	2.3073	0.8215	0.3296	0.1469	-1.3479
SA-T=2.0 s	2.2817	0.8291	0.3475	0.1492	-1.3613
SA-T=2.5 s	2.1890	0.8565	0.3793	0.1550	-1.3899
SA-T=3.0 s	1.9055	0.8897	0.4183	0.1593	-1.3392
SA-T=3.5 s	1.7471	0.9175	0.4585	0.1622	-1.3637
SA-T=4.0 s	1.5653	0.8968	0.4446	0.1813	-1.3578
SA-T=4.5 s	1.4035	0.8813	0.4405	0.1943	-1.3191
SA-T=5.0 s	1.2149	0.8502	0.4471	0.2119	-1.2842
SA-T=6.0 s	1.3876	0.8108	0.3116	0.2194	-1.3618

SA-T=7.0 s	1.2173	0.7802	0.3739	0.2240	-1.3649
SA-T=8.0 s	1.0810	0.7294	0.3793	0.2434	-1.3642
SA-T=9.0 s	0.9722	0.6758	0.3989	0.2613	-1.3677
SA-T=10 s	0.8701	0.6248	0.3916	0.2795	-1.3721
PGV	1.6593	0.3802	0.1713	0.2784	-1.4133

Table 2.2 Coefficients of the predictive model for events (ITA18) in the vertical direction.

IMs	c_3	**k**	f_1	f_2	τ
PGA	-0.0025	-0.2710	0.0840	0.0064	0.1687
SA-T=0.01 s	-0.0025	-0.2708	0.0838	0.0059	0.1690
SA-T=0.025 s	-0.0023	-0.2679	0.0881	0.0111	0.1729
SA-T=0.04 s	-0.0021	-0.2649	0.1030	0.0225	0.1854
SA-T=0.05 s	-0.0024	-0.2787	0.1167	0.0274	0.1889
SA-T=0.07 s	-0.0032	-0.2815	0.1320	0.0333	0.1884
SA-T=0.10 s	-0.0040	-0.2624	0.1201	0.0186	0.1844
SA-T=0.15 s	-0.0044	-0.2660	0.0997	-0.0032	0.1680
SA-T=0.20 s	-0.0042	-0.2559	0.0785	-0.0073	0.1598
SA-T=0.25 s	-0.0037	-0.2434	0.0654	-0.0172	0.1570
SA-T=0.30 s	-0.0033	-0.2504	0.0673	-0.0151	0.1523
SA-T=0.35 s	-0.0032	-0.2520	0.0611	-0.0238	0.1453
SA-T=0.40 s	-0.0030	-0.2517	0.0446	-0.0276	0.1424
SA-T=0.45 s	-0.0026	-0.2686	0.0372	-0.0270	0.1396
SA-T=0.50 s	-0.0022	-0.2768	0.0317	-0.0323	0.1374
SA-T=0.60 s	-0.0019	-0.2793	0.0130	-0.0597	0.1490
SA-T=0.70 s	-0.0014	-0.3086	0.0044	-0.0628	0.1514
SA-T=0.75 s	-0.0013	-0.3117	0.0025	-0.0623	0.1514
SA-T=0.80 s	-0.0012	-0.3099	-0.0055	-0.0623	0.1509
SA-T=0.90 s	-0.0010	-0.3089	-0.0078	-0.0632	0.1552
SA-T=1.0 s	-0.0008	-0.3315	-0.0135	-0.0697	0.1573
SA-T=1.2 s	-0.0006	-0.3648	-0.0270	-0.0708	0.1535
SA-T=1.4 s	-0.0003	-0.3639	-0.0417	-0.0694	0.1582
SA-T=1.6 s	-0.0001	-0.3557	-0.0414	-0.0735	0.1580
SA-T=1.8 s	0.0000	-0.3672	-0.0470	-0.0708	0.1581
SA-T=2.0 s	0.0002	-0.3724	-0.0597	-0.0778	0.1641
SA-T=2.5 s	0.0000	-0.3495	-0.0948	-0.0776	0.1712
SA-T=3.0 s	-0.0008	-0.3056	-0.1301	-0.0839	0.1884
SA-T=3.5 s	-0.0010	-0.2927	-0.1527	-0.0796	0.1878

SA-T=4.0 s	-0.0011	-0.2794	-0.1517	-0.0722	0.1875
SA-T=4.5 s	-0.0013	-0.2590	-0.1536	-0.0660	0.1871
SA-T=5.0 s	-0.0013	-0.2230	-0.1480	-0.0447	0.1829
SA-T=6.0 s	-0.0012	-0.1652	-0.1347	-0.0253	0.1679
SA-T=7.0 s	-0.0009	-0.1407	-0.0959	-0.0067	0.1633
SA-T=8.0 s	-0.0008	-0.1274	-0.0749	0.0030	0.1631
SA-T=9.0 s	-0.0007	-0.1139	-0.0663	-0.0030	0.1619
SA-T=10 s	-0.0007	-0.1153	-0.0581	-0.0037	0.1565
PGV	-0.0010	-0.2665	0.0086	-0.0408	0.1437

Table 2.3 Coefficients of the predictive model for events (ITA18) in the vertical direction.

IMs	ϕ_{S2S}	ϕ_0	M_h	M_{ref}	**h**
PGA	0.2014	0.1969	5.5000	5.3624	5.7642
SA-T=0.01 s	0.2018	0.1969	5.5000	5.3713	5.7526
SA-T=0.025 s	0.2078	0.1987	5.5000	5.5123	5.5344
SA-T=0.04 s	0.2220	0.2057	5.5000	5.8722	5.8036
SA-T=0.05 s	0.2295	0.2066	5.5000	5.9372	6.0391
SA-T=0.07 s	0.2378	0.2055	5.5000	5.7413	6.3284
SA-T=0.1 s	0.2410	0.2070	5.5000	5.3627	6.5854
SA-T=0.15 s	0.2297	0.2084	5.5000	4.8307	6.4418
SA-T=0.2 s	0.2158	0.2076	5.5000	4.3030	5.7495
SA-T=0.25 s	0.1992	0.2070	5.5000	4.1355	5.6541
SA-T=0.3 s	0.1932	0.2094	5.5250	3.9162	5.5935
SA-T=0.35 s	0.1901	0.2089	5.5500	3.4340	5.5359
SA-T=0.4 s	0.1908	0.2096	5.6000	3.4391	5.4960
SA-T=0.45 s	0.1888	0.2089	5.6500	3.4521	5.5044
SA-T=0.5 s	0.1874	0.2054	5.7000	3.4923	5.5046
SA-T=0.6 s	0.1904	0.2022	5.7500	3.3290	5.3198
SA-T=0.7 s	0.1899	0.2014	5.8000	3.3835	5.5947
SA-T=0.75 s	0.1886	0.2019	5.8000	3.3880	5.4556
SA-T=0.8 s	0.1900	0.2024	5.8000	3.3823	5.4787
SA-T=0.9 s	0.1950	0.2035	5.8000	3.2331	5.6511
SA-T=1 s	0.1961	0.2030	5.8000	3.0078	5.6522
SA-T=1.2 s	0.1960	0.2034	5.8000	2.9128	5.5685
SA-T=1.4 s	0.1953	0.2043	5.8000	3.0781	6.0306
SA-T=1.6 s	0.1943	0.1998	5.8000	3.3237	6.3996
SA-T=1.8 s	0.1893	0.2022	5.8000	3.6674	6.6556

SA-T=2 s	0.1854	0.2036	5.8000	3.7674	7.0692
SA-T=2.5 s	0.1784	0.2112	5.8000	3.7031	8.0252
SA-T=3 s	0.1710	0.2106	5.8000	3.1687	6.7836
SA-T=3.5 s	0.1647	0.2106	5.8000	2.7709	6.5001
SA-T=4 s	0.1599	0.2106	5.8000	2.8476	5.5451
SA-T=4.5 s	0.1600	0.2075	5.8000	2.9532	4.5699
SA-T=5 s	0.1534	0.2076	5.8000	3.1814	3.6750
SA-T=6 s	0.1487	0.2031	6.3000	2.8290	3.1530
SA-T=7 s	0.1476	0.1982	6.3000	2.9741	2.5910
SA-T=8 s	0.1449	0.1928	6.3000	3.3169	2.5678
SA-T=9 s	0.1408	0.1897	6.3000	3.6039	2.7886
SA-T=10 s	0.1385	0.1869	6.3000	3.8179	2.9419
PGV	0.1460	0.1942	5.7000	4.6341	5.5213

In the following, some explicative scenarios are reported for the PGA from ITA18-V model, assuming a Normal-Fault mechanism on the left, and a Strike-Slip mechanism on the right, referenced on rock site (EC8-A).

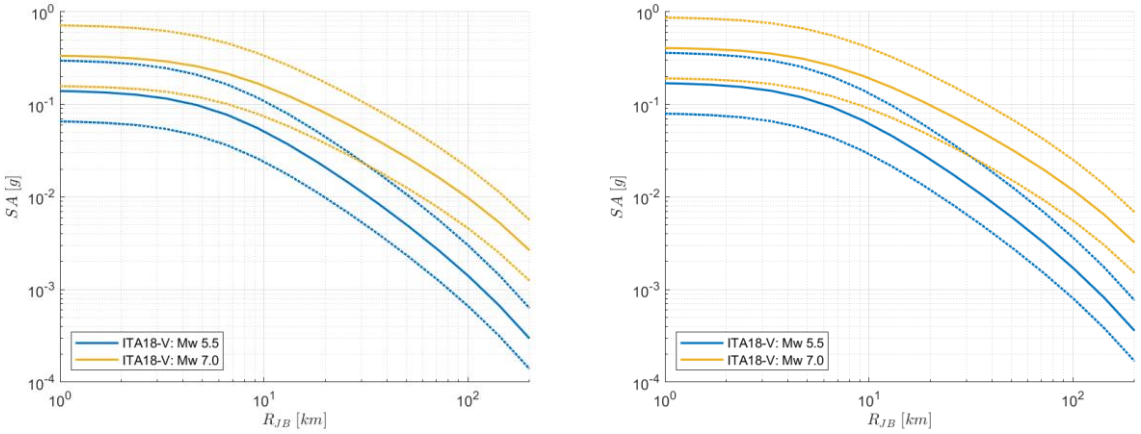

(a) Normal-Fault (b) Strike-Slip

Figure 2.5 Predictions of PGA from ITA18-V, for (a) NF and (b) SS mechanisms, rock site conditions (EC8-A), for different magnitude.

2.6. LL19

The earthquakes caused by volcanoes are of primary importance in the evaluation of seismic hazard in Italy because of the serious endanger of densely populated areas.

A typical feature of ground motion from volcanic events is the fast amplitude decay from shallow earthquake sources. Volcanic earthquakes occur as magma and volcanic gases rise to the surface from depth, which involves significant stress changes in the

crust as the material migrates upwards. Volcanic activities induce two main types of recognized earthquakes, the long-period earthquakes, and the volcanic-tectonic earthquakes. The first are caused by cracks resonating as magma and gases moving toward the surface; the second represent a brittle failure of rock, describing the same process that occurs along purely tectonic faults and have characteristics almost the same to events occurred in shallow active crustal regions [14].

Very few models for the prediction of ground motion induced by volcanic events are available since of scarce observations and less frequent volcanic earthquakes than crustal events. For instance, the regional predictive equations derived by De Natale [42] has been used in the latest release of the hazard model of Italy (MPS04, [3]) for volcanic area from weak-motion data recorded at the Campi Flegrei (Napels) and applied to all the active volcanic districts in Italy [43]. Whereas, the ground motion model developed by Faccioli [44] has been used for the 2013 European Seismic Hazard Model [45] although not specifically derived for volcanic areas [14].

Other areas of the world characterized by volcanic events have a similar situation to Italy, related to the very few models available which are calibrated from empirical data. The empirical relation of Munson and Thurber [46] is provided for instance for the peak ground acceleration for the volcanic earthquakes in Hawaiian Islands; whereas McVerry [47] propose coefficients for the correction of the GMMs to account for volcanic areas in New Zealand. Similarly, to McVerry [47], Atkinson [48] proposes coefficients for the correction of the model by Boor end Atkinson [49] for shallow crustal earthquake in active tectonic regions.

More recently, Tusa and Langer [50] developed empirical ground motion equations with a functional form accounting for source, attenuation and site effect derived for the Mount Etna region by separating the functional forms for shallow (depth < 5km) and deep (depth > 5 km) earthquakes.

As a result of the recent earthquakes in the Mount Etna (mainshock 26/12/2018 Mw 4.9) area and in the island of Ischia (mainshock 21/08/2017 Mw 3.9) it has been possible to increase the number of recordings for volcanic areas in Italy and, to increase the number of observations close to the epicenter.

Hence, a new empirical model has been calibrated in the volcanic context by [14] and adopted herein with improvements on the limited data of the previous models and on appropriate prediction of the ground motion observed in the near source. In fact, the new data allowed to robustly extend the magnitude range of pre-existing models to 4.9 and following Tusa and Langer [50] to include different attenuation with distance for shallow and deep events. The prediction of the amplitudes of several intensity measures relevant for engineering applications is proposed by Lanzano-Luzi [14] for volcanic areas in Italy (LL19). The peculiarity of the calibration is related to the distinction in the attenuation with distance between shallow and deep events, with discerning focal depth fixed at 5 km. The equations are valid for the geometric mean

of horizontal components of PGA, PGV and acceleration response spectra ordinates at 5% damping (in period range $T = 0.025 - 5\ s$), with a magnitude range $3.5 - 4.9$ and hypocentral distance range $1 - 200\ km$ [14].

The ground-motion functional form of LL19 is characterized by a linear dependance on magnitude; geometrical attenuation dependent on distance and the effect of anelastic attenuation is accounted for only in case of deep events.

$$\log_{10} Y = a + bM + F_D + F_S + \delta B_e + \delta S2S_S + \delta W_{0,es}, \tag{2.22}$$

Where a is the offset and M is the moment magnitude. The term distance F_D is:

$$F_D = \begin{cases} c_1 \log_{10} \sqrt{R_{hyp}^2 + h_1^2} & h \leq 5\ km \\ c_2 \log_{10} \sqrt{R_{hyp}^2 + h_2^2} + c_3 \sqrt{R_{hyp}^2 + h_2^2} & h > 5\ km \end{cases}, \tag{2.23}$$

Where R_{hyp} is the hypocentral distance and the pseudo-depth is equal to $h_1 = 2\ km$ for shallow earthquakes and $h_2 = 5\ km$ for deep events. The site term is $F_s = s_i$ with $i = 1, 2, 3$. In particular, $i = 1$ corresponds to rock sites belonging to the subsoil category EC8-A ($s_i = 0$), $i = 2$ for sites of class EC8-B and $i = 3$ for sites of class EC8-C and -D. The least squares calibration is performed with a linear mixed-effect model in which the coefficients a, b, c_1, c_2, c_3, s_1, s_2 and s_3 represent the fixed part.

In the following, some explicative scenarios are reported for the PGA from LL19 model for shallow depth, referenced on rock site (EC8-A).

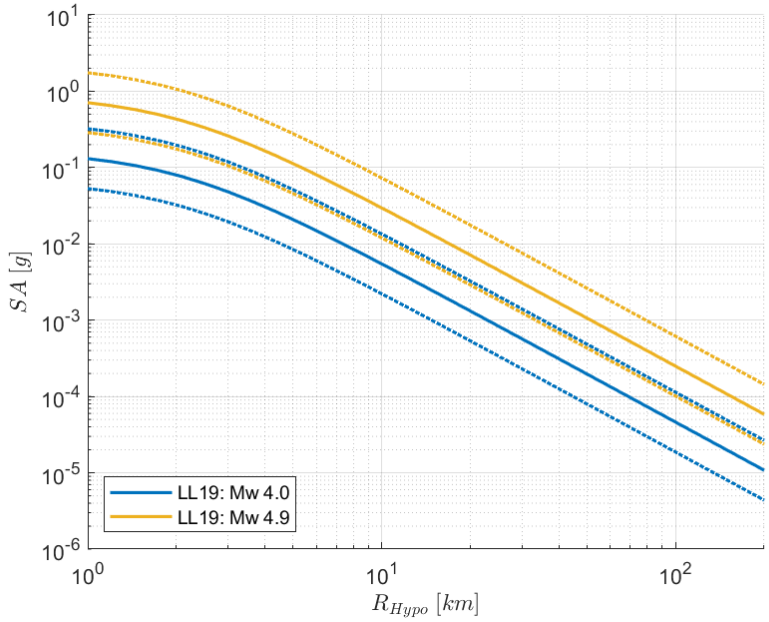

Figure 2.6 Predictions of PGA from LL19, depth = 2 km, rock site conditions (EC8-A), for different magnitude.

2.7. LL19-V

This model is not yet in the public domain, and it has been calibrated *ad-hoc* directly on the vertical records of the previously mentioned LL19 dataset for the proposal of the present work by Ramadan F of INGV (personal communication). The functional form is the same as the one proposed for the horizontal component, with the difference that the coefficients are now calibrated on the vertical direction and are reported in the table below.

Table 2.4 Coefficients of the predictive model for volcanic events (LL19) in the vertical direction.

IMs	a	b	c_1	c_2	c_3
PGA	-0.4922	0.7918	-2.1233	-1.5629	-0.0068
SA-T=0.025 s	-0.4127	0.7807	-2.1309	-1.5645	-0.0069
SA-T=0.04 s	-0.1683	0.7437	-2.1588	-1.57	-0.0073
SA-T=0.05 s	0.1917	0.6961	-2.2144	-1.6283	-0.0073
SA-T=0.07 s	0.4101	0.6965	-2.3124	-1.6277	-0.008
SA-T=0.1 s	0.4598	0.6966	-2.3096	-1.6208	-0.0078
SA-T=0.15 s	0.1611	0.7707	-2.2818	-1.6762	-0.0063
SA-T=0.2 s	-0.3727	0.8541	-2.1739	-1.5712	-0.0063
SA-T=0.25 s	-0.7695	0.9203	-2.1132	-1.5399	-0.0057
SA-T=0.3 s	-1.1758	0.9924	-2.0542	-1.5231	-0.0053
SA-T=0.35 s	-1.3767	0.9979	-1.9639	-1.5023	-0.0044
SA-T=0.4 s	-1.7384	1.0448	-1.8819	-1.4582	-0.0041
SA-T=0.45 s	-1.9023	1.0721	-1.8577	-1.4497	-0.0042
SA-T=0.5 s	-2.0336	1.0923	-1.8434	-1.4806	-0.0036
SA-T=0.6 s	-2.2874	1.1178	-1.791	-1.5003	-0.0033
SA-T=0.7 s	-2.5501	1.1468	-1.7271	-1.4733	-0.0032
SA-T=0.75 s	-2.5944	1.1485	-1.7121	-1.4871	-0.0029
SA-T=0.8 s	-2.6871	1.1654	-1.7176	-1.5181	-0.0026
SA-T=0.9 s	-2.9402	1.1927	-1.6804	-1.5019	-0.0023
SA-T=1 s	-3.0481	1.1866	-1.6352	-1.4774	-0.0022
SA-T=1.2 s	-3.4003	1.2369	-1.6048	-1.483	-0.0018
SA-T=1.4 s	-3.6915	1.2795	-1.5813	-1.4934	-0.0015
SA-T=1.6 s	-3.8121	1.2855	-1.5664	-1.5091	-0.0014
SA-T=1.8 s	-3.7201	1.2528	-1.5813	-1.5616	-0.0009
SA-T=2 s	-3.7283	1.2381	-1.5719	-1.5751	-0.0009
SA-T=2.5 s	-3.9383	1.2148	-1.4994	-1.5115	-0.0009

SA-T=3 s	-4.2	1.2222	-1.415	-1.4787	-0.001
SA-T=3.5 s	-4.0575	1.1491	-1.3629	-1.4609	-0.0012
SA-T=4 s	-4.1633	1.1377	-1.3178	-1.4335	-0.0015
SA-T=4.5 s	-4.0792	1.0961	-1.2982	-1.4558	-0.001
SA-T=5 s	-4.1212	1.0718	-1.2876	-1.4269	-0.0014
PGV	-2.9088	0.9724	-1.7466	-1.464	-0.0048

Table 2.5 Coefficients of the predictive model for volcanic events (LL19) in the vertical direction.

IMs	s_2	s_3	τ	ϕ_{S2S}	σ_0
PGA	0.0835	0.3315	0.1921	0.2351	0.2228
SA-T=0.025 s	0.0811	0.3254	0.1952	0.2401	0.2232
SA-T=0.04 s	0.0882	0.3296	0.2012	0.2571	0.2283
SA-T=0.05 s	0.082	0.3095	0.2179	0.2749	0.2342
SA-T=0.07 s	0.0614	0.3118	0.2177	0.3008	0.2372
SA-T=0.1 s	0.0402	0.3043	0.2248	0.289	0.2259
SA-T=0.15 s	0.0814	0.3165	0.2262	0.2825	0.2148
SA-T=0.2 s	0.067	0.3094	0.203	0.2632	0.2123
SA-T=0.25 s	0.0656	0.3399	0.1876	0.2493	0.2055
SA-T=0.3 s	0.0538	0.3165	0.1766	0.2325	0.2005
SA-T=0.35 s	0.08	0.3257	0.1654	0.2292	0.204
SA-T=0.4 s	0.0875	0.3258	0.1724	0.2302	0.2017
SA-T=0.45 s	0.085	0.3372	0.1693	0.2234	0.2003
SA-T=0.5 s	0.0996	0.3567	0.1748	0.222	0.1922
SA-T=0.6 s	0.1377	0.3313	0.151	0.2144	0.1902
SA-T=0.7 s	0.1189	0.335	0.147	0.2041	0.1934
SA-T=0.75 s	0.108	0.3155	0.1379	0.1978	0.1983
SA-T=0.8 s	0.1183	0.3315	0.1301	0.2016	0.1989
SA-T=0.9 s	0.1393	0.3934	0.1634	0.1997	0.1915
SA-T=1 s	0.1347	0.3987	0.1506	0.1884	0.1944
SA-T=1.2 s	0.1209	0.3608	0.1838	0.1931	0.1919
SA-T=1.4 s	0.1173	0.3102	0.2171	0.2008	0.1838
SA-T=1.6 s	0.1083	0.2848	0.2245	0.2017	0.1852
SA-T=1.8 s	0.1102	0.2776	0.218	0.2046	0.1836
SA-T=2 s	0.1035	0.2624	0.2199	0.2023	0.1848
SA-T=2.5 s	0.1194	0.2843	0.25	0.2074	0.1777
SA-T=3 s	0.1174	0.2974	0.2521	0.2045	0.1837

SA-T=3.5 s	0.0928	0.2645	0.2668	0.1874	0.1855
SA-T=4 s	0.0938	0.2544	0.2885	0.1802	0.186
SA-T=4.5 s	0.0881	0.2565	0.2708	0.1734	0.1889
SA-T=5 s	0.1062	0.2482	0.2699	0.177	0.1886
PGV	0.104	0.3601	0.1505	0.1783	0.2082

In the following, some explicative scenarios are reported for the LL19-V model for shallow depth, reference rock site (EC8-A).

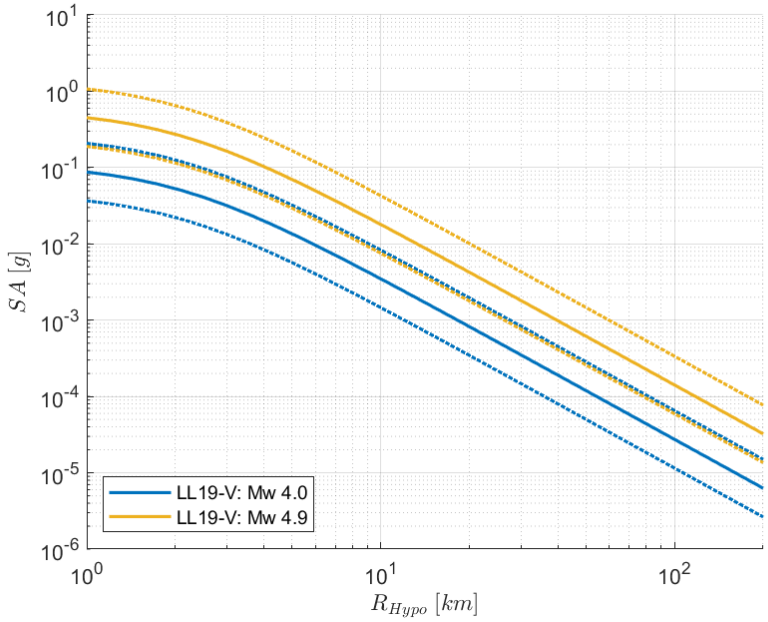

Figure 2.7 PGA from LL19-V, depth = 2 km, rock site conditions (EC8-A), for different magnitude.

2.8. ITA18 corrected with NESS2

The near-source effects are generally underestimated in current seismic design procedures, in fact, it has been demonstrated that elastic design spectral ordinates can be often exceeded in epicentral area, for moderate-to-high earthquakes. Indeed, the knowledge and the proper modelling of peculiar features of strong-motion records near the fault rupture are fundamental to quantify the seismic input in structural engineering, considering a distance within about 20-30 km from the fault rupture or even greater [7].

On one hand, NESS1 [51] is a worldwide strong-motion dataset including only high-quality recordings obtained in near-source conditions (velocity pulse, large vertical ground-motions, directional and hanging-wall (HW) amplification and fling-step) and consists of about 800 three-component waveforms relative to 700 accelerometric stations, caused by 74 crustal earthquakes with Mw ≥ 5.5 and R_{JB} up to 140 km [7]. On the other hand, the NESS2 is a new expanded and updated version which includes

both an increased number of earthquake records and new source metadata, particularly it accounts for seven events and 421 records which mainly contribute to magnitudes larger than 7.0 (more than 65% with respect to NESS1) [7] recorded in epicentral area, source metadata and intensity measures, comprising spectral displacements and fling-step amplitudes retrieved from the extended baseline correction processing of velocity time series.

The NESS2 dataset is suitable to increase the knowledge on the near-source features of ground motion and to constrain the existing regional and global GMMs near the epicentre. In particular, the NESS2 dataset is used to calibrate an empirical correction factor of ITA18 and to correct its median prediction, mainly based on far-field records, to account for near-source effect which are not fully captured by the reference model. The approach adopted by Sgobba et al. [7] is to implement the method proposed by Atkinson [52] [48] known as "Reference Empirical Approach" by performing a regression analysis on the residuals of ITA18 GMM with respect to NESS2 data, hence a calibrated correction factor of the median prediction of the regional model is obtained [7].

NESS2 flat file is compiled according to the following criteria:

1. Data relative to events with moment magnitude Mw ≥ 5.5 distributed worldwide;
2. Hypocentral depth ≤ 40 km;
3. Fully referenced information about finite-fault source model;
4. Maximum source-to-site distance defined through seismological considerations introduced by Pacor [53] by assuming the parameter k (i.e., number of fault length) equal to unity and average stress drop 10 MPa.

The latter criterion is fundamental to define a "near source" regime (based on a physics-informed metric instead of an arbitrary one).

The resulting dataset NESS2 consists of 81 events with moment magnitude ≥ 5.5 and hypocentral depth shallower than 40 km, corresponding to 1189 three-component waveforms, which are selected to have a maximum source-to-site distance within one fault length. Most of the events are in the United States (20 events) and Italy (20 events). The remaining earthquakes are distributed among Japan (10), Turkey (7), Greece (6), Iran (5), New Zealand (5), Montenegro (2), Mexico (2), Taiwan (2), Nepal (19, Uzbekistan (19, and Chile (1).

The dataset of ITA18 is composed of less than 7% of records at distances shorter than 20 km. On this model, a residual analysis has been applied by selecting the data of NESS2 with magnitude up to 7.5 for consistency purposes with the range of validity of the Italian model. The residuals depend on some parameters, such as moment magnitude Mw, Joyner-Boore source-to-site distance R_{JB}, focal mechanism and shear-wave velocity V_{S30}, which represent the explanatory variables usually considered for the calibration of empirical GMMs.

The results obtained by Sgobba et al. [7] evidences the need to introduce a different slope of the correction in two magnitude ranges and to adopt a bilinear scaling in the functional form of the correction term with a hinge magnitude equal to 6.7 [7]. In fact, the magnitude scaling of ITA18 has a more pronounced saturation at magnitudes larger than 6.7 with respect to that observed on NESS2 data, both for short and long periods; conversely, at magnitudes smaller than 6.7, the model tends to underestimate the observed ground motion. For similar reasons, the distance scaling is characterized by large positive residuals, particularly in the 10-20 km range, followed by a decreasing trend at longer distances.

The site dependency of the residuals with respect to V_{S30} shows a slightly negative bias at short periods (lower observations than ITA18 predictions) for $V_{S30} < 200m/s$, where besides, few data are available; for larger V_{S30}, the average trend increases very weakly. Therefore, a distortion of the intrinsic features of ITA18 original model and its predictive power in ranges not sufficiently sampled by the NESS2 data can follows. Consequently, the dependency on the explanatory variables has been simplified as much as possible, considering in the regression only its dependance on magnitude and distance. As a result, the residuals are modelled with the following functional form:

$$\delta_c(T) = a_R + F_M(M_w, SOF) + F_D(M_w, R) + dBe + dS2S + dW_0, \quad (2.24)$$

In which a_R is the offset, dW_0 is the remaining aleatory residual, whereas F_M and F_D are the magnitude and distance scaling, respectively, which are computed as

$$F_M(M_w, SOF) = b_R\left(M_w, M_{ref}\right) + f_{jR}SOF_{jR}, \quad (2.25)$$

$$F_D(M_w, R) = c_R \log_{10}(R_{JB}^2 + h_R^2)^{0.5}. \quad (2.26)$$

In equation (2.25), b_R is a positive value for $M_w \leq 6.7$, whereas it is zero for $M_w > 6.7$. this means that the magnitude scaling term is forced to be zero when negative, so that the ITA18 model corrected with NESS2 (NESS-ITA18 hereafter) always amplifies the predictions with respect to the uncorrected ITA18, thus, to provide safe predictions over all scenarios in near-source conditions. M_{ref} is set to 6.7 for the reasons explained above, the terms b_R, c_R and f_{jR} are the model coefficients (provided in Supplement S4 in Sgobba et al. [7]) for each IM, hence PGA, PGV, and SA at periods from 0.01 to 10 s along with the corresponding statistical significance [7].

The regression is performed in two steps: firstly, the earthquake pseudo depth is computed through a nonlinear regression, in the second step, a linear ordinary least-squares mixed-effect regression is performed [41] to obtain the model coefficients and the corresponding uncertainty. In the latter step, the random terms dBe, $dS2S$ and dW_0 of equation (2.24), which represent, respectively, the between-event, the site-to-site, and the remaining aleatory residuals, according to Al-Atik [32], are estimated, together with the corresponding standard deviations denoted by τ, ψ, ϕ_0 [7].

The obtained relation led to correct the GMM for NESS2 data, by logarithmically combining the ITA18 median predictions (SA_{ITA18}) with the correction factor δ_c, according to the following equation:

$$\log_{10}(SA_{ITA18-NESS}) = \log_{10}(SA_{ITA18}) + \delta_C. \tag{2.27}$$

For a conservative purpose, the factor delta δ_c is used to correct ITA18 only if positive.

In the following, some explicative scenarios are reported for the PGA from ITA18-NESS2 model, assuming a Normal-Fault mechanism on the left, and a Strike-Slip mechanism on the right, referenced on rock site (EC8-A).

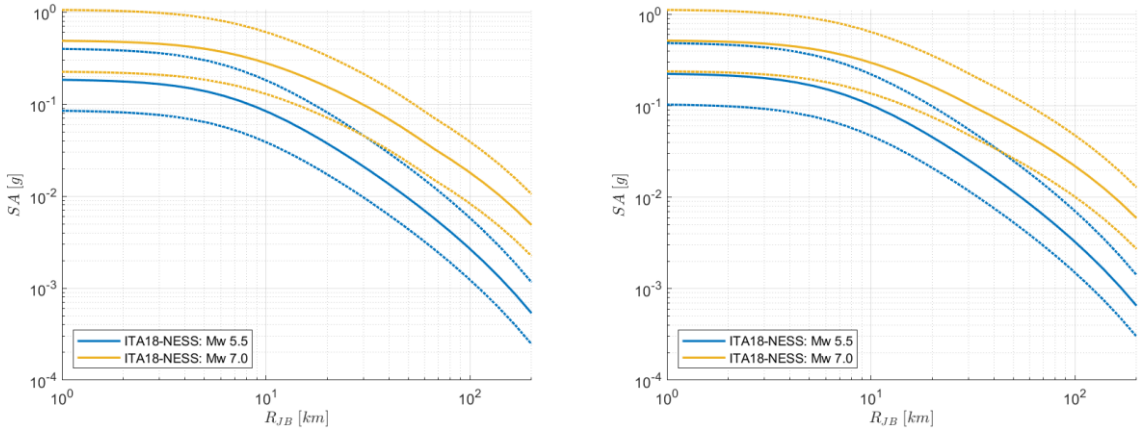

(a) Normal-Fault (b) Strike-Slip

Figure 2.8 Predictions of PGA from ITA18-NESS2, for (a) NF and (b) SS mechanisms, rock site conditions (EC8-A), for different magnitude.

2.9. ITA18-VH corrected with NESS1

The proposed GMM is introduced to obtain the vertical design spectra amplified by the near-source conditions, by scaling the corrected VH-NESS response spectral acceleration ratio with the horizontal UHS [13]. The VH model is compatible with the horizonal one developed by Lanzano et al. (ITA18), in fact the dataset, record processing and functional form are common to both.

The47mplifyication of VH spectral ratios is typically found in the proximity of the earthquake source and is accounted for by introducing an adjustment factor, leading to an improvement of the median predictions [13]. The procedure is the same as the one explicated in the previous subchapter 0: the factor is calibrated from the residual analysis of the reference GMM (i.e., calibrated using the ITA18 dataset) with respect to the worldwide (NESS1), following the Referenced Empirical Approach [52] [48].

The near-source factor is determined by fitting the residuals of ITA18 with respect to NESS1 data using a suitable functional form and is computed as:

$$\delta_C = \log_{10}\left(VH_{OBS,NESS}\right) - \log_{10}(VH_{ITA18}). \tag{2.28}$$

Where $VH_{OBS,NESS}$ represents the observed VH from NESS1 dataset and VH_{ITA18} represents the predicted rations from the ITA18 model.

The regression function of residuals is defined as:

$$\delta_C = a_R + F_{MR}(M_w, SoF) + F_{DR}(R) + F_{SR}(V_{S30}). \tag{2.29}$$

Where a_R is the offset, $F_{MR}(M_w, SoF)$ is the source function, $F_{DR}(R)$ is the distance function, and $F_{SR}(V_{S30})$ is the site terms:

$$F_{MR}(M_w, SoF) = b_R M_w + f_{jR} SoF_j, \tag{2.30}$$

$$F_{DR}(R) = c_R \log_{10}(R), \tag{2.31}$$

$$F_{SR}(V_{S30}) = k_R \log_{10}\left(\frac{V_0}{800}\right). \tag{2.32}$$

The coefficients, b_R, f_{jR}, c_R and k_R and variables R, M_w and V_0 definitions follow the VH ITA18 model [13].

The total variability of the ITA18-NESS model is simply estimated as the standard deviation of the residuals between the logarithmic VH predictions and observations included in the reference ITA18 dataset. Accordingly, the total standard deviation has been decomposed into the various components (τ, ψ and ϕ) and the propagation errors is applied to compute the variability of V predictions of the VH ITA18-NESS. The main contribution to the VH variability comes from the site-to-site variability (ψ), owing to the large uncertainties associate with the adopted model for site response [13].

In the following, some explicative scenarios are reported for the PGA from ITA18-V(VH)-NESS1 model, assuming a Normal-Fault mechanism on the left, and a Strike-Slip mechanism on the right, referenced on rock site (EC8-A).

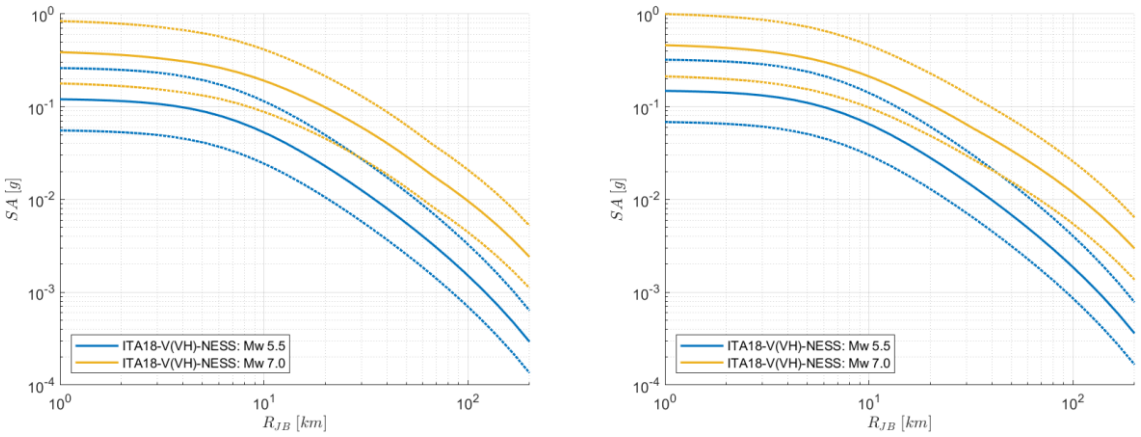

(a) Normal-Fault (b) Strike-Slip

Figure 2.9 Predictions of PGA from ITA18-V(VH)-NESS1, for (a) NF and (b) SS mechanisms, rock site conditions (EC8-A), for different magnitude.

3 Analyses of PSHA in R-CRISIS

3.1. Introduction to the software R-CRISIS

The software R-CRISIS [11] aims to perform probabilistic seismic hazard analyses based on the occurrence probabilities, attenuation characteristics and geographical distribution of earthquakes. The user can select different seismicity and geometrical models [11] for each computation site, whose seismic hazard results are mainly expressed within different time frames, in terms of probabilities of exceeding a given intensity value, correspondent to a return period obtained with the following formula:

$$Tr = \frac{-N}{\ln(1 - P_N)}, \tag{3.1}$$

Where N is the time frame expressed as number of years and P_N is the probability of exceedance in the next N years.

The user is allowed to define several seismogenic sources, selecting which ones are to be used in the calculation (see Figure 3.1), meaning that the software allows us to "activate" those source zones in which we are interested in, and to disable the others. The rule of thumb considered in the present work is to activate the seismogenic zone in which the site is located and those adjacent.

The result of the combined possible magnitude, distance and ground motion amplitude that contribute to the outcome of the PSHA is defined by the Uniform Hazard Spectra (UHS), evaluated for a given annual rate of exceedance probability, with the use of software R-CRISIS [11], according to the Cornell scheme [16] and to the new time-independent probabilistic seismic hazard model for Italy MPS19 [5].

3.1.1. Geometry models

To start with, the software requires the user to define the sites for which we want to perform the analysis in terms of a grid, which origin, increment and number of lines in the two orthogonal directions are specified by the analyst. The geometry of the seismic sources (plane coordinates and depth) may be defined manually or uploading a predefined shape file; in this study, the plane coordinates of ZS16 defined by Visini et al. [4] were uploaded from the shapefile of the authors.

In R-CRISIS, seismic sources can be described though different geometry models:

- Area sources (modelled as planes by means of a set of vertexes that account for a three-dimensional representation);
- Line sources (modelled as polylines with constant or variable depths);
- Point sources (where grid sources are case).

In the present work the geometry has been modelled using area sources (polygon divided into triangles).

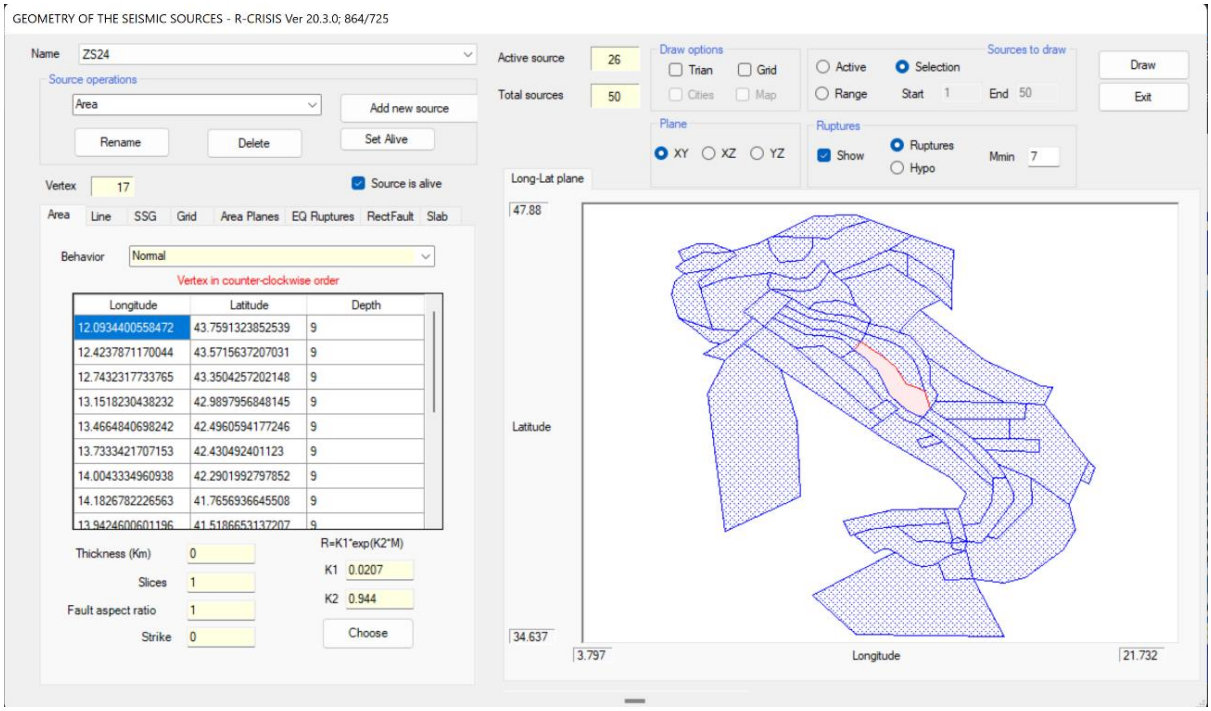

Figure 3.1 Example of settings of geometry in R-CRISIS for the Source Zone 24 (SZ24) according to [4].

Since attenuation relations (or ground motion models GMMs) rely on different distance measures (i.e., focal distance R_F, epicentral distance R_{EPI}, Joyner and Boore distance R_{JB} and closest distance to rupture area R_{RUP}), when R_{RUP} or R_{JB} distances are at play, the rupture area (or length) is expressed as a function of magnitude.

For area and smoothed seismicity (gridded) sources, R-CRISIS initially assumes a circular rupture, which radius R (in km) relates with the magnitude M as follows:

$$A = \pi R^2, \qquad (3.2)$$

where:

$$R = K_1 \cdot e^{K_2 M}, \qquad (3.3)$$

and K_1 and K_2 are constants of the relationship between the magnitude and the rupture area A.

Equation (3.2) can be rewritten thus as:

$$A = \pi {K_1}^2 \cdot e^{2K_2 M}. \qquad (3.4)$$

The rupture areas are contained in the plane of the source areas itself and are treated with a normal behavior, meaning that the software allows the rupture area to expand outside of the source area geometry, behaving as *leaky boundary* (see Figure 3.2).

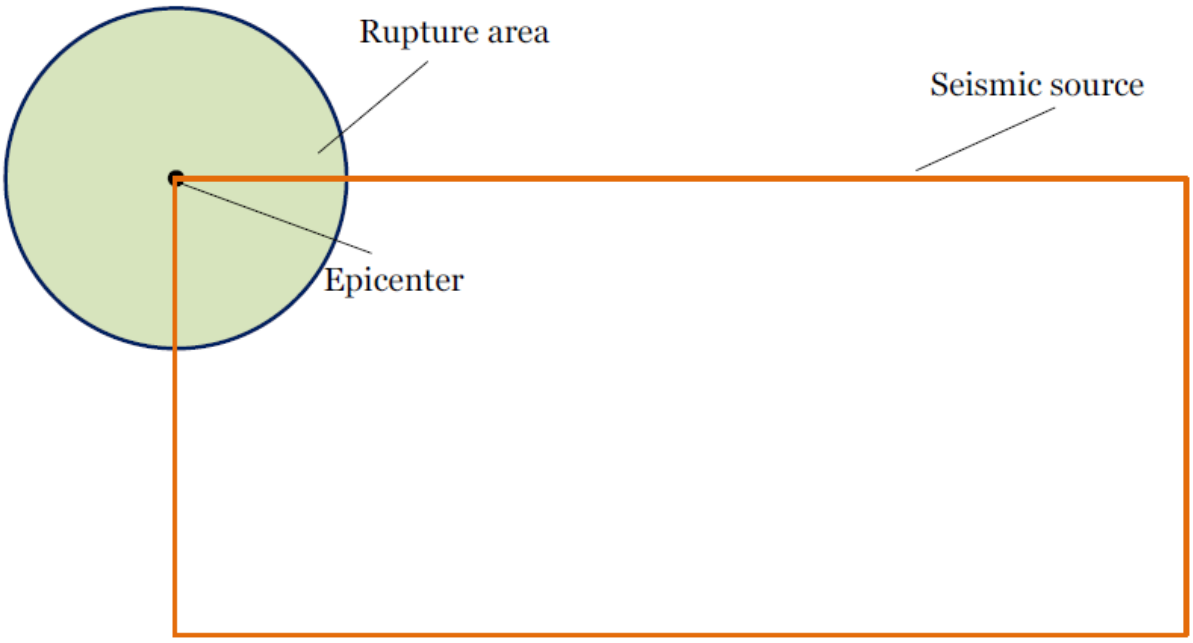

Figure 3.2 Schematic representation of the leaky boundary behavior.

Several regression analyses performed to study the relationship between magnitude and rupture area [54] adopt the following regression form:

$$\log A = a + bM. \qquad (3.5)$$

Where A is the rupture area, M is the magnitude and a, and b are the regression coefficients.

If equation (3.5) is rewritten as:

$$A = 10^a \cdot 10^{bM}, \qquad (3.6)$$

Equations (3.4) and (3.6) end with a similar structure with the following equivalences:

$$\pi {K_1}^2 = 10^a, \qquad (3.7)$$

$$e^{2K_2M} = 10^b. \qquad (3.8)$$

The correctness of the equivalences shown in equations (3.7) and (3.8) are verified through the regression coefficients, the R-CRISIS coefficients and the equivalences shown from the tables Table 3.1 to Table 3.3 [11].

Table 3.1: Wells and Coppersmith (1994) rupture area regression coefficients.

Model	a	b
Strike-slip	-3.42	0.90
Reverse	-3.99	0.98
Normal	-2.87	0.82
All	-3.49	0.91

Table 3.2: R-CRISIS rupture area coefficients for the Wells and Coppersmith (1994) model.

Model	K1	K2
Strike-slip	0.01100	1.03616
Reverse	0.00571	1.12827
Normal	0.02072	0.94406
All	0.01015	1.04768

Table 3.3: Equivalences between R-CRISIS and Wells and Coppersmith (1994) rupture are coefficients.

Model	Eq		Eq	
	10^a	$\pi {K_1}^2$	10^b	e^{2K_2M}
Strike-slip	3.80E-04	3.80E-04	7.943	7.943
Reverse	1.02E-04	1.02E-04	9.550	9.550
Normal	1.35E-03	1.35E-03	6.607	6.607
All	3.24E-04	3.24E-04	8.128	8.128

The rupture area coefficients are defined according to the respective style of faulting, and the source depth specified for the seismogenic zones of interest and to set alive the area sources for which the PSHA is performed.

3.1.2. Seismicity models

The seismicity is described in R-CRISIS by means of the probabilities of having a given number of earthquakes of given magnitude, at a given location, during the next T_f years. The most frequently used model is the Gutenberg-Richter [17], which is associated to Poissonian occurrences (assumed in the present study), and so, the probability of exceeding the intensity level a in the next T_f years, given that the earthquake with magnitude M occurred at a distance R from the site of interest.

The source seismicity expressed through the modified Gutenberg-Richter model is defined for each seismogenic zone and follows the first approach defined by Visini et al. [4]. The parameters needed are the minimum and maximum values of the magnitude to be considered in the calculations, the rate at the min M and the expected value of β that is defined as:

$$\beta = b \cdot \ln 10, \tag{3.9}$$

where b is the slope of the G-R relation in semilogarithmic scale.

R-CRISIS allows to consider the uncertainty in the definition of b and the maximum magnitude, using the coefficient of variation of beta and the standard deviation, respectively. In this work, a value of 0.1 and 0.2 has been adopted (see Figure 3.3).

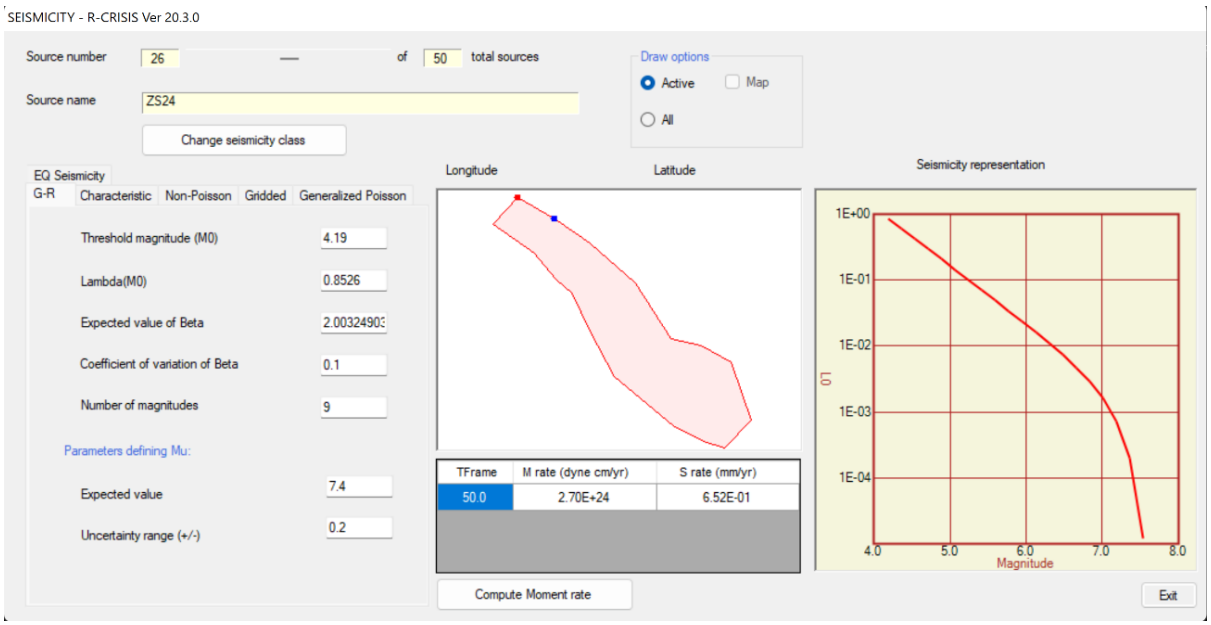

Figure 3.3 Illustration of Gutenberg-Richter seismicity model (SZ24) in R-CRISIS.

3.1.3. Strong ground motion attenuation models

R-CRISIS allows the user to choose among three different "families" of GMM included in the seismic hazard analysis project (see Figure 3.4):

1. GMM tables: to be prepared externally by the user, with the prediction of the GMM given as a function of magnitude, structural period and source-to-site distance;
2. Built-in GMM: popular models published in the literature included in R-CRISIS and selectable by the user;

3. Generalized models: generalized attenuation models with a non-parametric probabilistic description of the ground motions, to be given externally by the user.

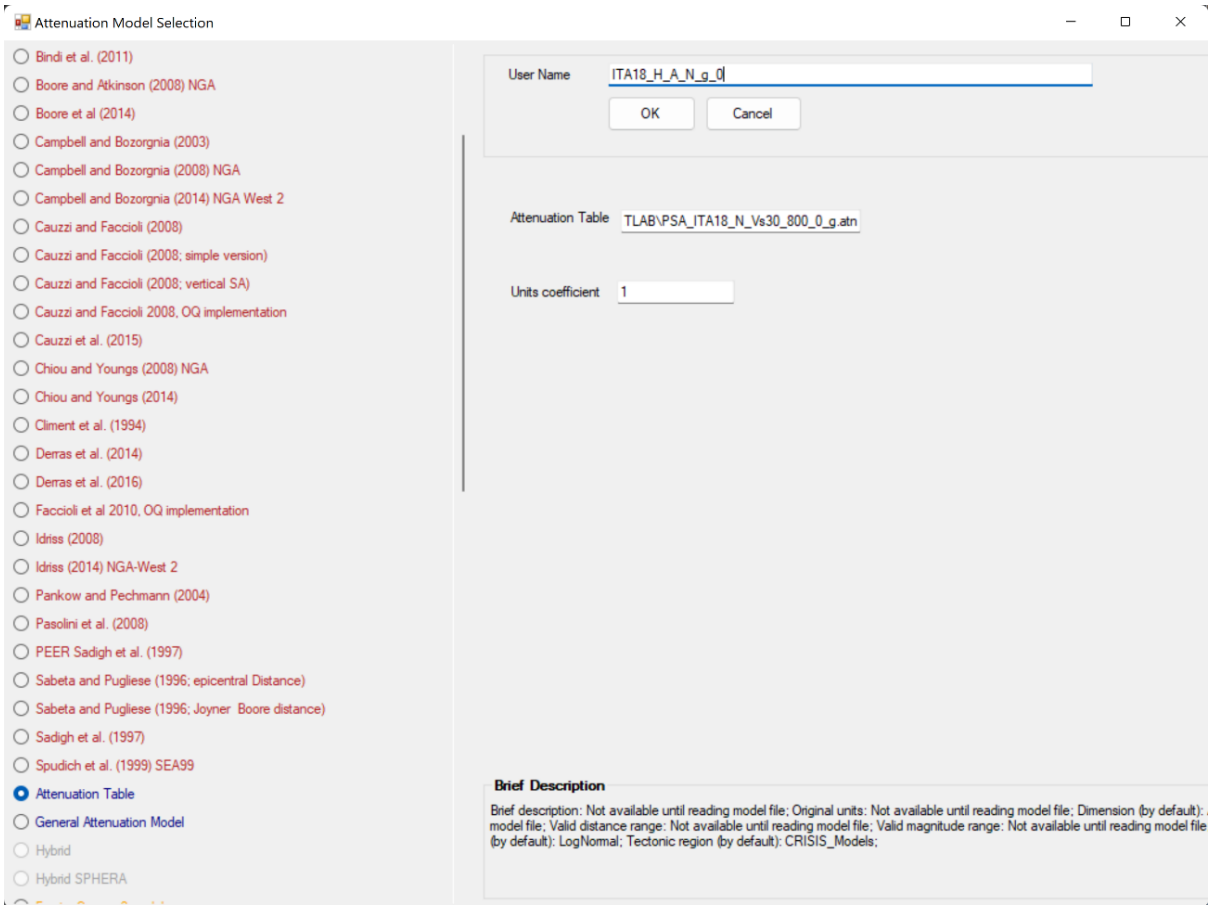

Figure 3.4 Attenuation model selection in R-CRISIS.

The attenuation models used in this work were prepared as external tables, using an *ad hoc* MATLAB code. For each spectral ordinate, the attenuation table includes a matrix that contains the median intensities associated to the magnitudes (rows) and to the distances (columns).

Note that a truncation can be applied to the hazard intensity values, meaning that the integration across the attenuation relation uncertainty implied, is conducted up to a certain value denoted as TC sigma truncation. Here, no truncation was applied.

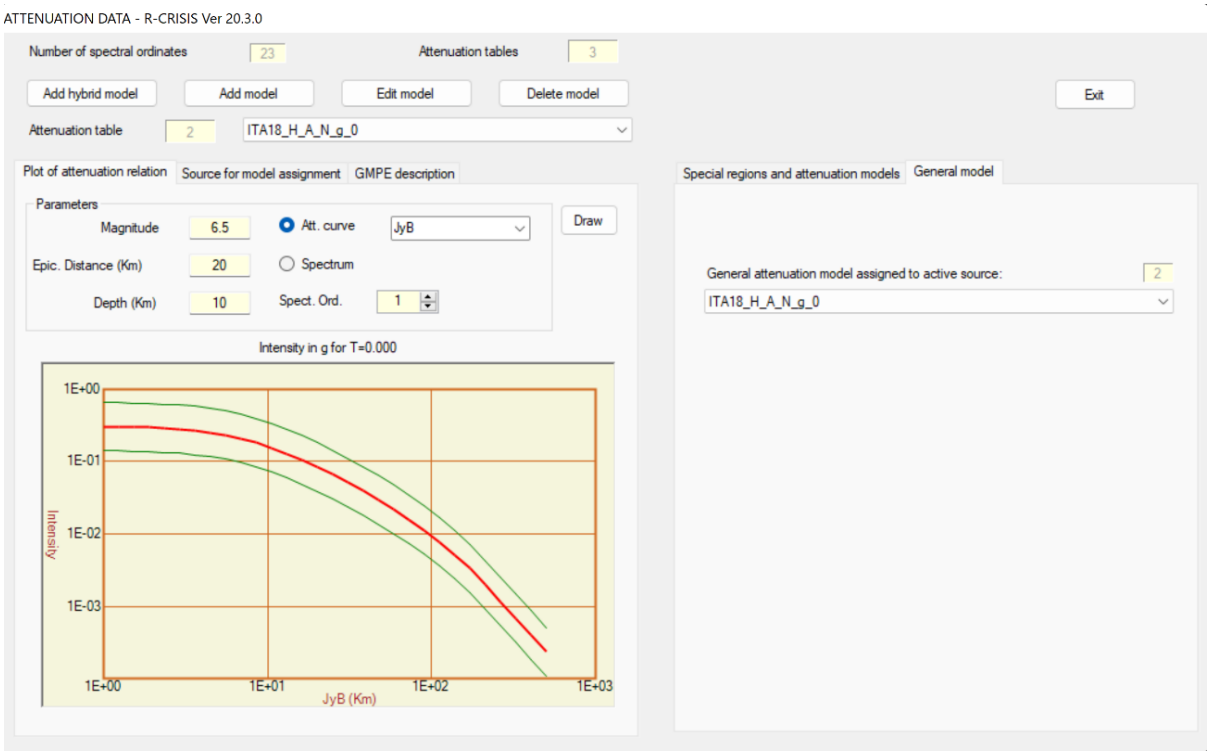

Figure 3.5 Illustration of attenuation data in R-CRISIS.

4 Case-studies

The aim of this work focuses on the impact, within the seismic hazard calculation, of new GMMs specifically calibrated for the Italian context for shallow crustal earthquakes [6], as well as on the empirically derived correction factors used to adjust the median predictions of these GMMs to consider the effects of near source.

The main cases study examined for the thesis are L'Aquila (Abruzzo), sited in a tectonic region of high seismicity and characterized by a Normal-Fault mechanism, and Zafferana Etnea (Sicily), located in a volcanic zone, with Strike-Slip mechanism. The site of L'Aquila has been analysed in terms of seismic hazard to evaluate the impacts of the horizontal and the vertical GMMs, calibrated for shallow crustal earthquakes in the Italian active tectonic regions [6] (ITA10 and ITA18) and to assess the ground motion effects in near-source conditions (ITA18-NESS), also with reference to vertical components of motion that may be of particular relevance in the near field.

Thereafter, the site of Gemona del Friuli (Friuli-Venezia Giulia) is also examined for the sole purpose of verifying the performance of the UHS calculated in near-source conditions, for a different style of faulting (prevailed by a reverse mechanism), for which we expect more significant effects produced by the NESS correction, mainly over short periods, both for the horizontal and the vertical components, calibrated for shallow crustal earthquakes in the Italian active tectonic regions [6] (ITA18-NESS).

While the site of Zafferna Etnea is introduced to obtain an in-depth analysis of the impacts of a shallow volcanic GMM (the LL19 model) with respect to active shallow crustal one, therefore the prediction models of ITA18 and LL19 have been compared in terms of PSHA results for the volcanic area source.

We chose these cities because they lie in different tectonic settings and are located inside area sources characterized by different levels of seismic activity [4].

4.1. L'Aquila case study

The municipality of L'Aquila (Lat: 42.3540; Lon: 13.391992) is sited in the Italian region of Abruzzo, along the central Apennine, mainly characterized by normal faults; the Adria Microplate dives beneath the Eurasian Plate where the Apennine Mountains rise and the Eurasian and African plates collide, creating compression and thrusting at depth, and extension and normal faults at the surface [55].

The area of interest is known to be seismically active since a long time and is also characterized by high seismicity as demonstrated by the recent earthquake (i.e., Mw 6.1 L'Aquila event of April 6, 2009) which caused about three hundreds of fatalities, more than a thousand injuries, and extensive and severe damage to buildings and other structures; about 66.000 residents were temporarily evacuated, and more than 25.000 were medium-term homeless. Several events with a comparable magnitude to this last earthquake are reported by the national seismic catalogue [56]: the main documented events (magnitude larger than 6.5) date back to 1315, 1349,1461,1703 and 1915, while the first contemporary seismic classification of L'Aquila date to 1915, after the catastrophic Avezzano earthquake [56].

Moreover, seismic demand during the 2009 earthquake was locally much larger than the design one, also related to near-source directivity effects that were found in the records of L'Aquila earthquake (large velocity pulses concentrating energy in the starting phase of the Normal- Fault component), that depend on the relative position of the site with respect to the fault rupture [56].

From this perspective, the site of L'Aquila has been considered in terms of seismic hazard to evaluate the impacts of the horizontal and the vertical GMMs, calibrated for shallow crustal earthquakes in the Italian active tectonic regions [6] (ITA10 and ITA18) and to assess the ground motion effects in near-source conditions (ITA18-NESS), also with reference to vertical components of motion that may be of particular relevance in the near field. The seismogenic zones considered for the seismic hazard evaluation are highlighted in the figure below: the area source #24 where L'Aquila is sited, and those adjacent #23, #25, #26, #33 defined in ZS16 [4].

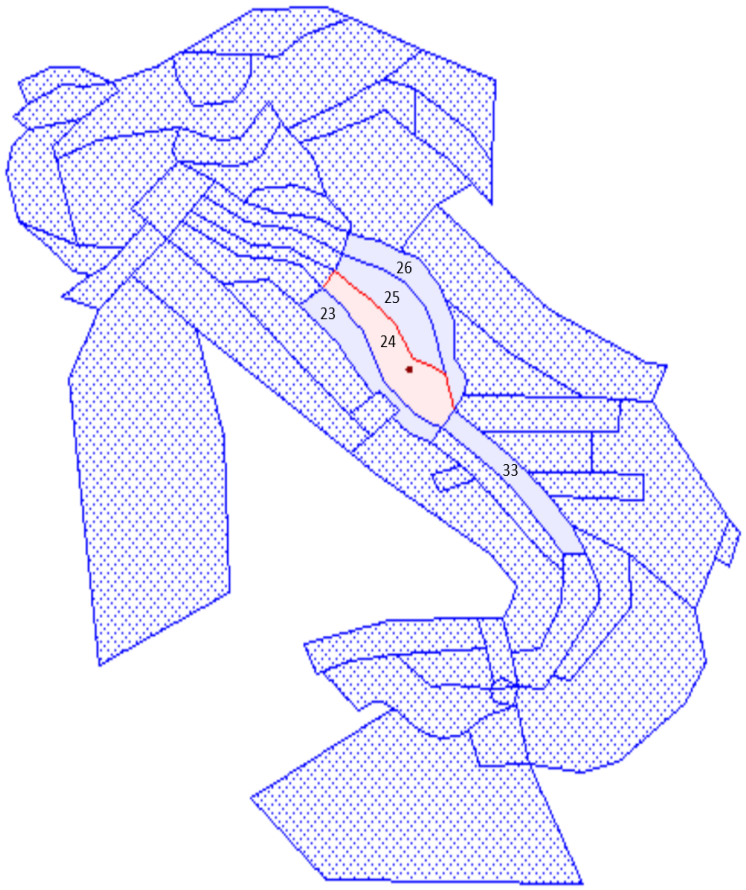

Figure 4.1 Map of Italy – case study of L'Aquila: the SZ considered are those with uniform blue color, the SZ containing the site is colored in red, other SZ are in dotted blue and are neglected.

The seismicity of each area source is defined according to Visini et al. [4] and is summarized in the following table: b is a regression coefficient of the rupture area (slope of the G-R law [17]); M_0 is the threshold magnitude; $\lambda(M_0)$ is the rate of occurrence of ground motion earthquake; M_{max} is the maximum magnitude; *Sof* define the rupture mechanism; *Hypo* is the depth; *K1* is a constant related to the regression coefficient a (defined in the previous chapter 3).

Table 4.1 Gutenberg-Richter parameters, styles of faulting and depth for the SZ adopted in the PSHA study of L'Aquila.

GR	SZ24	SZ23	SZ25	SZ26	SZ33	Rif.
b	0.87	1.2	0.96	0.77	0.72	Suppl. 3
M_0	4.19	4.19	4.19	4.19	3.96	Suppl. 3
$\lambda(M_0)$	0.8526	0.0772	0.2221	0.1649	0.2376	Suppl. 3
β	2.00325	2.76310	2.21048	1.77299	1.65786	$ln(10) \cdot b$
M_{max}	7.4	7.4	7.1	7.1	7.5	Suppl. 3
Sof	NF	SS	SS	SS	NF	Visini2022
Hypo	9	6	8	7	7	Suppl. 1
K1	0.0207	0.011	0.011	0.011	0.0207	W&C

To start with, a comparison of the UHS obtained using different attenuation models (ITA10 and ITA18) is done, considering the hazard from the single SZs, activated singularly from all the SZs, together (SZALL) for two values of probability of exceedance fixed at 10% and at 2%, considering a time frame of 50 years, corresponding to a return period 475 and 2475 years, respectively.

The obtained results are validated with the GMMs attenuation curves, plotted according to the predominant scenario obtained from the disaggregation analyses, evidencing the combination of magnitude and distance that mostly contribute to the seismic hazard at the site.

Thereafter, a sensitivity analysis follows for the dominant area source #24. A study on the ground motion variability is implemented in terms of PSHA when adopting ITA18 heteroscedastic variability [6], by making explicit the magnitude dependance expressed in terms of event- and site-corrected standard deviation at different periods.

In the case study, the hazard spectra for the vertical components are derived from the empirical model of the horizontal-to-vertical V/H spectral ratio calibrated for ITA18 [13] and scaled by the horizontal component. This simplified procedure was validated by the comparison with the vertical UHS, based on an ITA18-V model, i.e., calibrated directly on the V components. Finally, the UHS is calculated considering the effects of nearby sources by introducing the ITA18-NESS model for the L'Aquila site within the software.

4.1.1. ITA10 vs ITA18

As previously mentioned, the GMM implemented by Lanzano et al. (ITA18) [6] is calibrated on the most up-to-date strong motion dataset for Italian crustal earthquakes, extending the dataset implemented by Bindi [12] to magnitudes larger than 6.9, with variation periods up to 10 seconds. Hence, the impact on the UHS obtained with the

most recent model ITA18 is compared with the previous ITA10, focusing the attention on the most dangerous area source, which dominates the seismic hazard due to a higher spectral acceleration amplitude and probability of exceedance. In the next figures, the UHS calculated for the site of L'Aquila are shown, considering the use of the area sources, individually (i.e., SZ23, SZ24, SZ25, SZ26, SZ33) and together (i.e., SZALL), once with a return period of 475 years and then of 2475 years; the comparison between the UHS modelled with two different model (i.e., ITA10 and ITA18) follows.

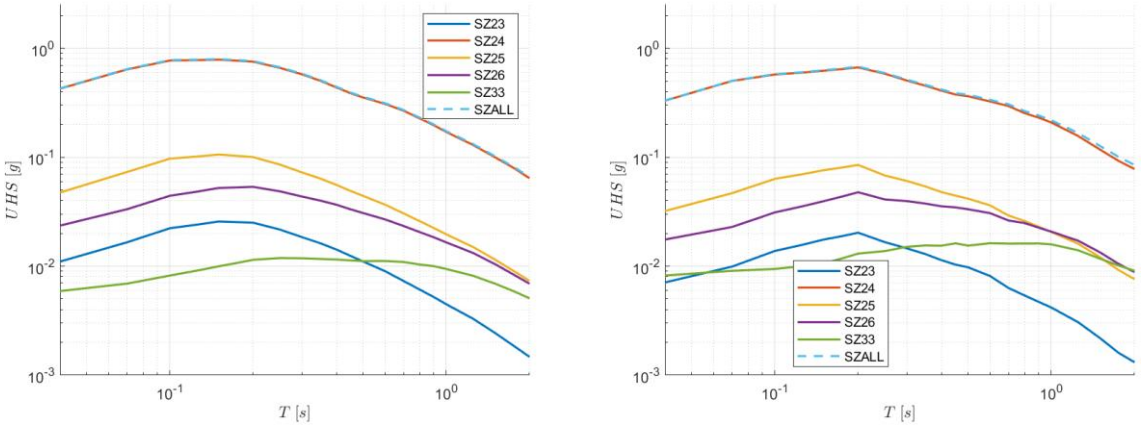

(a) ITA18 (b) ITA10

Figure 4.2 Uniform hazard spectra for the site of L'Aquila, return periods 475 years, calculated using (a) ITA18 model and (b) ITA10 one. In the figures, the contributions to the total hazard (SZALL) from the different SZ are also shown.

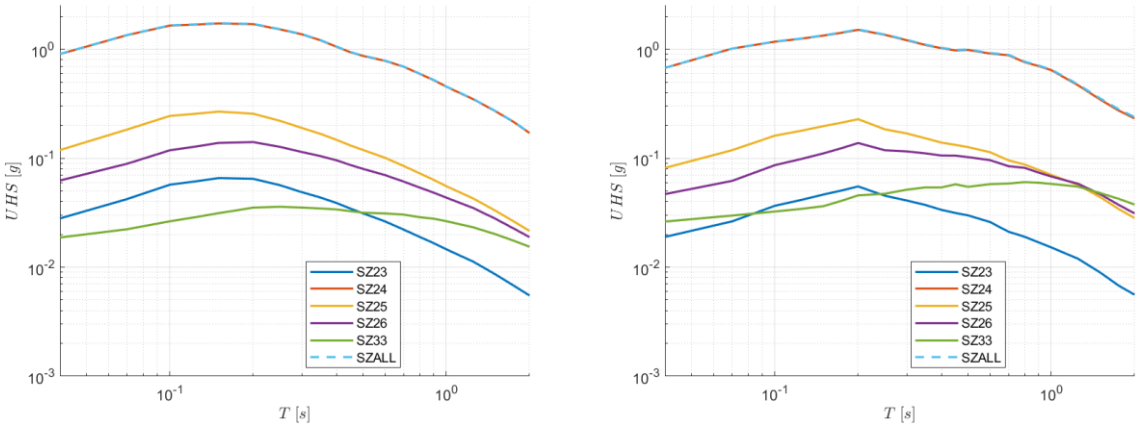

(a) ITA18 (b) ITA10

Figure 4.3 Uniform hazard spectra for the site of L'Aquila, return periods 2475 years, calculated using the (a) ITA18 model and the (b) ITA10 one. In the figures, the contributions to the total hazard (SZALL) from the different SZ are also shown.

As expected, the dominating seismogenic zone is the one where the site of L'Aquila is located (SZ24), as highlighted in Figure 4.2 and Figure 4.3, and overlap the SZALL curve across all vibration periods, for both the return periods, 475 and 2475 years, respectively.

To be noticeable, a crosscurrent is observed for SZ33 spectral shape with respect to other curves, due to the influence of the maximum magnitude (as reported in Table 4.1, Mw 7.5 is the higher) at long vibration periods, leading to an increasing trend. Indeed, the area source #33 is characterized by a significant amount of released energy and identify the Sannio-Irpinia seismic zone, which includes the most dangerous event that we have faced in Italy: 1980 Irpinia Mw 6.9 event.

A disaggregation hazard analysis is also implemented and reported in Figure 4.4 and Figure 4.5, for a return periods of 475 and 2475 years, respectively by considering all the source zones of L'Aquila case study, relating the ITA18 model to the source zones SZ23, SZ24,SZ25, SZ26, SZ33); the value at each cell corresponds to the probability that the selected intensity level is exceeded in 50 years, considering magnitude and distances within the accounted range [11].

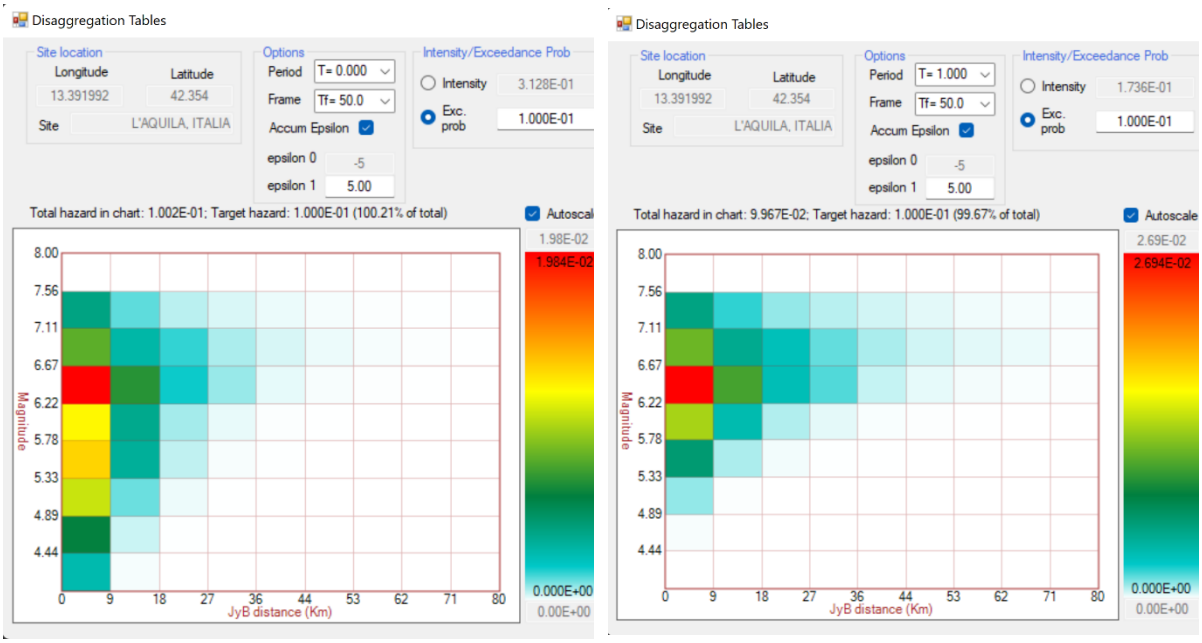

(a) T = 0 s (b) T = 1 s

Figure 4.4 Plots of disaggregation analysis from R-CRISIS, for the site of L'Aquila, with ITA18 GMM, Tr = 475 years, for (a) PGA and (b) 1s.

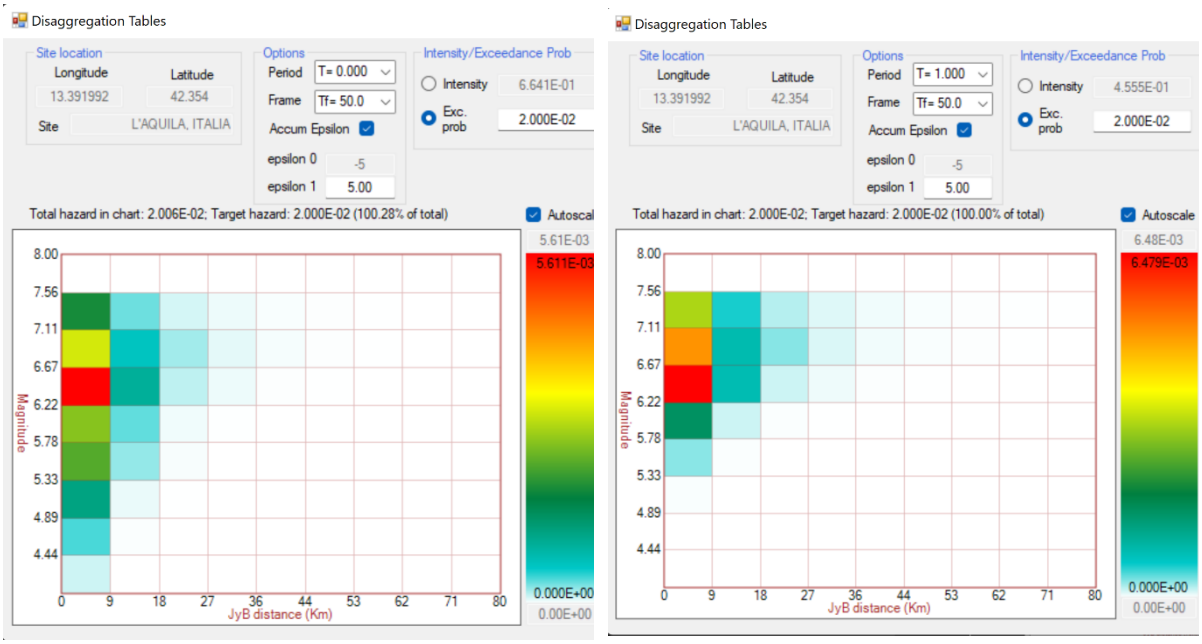

(a) T = 0 s (b) T = 1 s

Figure 4.5 Plots of disaggregation analysis from R-CRISIS, for the site of L'Aquila, with ITA18 GMM, Tr = 2475 years, for (a) PGA and (b) 1 s.

The predominant scenario obtained from the disaggregation analysis is identified in the red bin of figures above and ranges in magnitude Mw 6-22-6.67 and distances 0-9 km.

The comparison implemented above between the UHS obtained adopting the two attenuation models (i.e., ITA18 and ITA10) is done again in Figure 4.6, focusing the attention on the SZ24 curve, to capture as best as possible the peculiarities of the models; the results are supported by the illustration of the spectral acceleration of ground motion models of Figure 4.7, interpreted at the light of the disaggregation analyses reported above, according to the most relevant scenario (Mw 6.22-6.67 and R = 0-9 km).

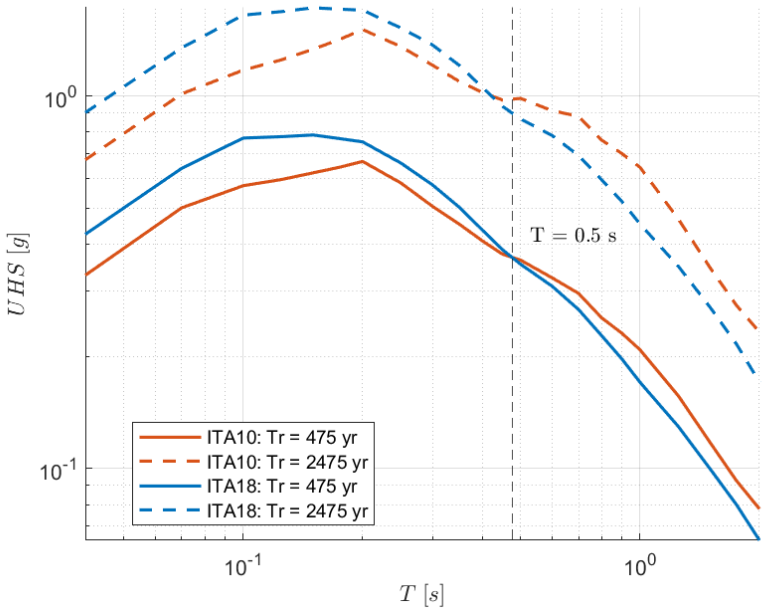

Figure 4.6 Uniform hazard spectra for the site of L'Aquila, with the single SZ24, comparison between the return periods of 475 and 2475 years, prediction models ITA10 and ITA18.

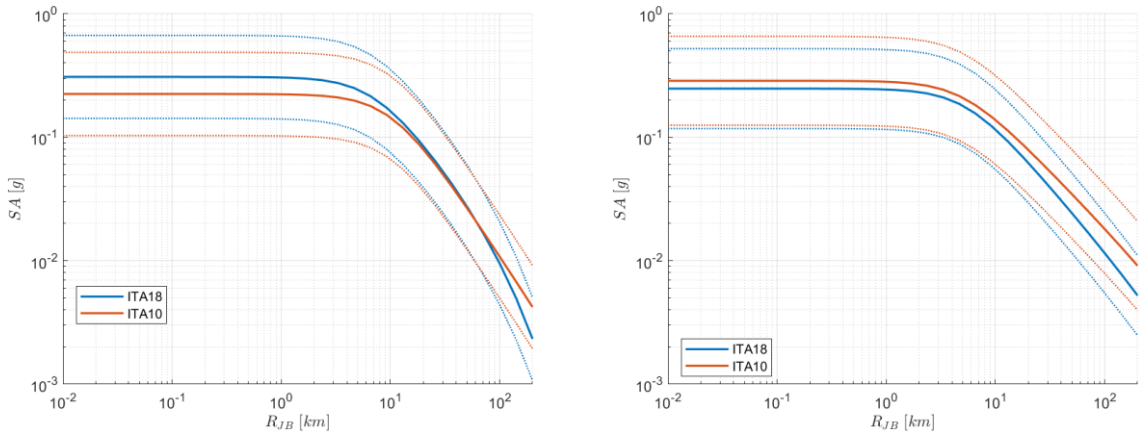

(a) T = 0 s (b) T = 1 s

Figure 4.7 SA predictions according to ITA10 and ITA18, for Mw = 6.5, NF mechanism and reference rock site (EC8-A) for (a) PGA and (b) 1 s.

Figure 4.6 shows an inversion of trend around 0.5 seconds; in particular, at short vibration periods, the two models are strongly influenced by the median predictions, accordingly ITA18 predicts higher values than ITA10 (see Figure 4.7), probably because of a better constraint of ITA18 to lower magnitudes (the dataset is calibrated on a higher number of small earthquakes). Instead, at intermediate-long periods, the overprediction of ITA10 comes to light; this is evidenced particularly for higher return period (Tr = 2475 years) and can be justified with a higher related sigma value with respect to ITA18 attenuation model, which are for instance, according to the dominant

scenario (Mw 6.5, R = 0km) and for a period $T = 1s$: $\sigma_{ITA10,T=1s} = 0.3600$, $\sigma_{ITA18,T=1s} = 0.3235$.

The numerical differences between the spectral accelerations implemented with the two models are better represented in the Figure 4.8 and Figure 4.9, by implementing the spectral ratios between the two SA (ITA18/ITA10 for the dominant scenario: Mw 6.5, R = 0 km) and UHS (ITA18/ITA10 for the SZ24), respectively. Also, the spectral acceleration ratios are also shown as function of distance, both at short and long periods in Figure 4.10.

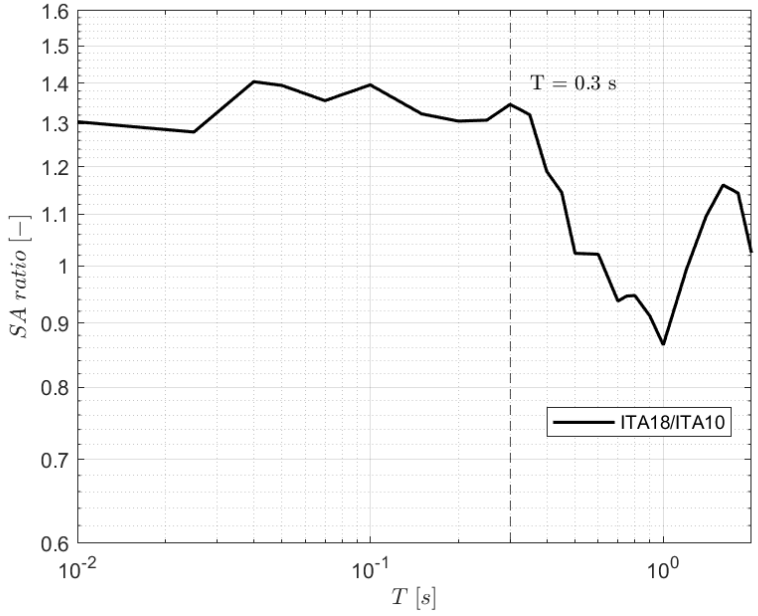

Figure 4.8 Spectral ratio between the prediction models ITA18 and ITA10 for Mw 6.5, R = 0 km, NF, EC8-A.

The spectral acceleration ratio represented in Figure 4.8 is characterized by an average ratio equal to 1.3 when we are close to the source (R = 0 km) and until a vibration periods T = 0.3 s, meaning that the ITA18 spectral acceleration is slightly larger than ITA10, while for higher periods, the differences between the two models are almost negligible (average ratio equal to 1.04).

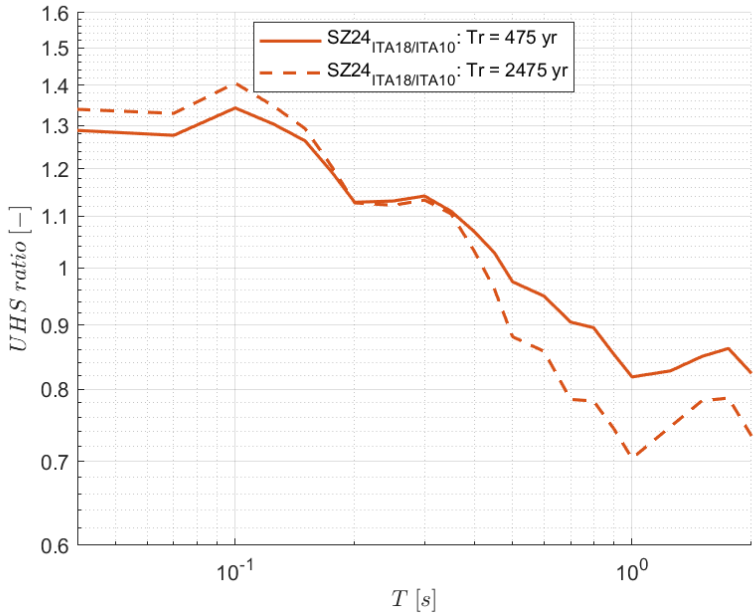

Figure 4.9 UHS ratio in SZ24 for Tr = 475 and Tr = 2475 years from prediction models ITA18 and ITA10.

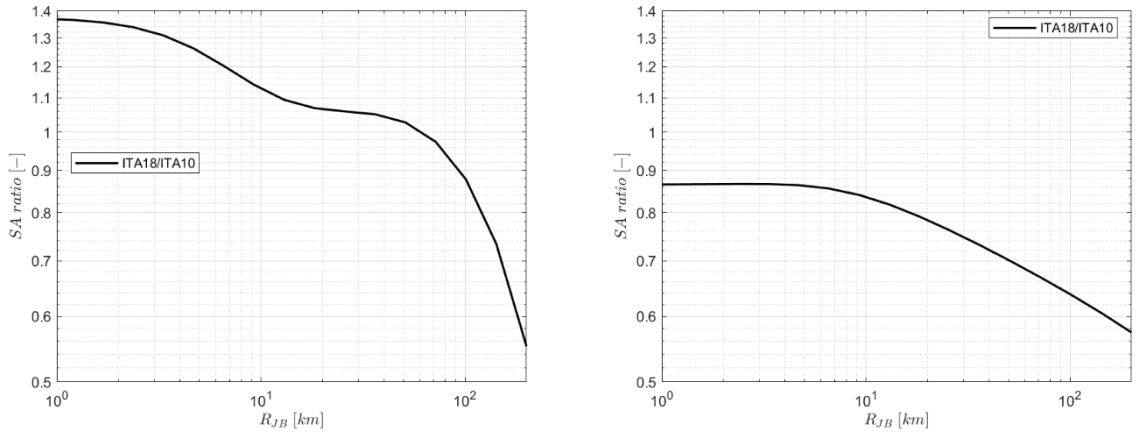

(a) T = 0 s (b) T = 1 s

Figure 4.10 Spectral acceleration ratio ITA18/ ITA10, for Mw = 6.5, NF mechanism and reference rock site (EC8-A) for (a) PGA and (b) 1 s.

On the other hand, the average spectral ratios of UHS of Figure 4.9 evidence the same trend as SA prediction ratios, both at Tr = 475 years and at Tr = 2475 years. Substantial differences between the two GMMs come to light for higher distances and as the vibration periods increases, as reported in Figure 4.10, in fact, the average mean at T = 0 s is 0.87, while at T = 1 s is 0.66, meaning that for long vibration periods ITA10 predicts almost half of ITA18 spectral acceleration.

4.1.2. Variability of ITA18

In this section, the effect of the heteroscedastic model of ITA18 GMM (deeply described in the subchapter 2.3.2) on UHS is shown, as a function of magnitude and with a fixed V_{S30} value to 800 m/s (i.e., rock site corresponding to EC8 – A site category). According to Lanzano et al. [6] the ground motion variability is expected to reduce at increasing magnitude and V_{S30}; this is partially shown in Figure 4.11, where the magnitude-dependent model ϕ_0 is shown as a function of Mw, assuming zero distance, three different values of periods (0, 0.1 and 1 seconds), and a constant ϕ_{S2S}, since it has been modelled with a single fixed value ($V_{S30} = 800m/s$). Also, the total standard deviation σ is shown in Figure 4.12 as a function of the structural period, for $R = 0\ km$ and for two different magnitudes (Mw 4.5 and 6.5).

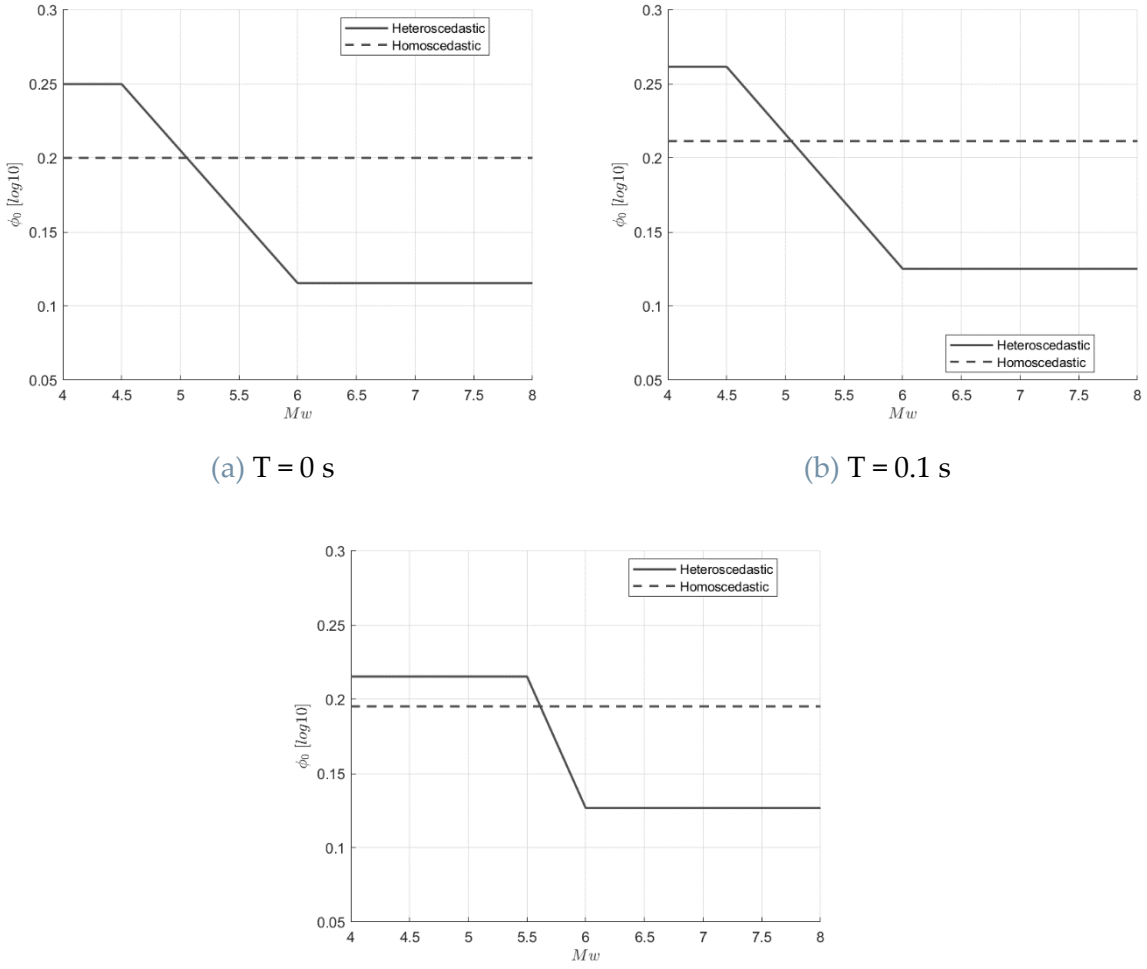

(a) T = 0 s

(b) T = 0.1 s

(c) T = 1 s

Figure 4.11 Heteroscedastic model of ITA18: magnitude dependent ϕ_0 model, function of magnitude, R= 0 km for (a) PGA, (b) 0.1 s and (c) 1s.

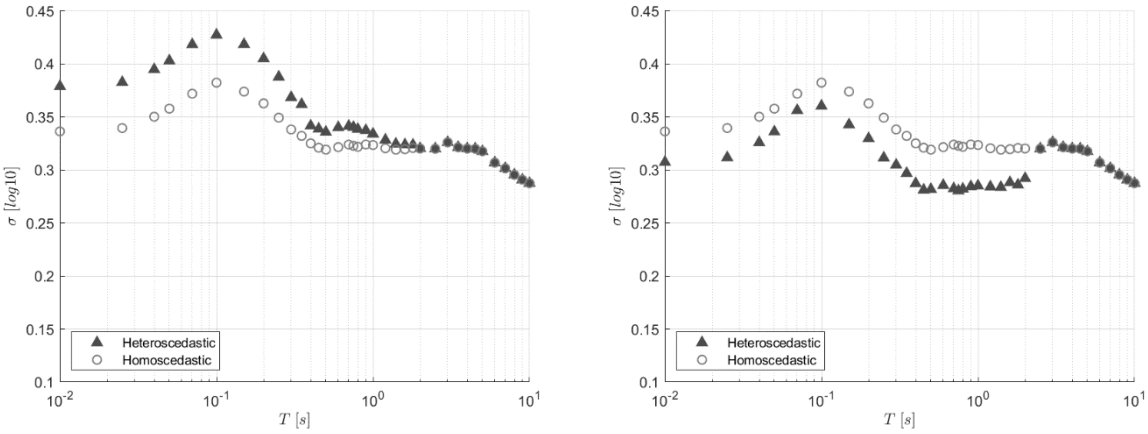

(a) Mw = 4.5 (b) Mw = 6.5

Figure 4.12 Ground motion variability in terms of standard deviation σ, as a function of T, for ITA18 model, Vs30 = 800 m/s, R = 0 km for (a) Mw 4.5 and (b) Mw 6.5.

The heteroscedastic sigma assumes higher values with respect to the homoscedastic one, for magnitude lower than about 5.5 (Figure 4.11 to support), and up to 2 seconds (beyond which no differences are observable); while for higher magnitudes, the homoscedastic sigma model is dominant, as clear from Figure 4.11.

Therefore, the ITA18 attenuation models have been used in CRISIS, with the single SZ24, for the site of L'Aquila and the obtained UHS curves are reported in Figure 4.13, according the two considered approaches (i.e., homoscedastic, and heteroscedastic) and for three different return periods (i.e., 30, 475 and 2475 years).

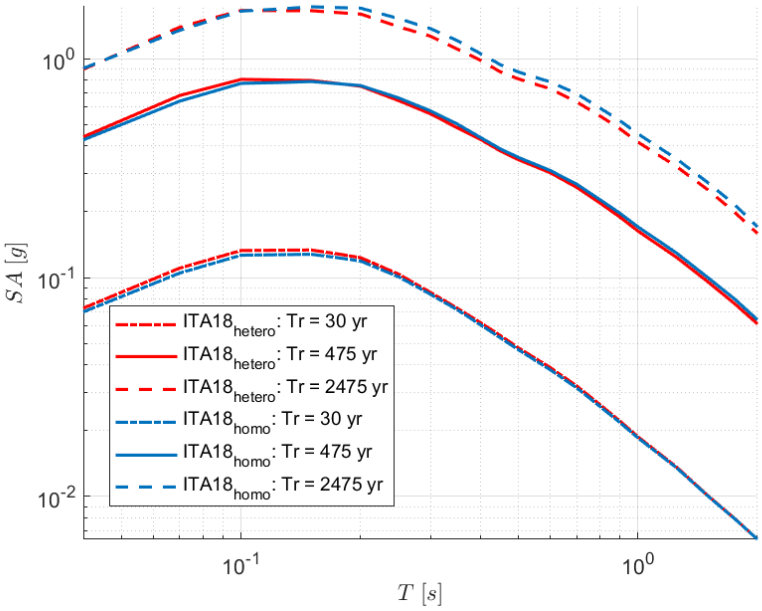

Figure 4.13 UHS for the site of L'Aquila, with the single SZ24: comparison between the return periods of 30, 475 and 2475 years, and the prediction model ITA18, with sigma homoscedastic and heteroscedastic.

For high return period, where the role of the GMM variability is higher, the spectral accelerations modelled with σ_{hetero} were expected to be lower than the one modelled considering σ_{homo}, and vice versa, since high return periods are related to higher values of magnitude. Figure 4.13 shows this expected trend: the ITA18 heteroscedastic modelling of the site-to-site and event- and site-corrected variability is effective in reducing the estimated hazard only at very long return periods (even though this reduction is quite limited). At ordinary return periods, we do not evidence any significant differences in terms of seismic hazard between the two models, meaning that the heteroscedastic model can be neglected.

4.1.3. ITA10-V vs ITA18-V

As previously mentioned, the vertical ground motion can be obtained with two alternative methods:

1. A GMM specifically developed for the vertical component, with the variability directly associated to the vertical model;
2. A GMM obtained multiplying the IMs of the Vertical-to-Horizontal (VH) ratio by the horizontal component, with the variability of the predicted vertical ground motion obtained from the error propagation of various component of the standard deviation considering the correlation between VH and H random variables under the assumption that they are log-normally distributed, as described in subchapter 2.4.

As already discussed, the relevance of the vertical ground motion component in the hazard assessment stems from the fact that it can be significantly larger than its horizontal counterpart, especially in the near-source region of earthquake and at short periods ($T < 0.3\ s$), with potential impact for short-period structures. A comparison of the UHS obtained with the vertical models with the two approaches mentioned above (i.e., ITA18-V and ITA18-V(VH)) is implemented and compared with respect to the horizontal one (ITA18-H) [6], for the dominant seismogenic zone #24, for two different return periods (475 and 2475 years). Also, the curves are compared as well with the most simplified approach, obtained by multiplying the IMs of the Vertical-to-Horizontal (VH) ratio by the horizontal UHS, considering the magnitude and distance coming from the disaggregation analysis results.

In addition, the impact on the UHS obtained with the most recent model (ITA18) is compared with the older (ITA10), as depicted below in Figure 4.14 and Figure 4.15, respectively.

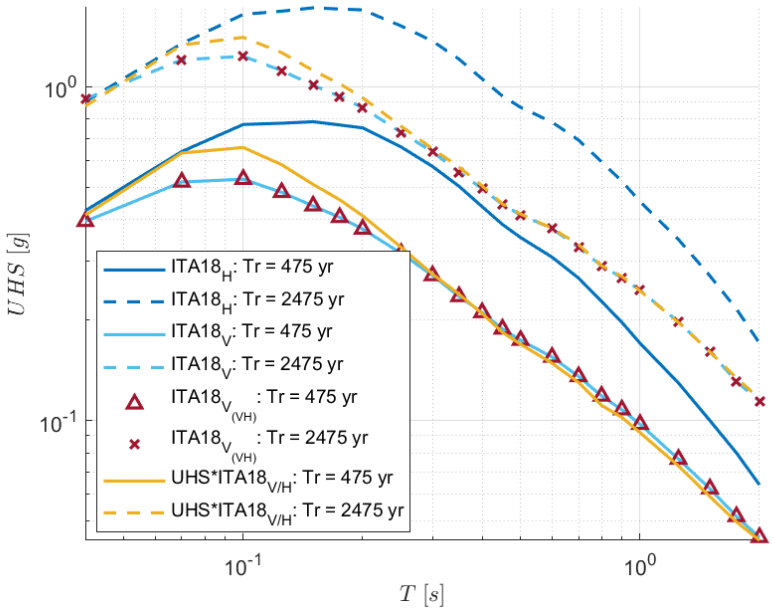

Figure 4.14 UHS for the site of L'Aquila, with the single SZ24: comparison between the return periods of 475 and 2475 years, in horizontal and vertical directions according ITA18 model.

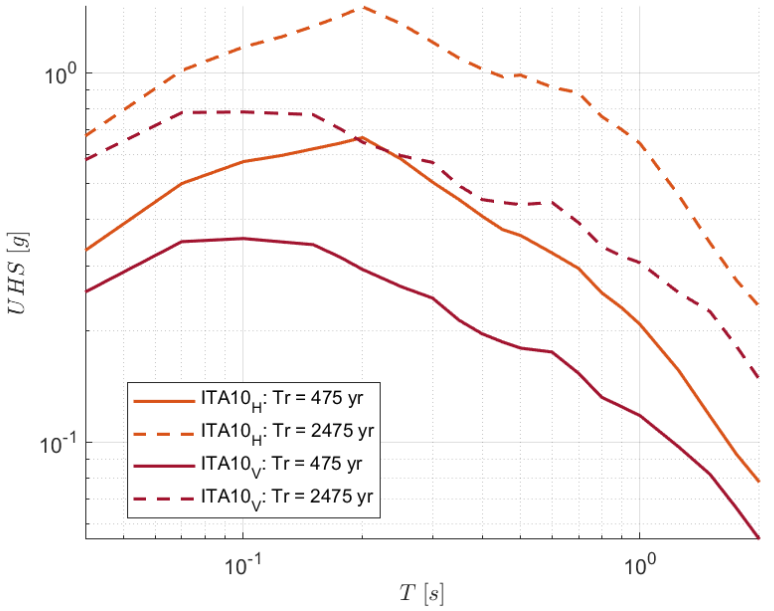

Figure 4.15 UHS for the site of L'Aquila, with the single SZ24: comparison between the return periods of 475 and 2475 years, in horizontal and vertical directions according ITA10 model.

Results show that the UHS calculated with the two approaches for the ITA18-V are almost coincident with one another and have a lower impact on the seismic hazard with respect to the horizontal component, which is characterized by higher spectral accelerations, similarly to ITA10 spectral accelerations; however, the vertical component becomes more significant at shorter periods, particularly for the simplified

approach for which comparable amplitudes are obtained with respect to the horizontal component of the ITA18 model, particularly at longer return periods.

A strong emphasis is laid first on ITA18 models, whose results agree with the spectral acceleration predictions of the ground motion models calculated with reference to the predominant scenario (Mw 6.5, R = 0 km) and reported in Figure 4.16, also characterized by a comparable ground motion variability. A complete view of the spectral accelerations trends is supported in Figure 4.17 with the introduction of various magnitude and then distances.

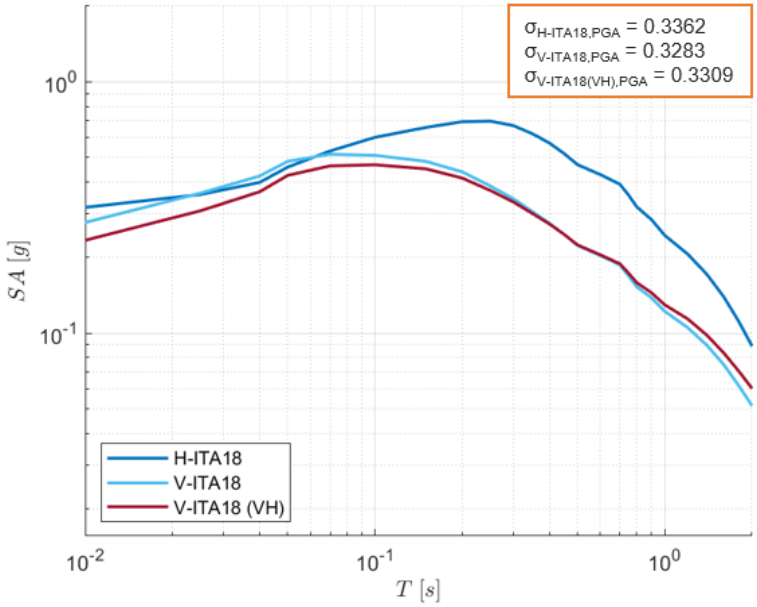

Figure 4.16 Spectral accelerations calculated with ITA18-H, ITA18-V, and ITA18-V(VH) prediction models, for R = 0 km, Mw = 6.5, NF mechanism and rock site conditions (EC8-A).

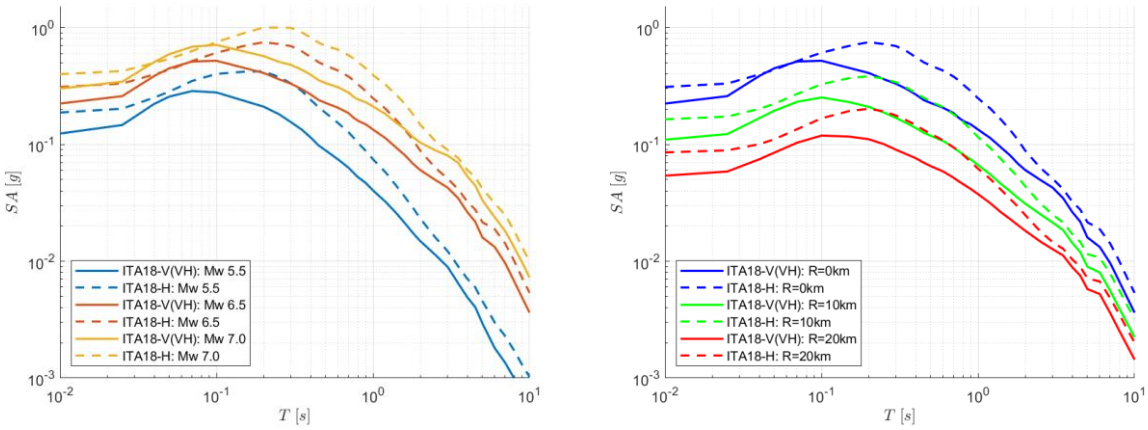

(a) R_{JB} = 0 km, for Mw = 5.5; 6.5; 7.0 (b) Mw = 6.5 for R_{JB} = 0; 10; 20 km

Figure 4.17 Spectral accelerations from ITA18-H and ITA18-V(VH) prediction models, for NF mechanism and rock site conditions (EC8-A), for (a) different magnitude and (b) different distances.

The vertical spectral acceleration has always lower or at least the same amplitude with respect to the horizontal one, also in proximity of the source (see Figure 4.17) and is generally of higher frequency (shifted to the short periods), with a sudden attenuation [13]; also, the spectral acceleration increases for increasing magnitude and decreasing distance (Figure 4.17).

The previous findings must be interpreted at the light of the disaggregation analyses performed with ITA18 model for horizontal (from Figure 4.4 and Figure 4.5) and vertical components (from Figure 4.18 to Figure 4.21) by considering all the source zones of L'Aquila case study, relating the ITA18 model to the source zones SZ23, SZ24,SZ25, SZ26, SZ33), whose results must be checked since the distance-magnitude scenario associated to one component can be different from the one associated to its orthogonal, leading to different results. Hence, in the following, the disaggregation analysis is implemented again for the site of L'Aquila considering the two different model for the vertical component.

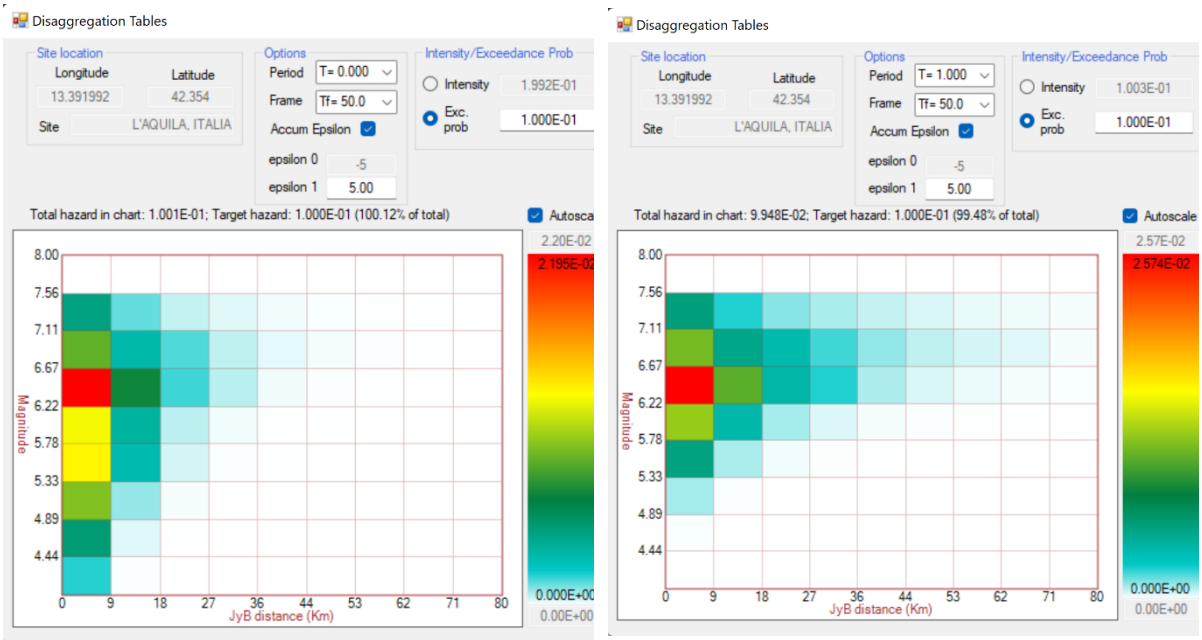

(a) T = 0 s (b) T = 1 s

Figure 4.18 Plot of disaggregation analysis from R-CRISIS, for the site of L'Aquila, with ITA18-V(VH) GMM, Tr = 475 years, for (a) PGA and (b) 1 s.

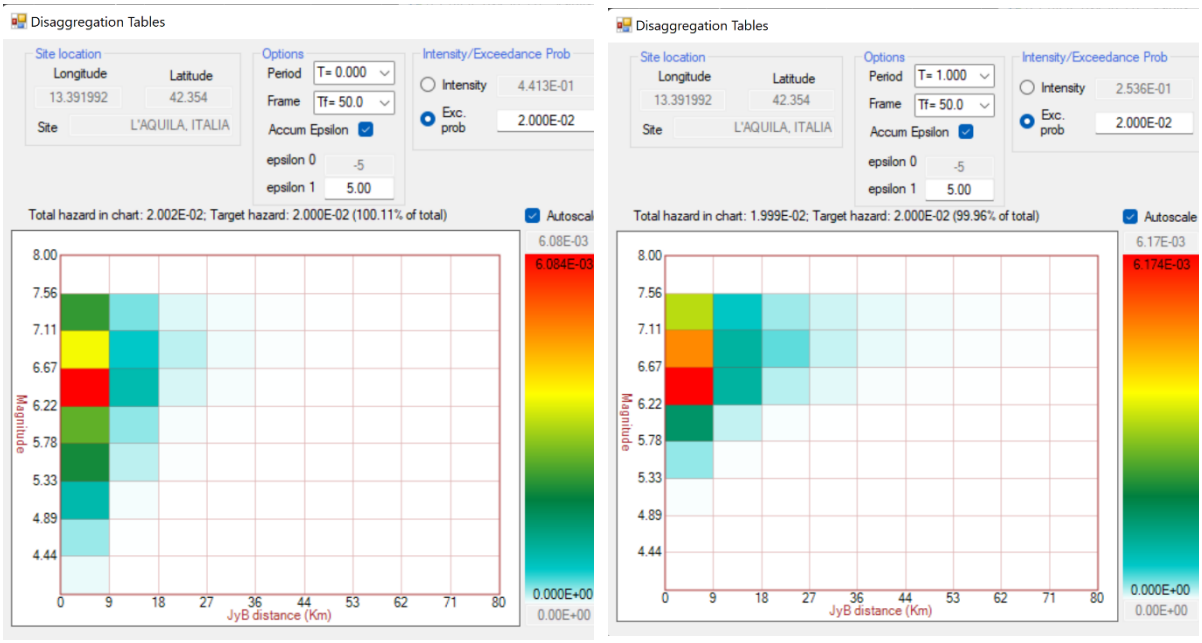

(a) T = 0 s (b) T = 1 s

Figure 4.19 Plot of disaggregation analysis from R-CRISIS, for the site of L'Aquila, with ITA18-V(VH) GMM, Tr = 2475 years, for (a) PGA) and (b) 1 s.

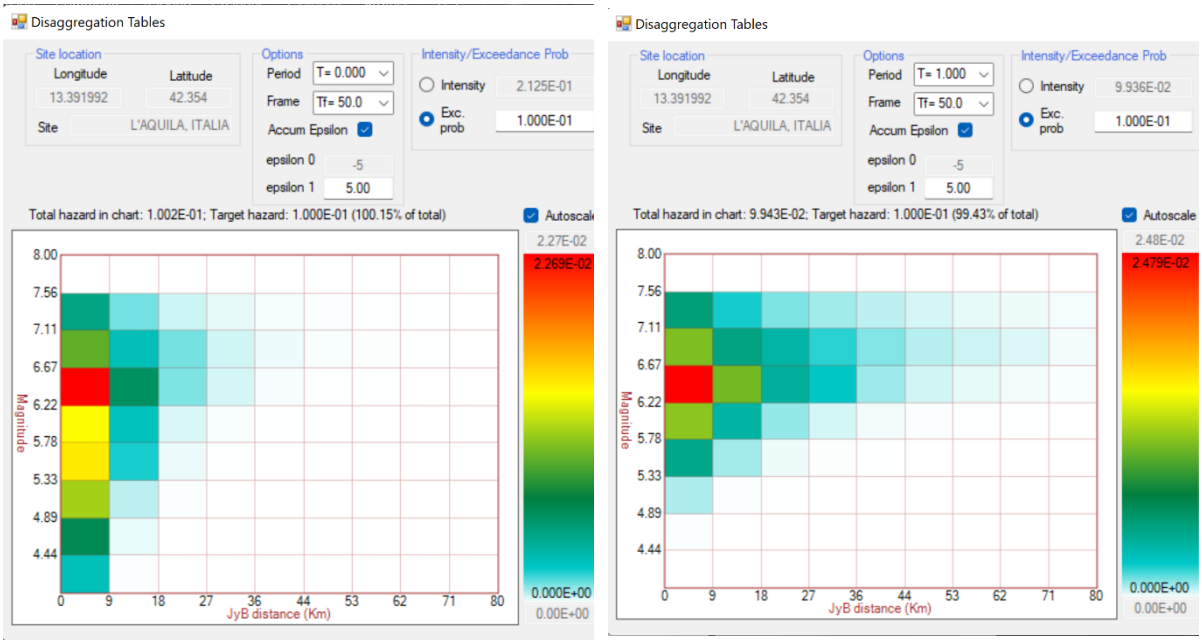

(a) T = 0 s (b) T = 1 s

Figure 4.20 Plot of disaggregation analysis from R-CRISIS, for the site of L'Aquila, with ITA18-V GMM, Tr = 475 years, for (a) PGA and (b) 1 s.

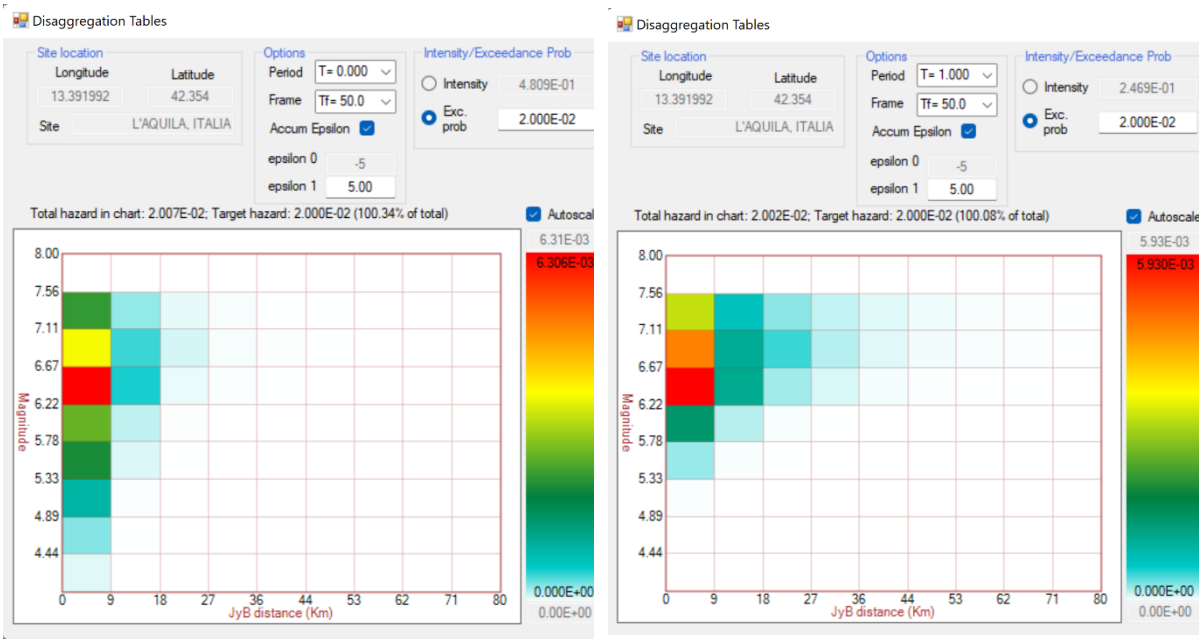

(a) T = 0 s (b) T = 1 s

Figure 4.21 Plot of disaggregation analysis from R-CRISIS, for the site of L'Aquila, with ITA18-V GMM, Tr = 2475 years, for (a) PGA and (b) 1 s.

The predominant scenario obtained from the vertical direction with the two approaches (see Figure 4.18 to Figure 4.21) returns the same range of distance-

magnitude (Mw 6.22-6.67 and R 0-9 km) and very similar values of probability of exceeding the selected intensity level in 50 years in the worst range correspondent to the predominant scenario (identified in figures by a red bin), to those of the horizontal component (see Figure 4.4 and Figure 4.5) which are summarized in Table 4.2.

Table 4.2 Predominant scenario of ITA18 components.

GMM	Tr = 475 years		Tr = 2475 years	
	$T = 0s$	$T = 1s$	$T = 0s$	$T = 1s$
ITA18-H	1.98E-02	2.69E-02	5.61E-03	6.48E-03
ITA18-V(VH)	2.20E-02	2.57E-02	6.08E-03	6.17E-03
ITA18-V	2.27E-02	2.48E-02	6.30E-03	5.93E-03

V/H spectral ratios computed between the UHS calculated with SZ24 and with the corresponding prediction models (ITA18V/ITA18H for the dominant scenario) are shown in Figure 4.22 and Figure 4.23, respectively, to furtherly highlight the difference between the vertical and the horizontal components. Also, the spectral acceleration ratios are shown as function of distance, both at short and long periods in Figure 4.24.

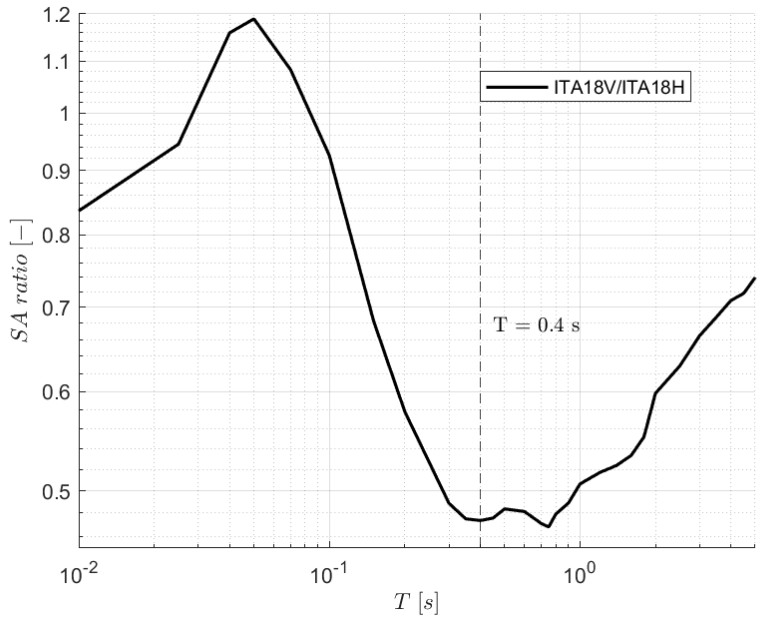

Figure 4.22 Spectral ratio between the prediction models ITA18-V and ITA18-H for Mw 6.5, R = 0 km, NF, EC8-A.

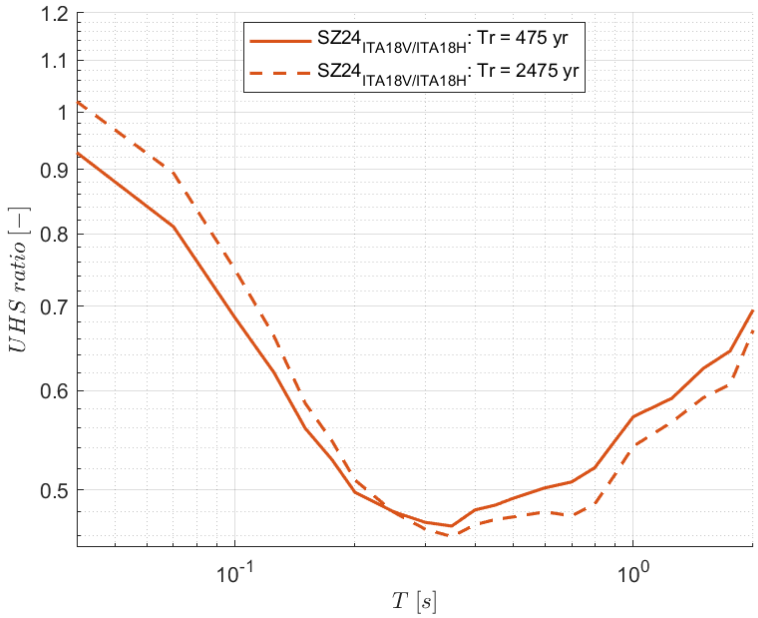

Figure 4.23 UHS ratio in SZ24 for Tr = 475 and Tr = 2475 years from prediction models ITA18-V and ITA18-H.

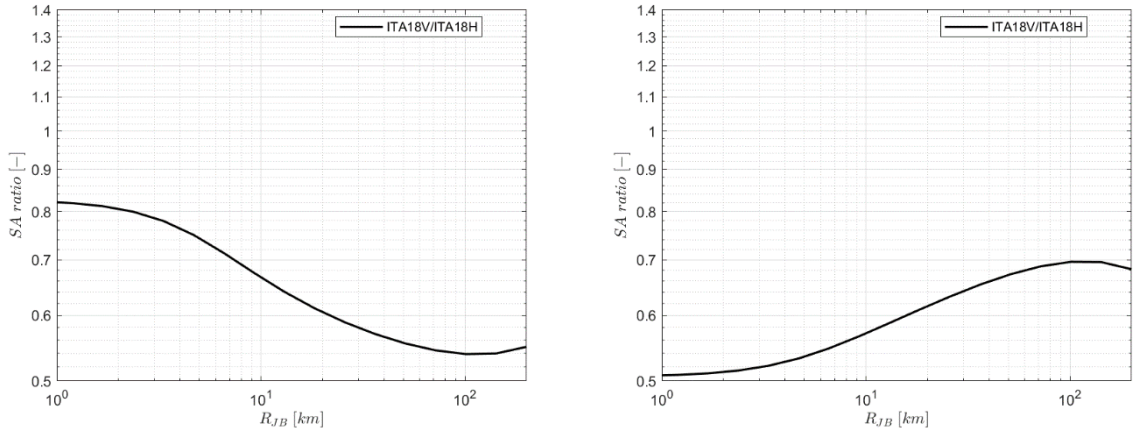

(a) T = 0 s (b) T = 1 s

Figure 4.24 Ground motion prediction models ratio ITA18V/ ITA18H, for Mw = 6.5, NF mechanism and reference rock site (EC8-A) for (a) PGA and (b) 1 s.

As a general comment, the ratio is sensitive to distance and spectral periods, tending to decrease as the period T increases, as expected. In detail, the ratio of the SA assumes an average unitary value at short periods, in accordance to the UHS trend (particularly for long return periods, i.e., 2475 years), meaning that the vertical component shall not be neglected for seismic design purposes; this trend tends to decrease for increasing structural periods, with a minimum of 0.45 at around T = 0.4 s, in agreement with the UHS ratios obtained at Tr = 475 years and at Tr = 2475 years. The same results are also obtained for the two relations attenuating with distances characterized by specular

trends: for increasing periods, the ratio reduces in near-source and increases for higher distances (see Figure 4.24).

Finally, the same calculations and plots performed for ITA18 are done for ITA10 model and shown below in Figure 4.25 and Figure 4.26: spectral ratios computed between the prediction models (ITA10V/ITA10H for the dominant scenario) and the UHS ratio calculated with SZ24 from the prediction models (ITA10-V/ITA10-H), respectively.

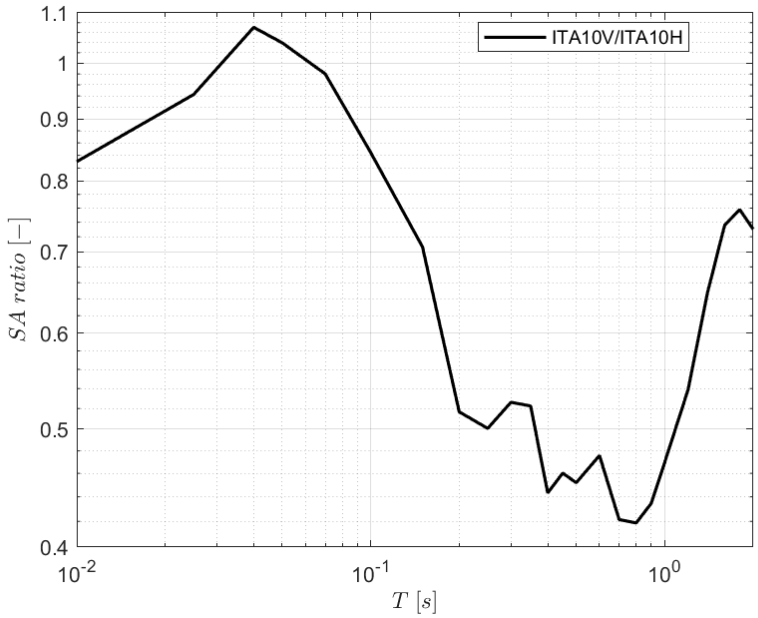

Figure 4.25 Spectral ratio between the prediction models ITA10-V and ITA10-H for Mw 6.5, R = 0 km, NF, EC8-A.

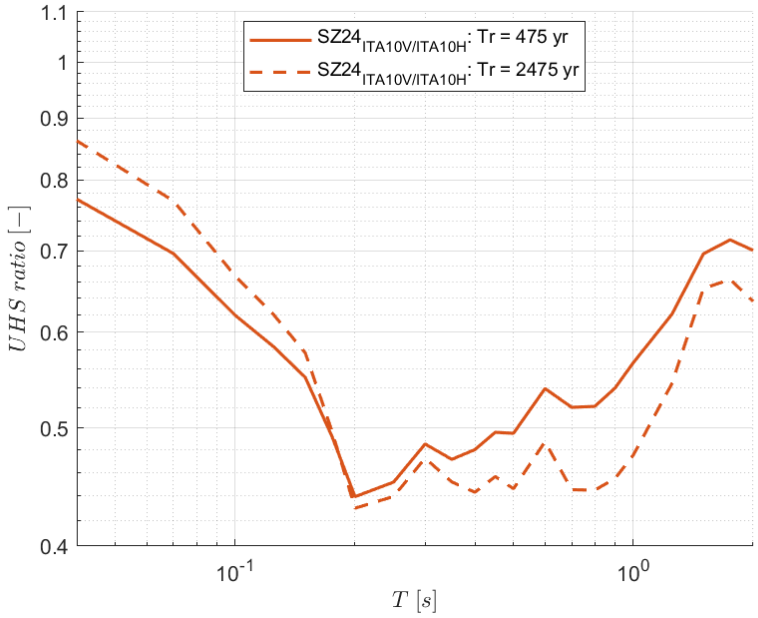

Figure 4.26 UHS ratio in SZ24 for Tr = 475 and Tr = 2475 years from prediction models ITA10-V and ITA10-H.

The spectral ratio is almost unitary at short periods, when we are close to the source (R = 0 km), while for increasing periods the vertical component of ITA10 tends to predict almost half of the respective horizontal spectral acceleration, in accordance with the UHS ratios obtained at Tr = 475 years and at Tr = 2475 years.

Finally, an interesting comparison is also done between the two vertical prediction models ITA18-V and ITA10-V, as shown figures below.

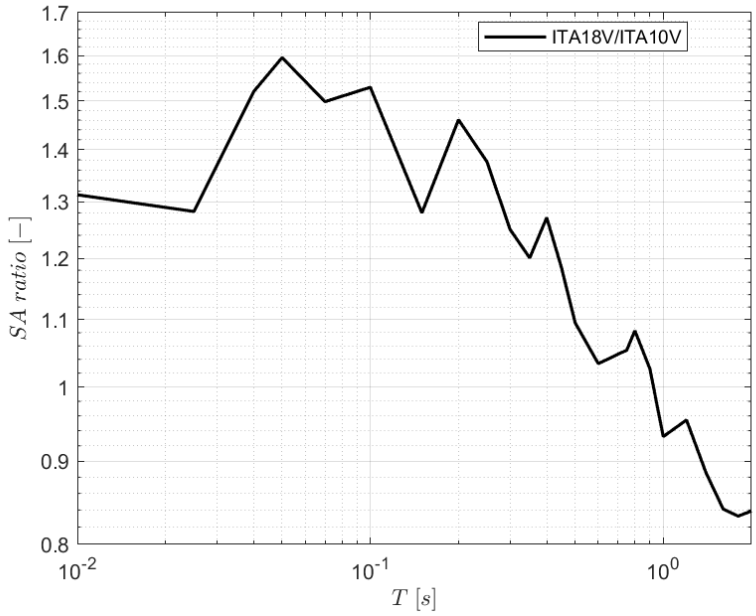

Figure 4.27 Spectral ratio between the prediction models ITA18-V and ITA10-V for Mw 6.5, R = 0 km, NF, EC8-A.

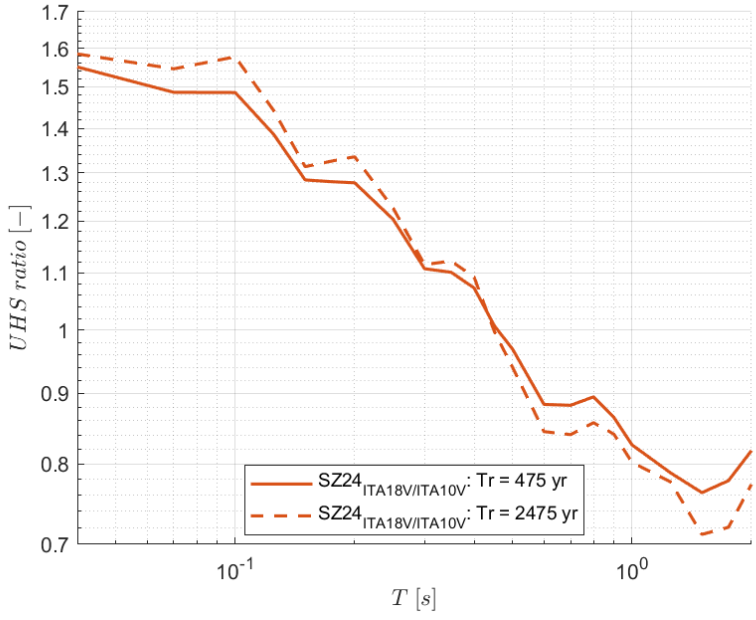

Figure 4.28 UHS ratio in SZ24 for Tr = 475 and Tr = 2475 years from prediction models ITA18-V and ITA10-V.

The results obtained in Figure 4.27 from the ratio of the two GMMs (ITA18V/ITA10V) for the dominant scenario are slightly larger than those found in the subchapter 4.1.1 for the horizontal component, in fact, the average ratio is equal to 1.4 when we are close to the source (R = 0 km) and until a vibration period around T = 0.3 s, while for higher periods, the differences between the two models are almost negligible (average ratio equal to 1.04) as for the horizontal ratios. The average spectral ratios of UHS shown in Figure 4.28 evidence the same trend both at Tr = 475 years and Tr = 2475 years.

4.1.4. Impact of Near-source adjustment to ITA18

The global near-source effects in L'Aquila are accounted for by applying the NESS2 correction implemented by Sgobba et al. [7] to the ITA18 median predictions; indeed, ITA18 is affected by a bias due to the paucity of large-magnitude and short-distance records in its calibration dataset.

UHS are then calculated with reference to the seismogenic source zone 24 by using the ITA18-NESS2 model and comparing with the hazard estimates produced with the ITA18 model (i.e., without correction), as shown in Figure 4.29.

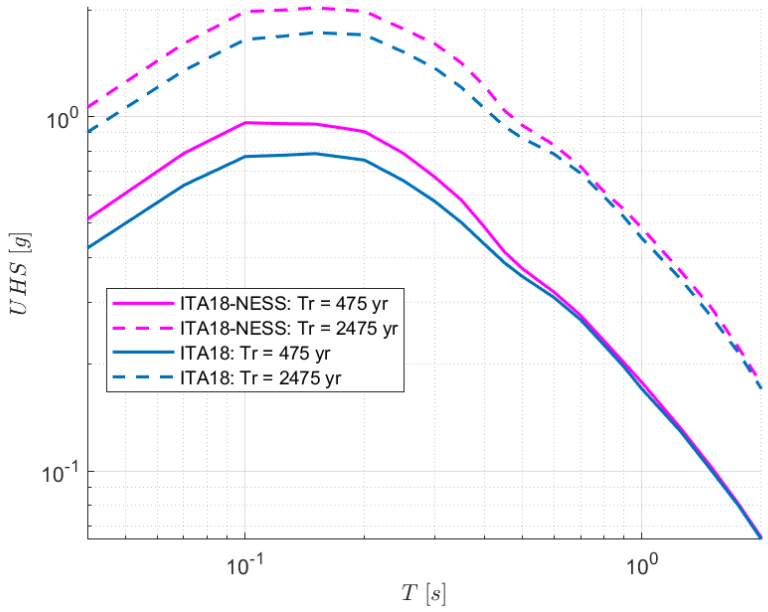

Figure 4.29 UHS for the site of L'Aquila, with SZ24, comparison between the return periods of 475 and 2475 years, for prediction models ITA18 and ITA18-NESS2 with homoscedastic sigma.

The trend observed in the UHS, obtained in Figure 4.29, is supported by the trend of the NESS2 corrective factor and by the spectral accelerations at zero distance (in accordance with the dominant scenario) and Normal-Fault mechanism as shown below.

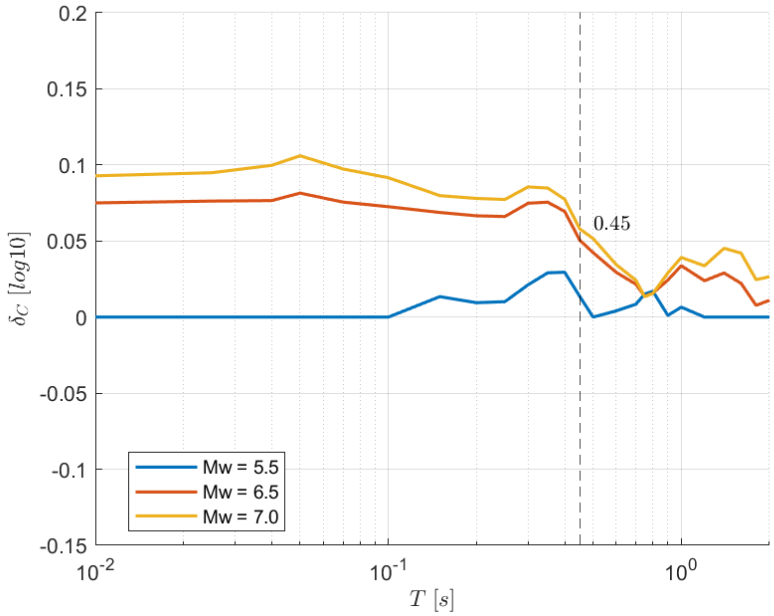

Figure 4.30 Corrective factor in ITA18-NESS, R = 0 km, Mw = 5.5; 6.5; 7.0 with Normal-Fault mechanism.

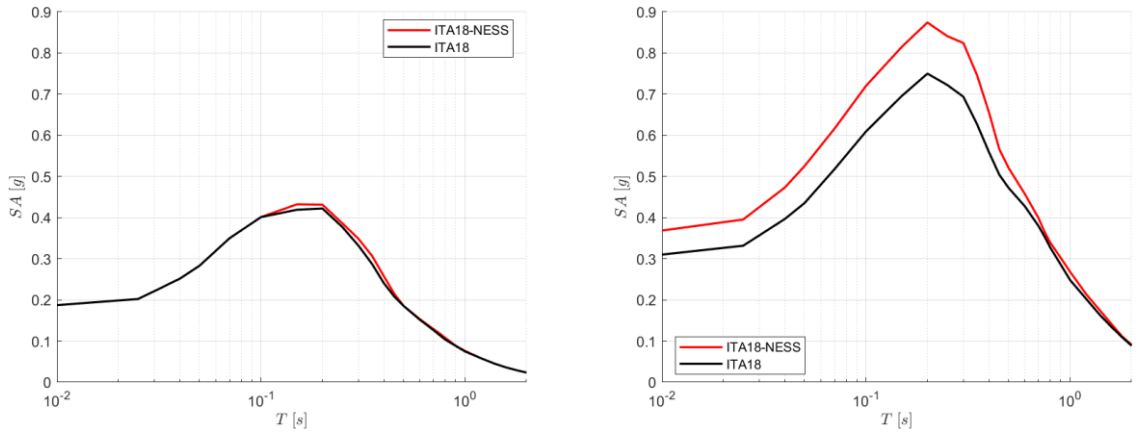

(a) Mw = 5.5 (b) Mw = 6.5

Figure 4.31 Comparison between the horizontal acceleration spectral predictions of ITA18 and ITA18-NESS with Normal-Fault mechanism, R = 0 km.

In more detail, the impact of the NESS2 adjustment is mainly evidenced at short periods, for the area source #24, although the main near-source features identified in the NESS2 dataset are expected to produce larger effects at longer periods. This evidence could depend on the presence of a bias in the residuals between ITA18 and the NESS2 observations at Mw 6.5 (dominant magnitude obtained from the disaggregation analysis of Figure 4.4 and Figure 4.5), in agreement with Paolucci et al. [57]. In fact, the NESS2 correction is modelled on the total residuals and therefore incorporates global near-source effects, also related to inter-event biases caused by a

different average stress-drop and different tectonic environments of NESS events with respect to Italian events.

The near-source corrective factor can be considered negligible for $Mw \leq 5.5$; and for a given threshold $\delta_C = 0.05$ set to be the significant one; in particular, the correction is relevant for the NF mechanisms until periods of about 0.45 s, as shown in Figure 4.31, where the influence of magnitude is also highlighted. A complete view of the spectral accelerations trends is supported in Figure 4.32 with the introduction of various magnitude and then distances.

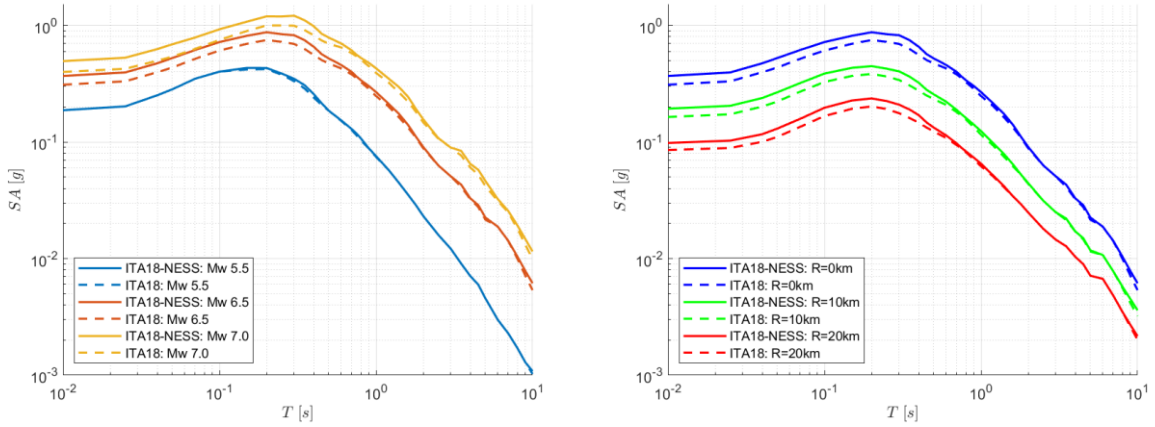

(a) R_{JB} = 0 km, for Mw = 5.5; 6.5; 7.0 (b) Mw = 6.5 for R_{JB} = 0; 10; 20 km

Figure 4.32 Spectral accelerations from ITA18-NESS and ITA18, for NF mechanism and reference rock site conditions (EC8-A), for (a) different magnitude and (b) different distances.

The near-source correction for NF mechanisms thus provides a more significant contribution to the spectral amplification with increasing magnitudes and at decreasing distances, mainly at short-medium periods as shown in Figure 4.32 and Figure 4.30, in agreement with Sgobba et al. (2021).

UHS are then calculated again in Figure 4.33, with reference to the seismogenic source zone 24, by implementing the near-source adjustment for the vertical component ITA18-V(VH) according to the NESS1 dataset [51] and comparing with the hazard estimates produced with the ITA18-V and ITA10-H models (i.e., without correction). A complete view of the spectral accelerations trends is supported in Figure 4.34 with the introduction of various magnitude and then distances.

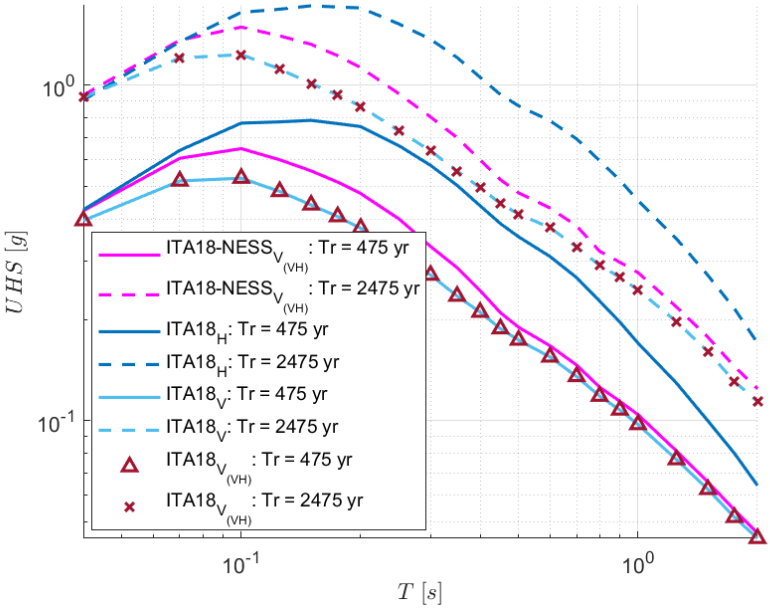

Figure 4.33 UHS for the site of L'Aquila, SZ24, comparison between the return periods of 475 and 2475 years, prediction models ITA18H, ITA18V, ITA18V(VH) and ITA18V(VH)-NESS1.

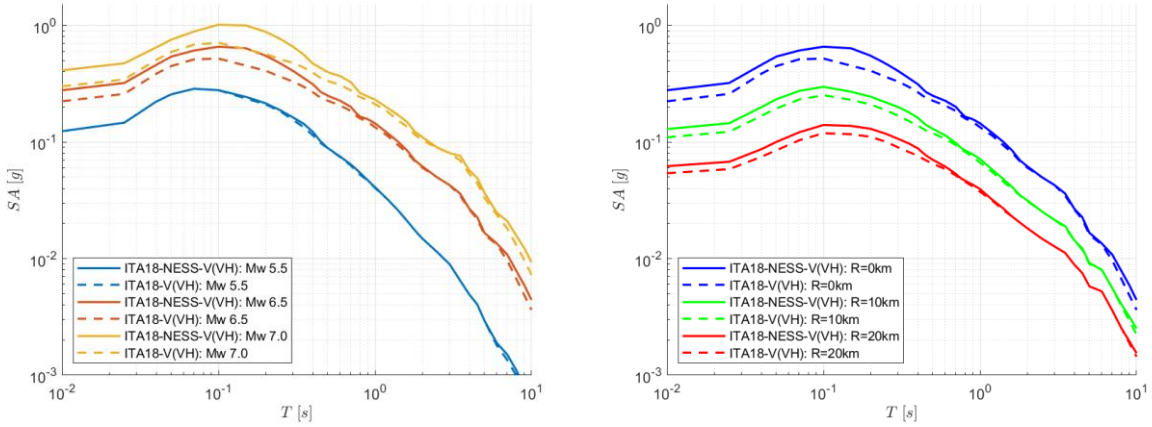

(a) R_{JB} = 0 km, for Mw = 5.5; 6.5; 7.0 (b) Mw = 6.5 for R_{JB} = 0; 10; 20 km

Figure 4.34 Spectral accelerations from ITA18-NESS and ITA18 for V(VH) direction, for NF mechanism and rock site conditions (EC8-A), for (a) different magnitude and (b) different distances.

The same observation evidenced until now are obtained with larger impact at short periods (see Figure 4.33 and Figure 4.34) and slightly larger amplification at long return periods, and a more significant contribution to the spectral amplification with increasing magnitudes and at decreasing distances. Even though the near-source correction amplifies the spectral acceleration of the vertical component, the horizontal one remains the dominant UHS curve.

V/H spectral ratios computed between the UHS calculated with SZ24 and with the corresponding prediction models (considering the predominant scenario Mw 6.5 and

R = 0 km) are shown below by comparing the results obtained from ITA18-V(VH)-NESS/ITA18H and ITA18V/ITA18H in Figure 4.35 and Figure 4.36, respectively for the prediction ratios and UHS ratiosFigure 4.22, to furtherly highlight the difference between the vertical component with and without near source correction and the horizontal components not corrected.

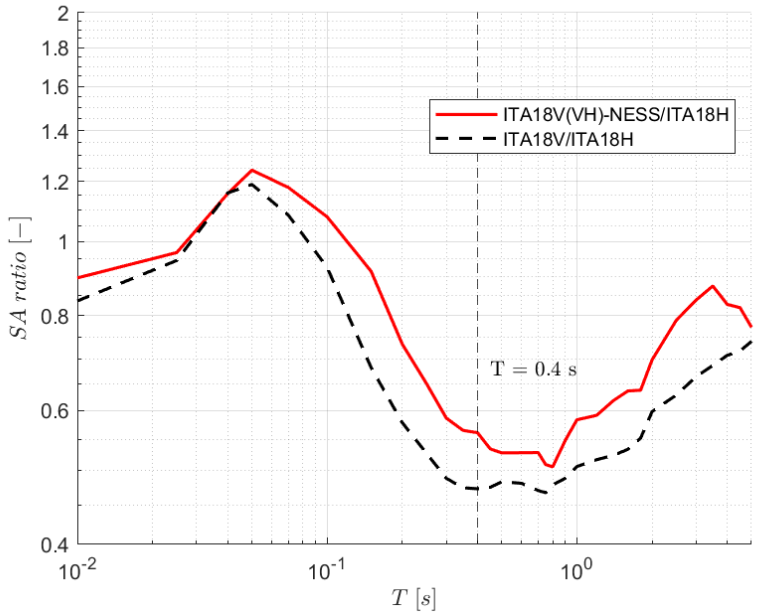

Figure 4.35 Spectral ratio between the prediction models ITA18-V(VH)-NESS and ITA18-H for Mw 6.5, R = 0 km, NF, EC8-A.

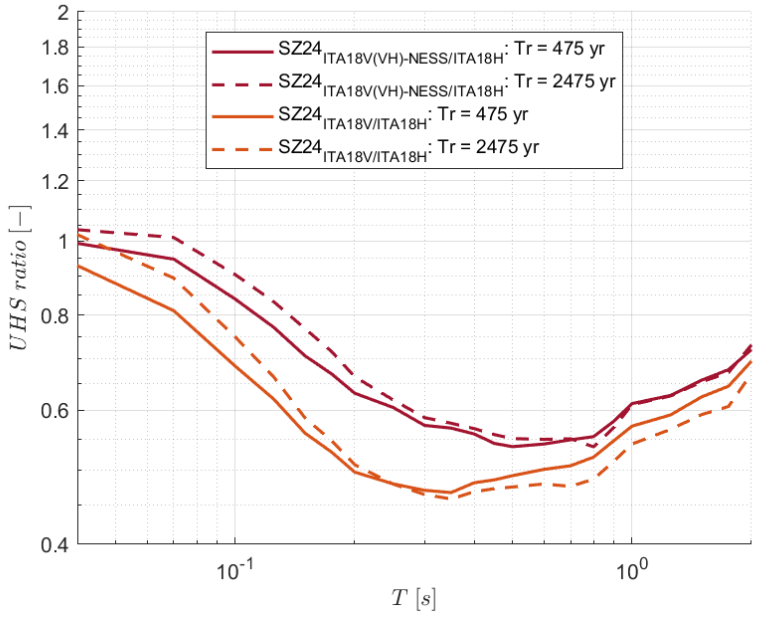

Figure 4.36 UHS ratio in SZ24 for Tr = 475 and Tr = 2475 years from prediction models ITA18-V(VH)-NESS and ITA18-H.

As a general comment, the ratio is sensitive to distance and spectral periods, tending to decrease as the period T increases, as expected. In detail, the ratio of the SA assumes an average unitary value at short periods, in accordance with the UHS trend (for both the return periods, i.e., 475 and 2475 years), meaning that the vertical component shall not be neglected for seismic design purposes; this trend tends to decrease for increasing structural periods, with a minimum of 0.55 at around T = 0.4 s. As expected, as the near-source correction account for major adjustment to the amplification ratios.

4.2. Gemona del Friuli case study

In the previous section, it was shown that in the case of the L'Aquila site, which is characterized by normal faults, the NESS2 correction produces more significant effects mainly over short periods. In the following, we intend to assess whether the NESS2 correction may have a different effect in the case of sites characterized by a different style of faulting, as highlighted by Sgobba et al. [7]. Therefore, we examine the hazard at Gemona del Friuli test site, where reverse styles of faulting prevail, for the sole purpose of verifying the performance of the UHS calculated using the ITA18-NESS2 model. For further details, the Appendix A have a complete description of the PSHA results.

The municipality of Gemona del Friuli (Lat: 46.279; Lon: 13.135) is sited in Northern-East part of Italy in the region of Friuli-Venezia Giulia, it is characterized by a Thrust-Fault mechanism, and it is known for one of the largest events (i.e., Mw 6.5 Friuli earthquake May 6, 1976) recorded in Northern Italy, more precisely in the Southern Alps within the active collision zone between Eurasia and Adria plates.

The site of Gemona del Friuli has been examined in terms of seismic hazard to evaluate the ground motion effects in near-source conditions of the horizontal and the vertical components, calibrated for shallow crustal earthquakes in the Italian active tectonic regions [6] (ITA18-NESS). The seismogenic zones considered for the seismic hazard evaluation is shown in the figure below: the area source #3 where Gemona del Friuli is sited, and those adjacent #1, #2, #4, #13 defined in ZS16 [4].

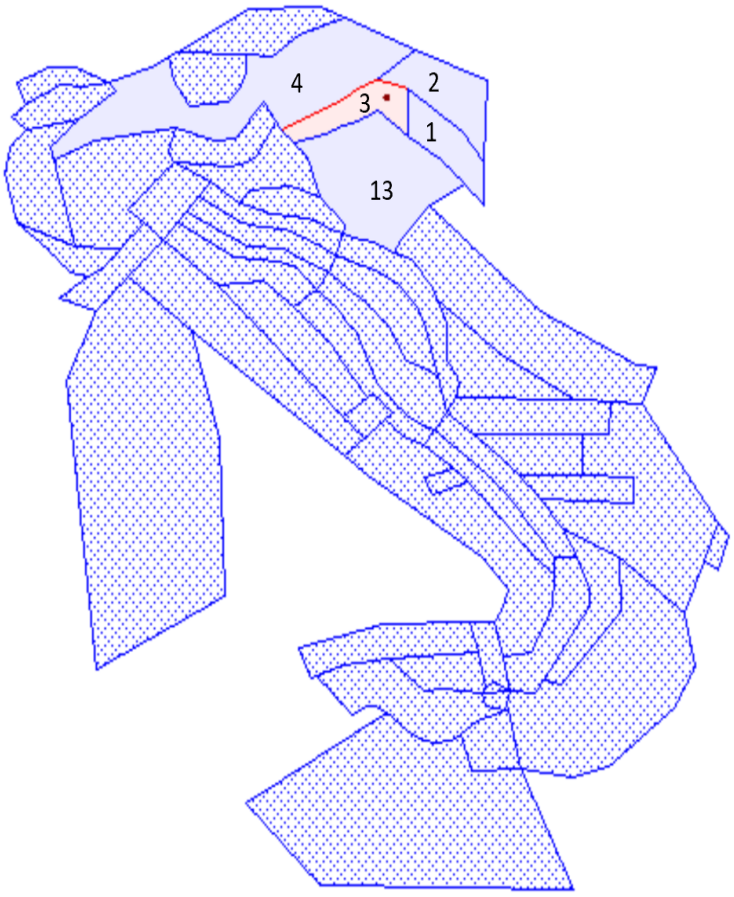

Figure 4.37 Map of Italy - case study of Gemona del Friuli: the SZ considered are those with uniform blue color, the SZ containing the site is evidenced in red, other SZ are in dotted blue and are neglected.

The seismicity of each source areas is taken from Visini et al. [4] and is defined by the Gutenberg-Richter relationship, whose parameters are summarized in the following table.

Table 4.3 Gutenberg-Richter parameters, styles of faulting and depth for the SZ used in the SH for the site of Gemona del Friuli.

GR	SZ3	SZ1	SZ2	SZ4	SZ13	Rif.
b	0.93	1.1	1.2	1.2	1	Suppl. 3
M_0	4.42	4.19	4.19	4.19	4.42	Suppl. 3
$\lambda(M_0)$	0.3579	0.1663	0.227	0.0651	0.0032	Suppl. 3
β	2.14140	2.53284	2.76310	2.76310	2.30259	$ln(10) \cdot b$
M_{max}	6.9	6.9	6.9	6.7	6.9	Suppl. 3
Sof	TF	SS	SS	SS	U	Visini2022
Hypo	7	10	7	8	5	Suppl. 1
K1	0.00571	0.011	0.011	0.011	0.0101	W&C

As anticipated, analysis at the site aims to show the global impact on near-source effects of a different style of faulting; hence, the UHS is provided in Figure 4.38, considering the dominant source zone (SZ03), with and without the NESS correction.

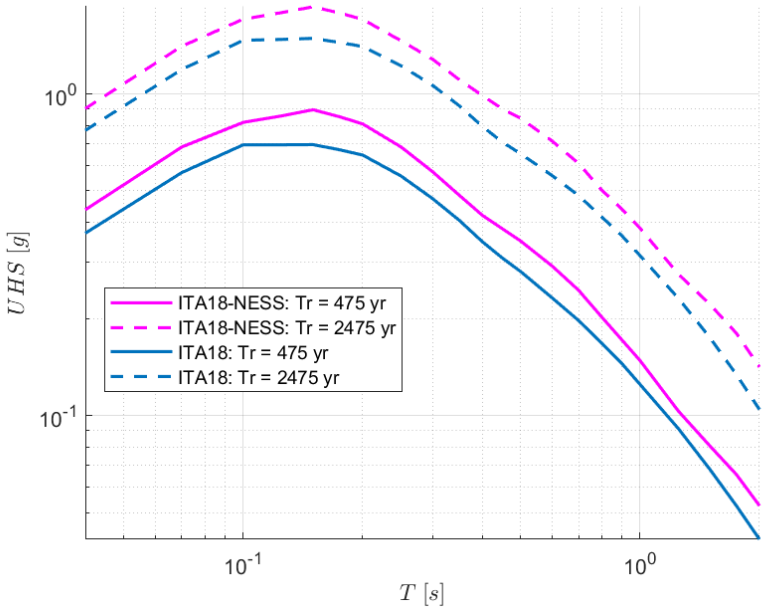

Figure 4.38 UHS for the site of Gemona del Friuli, SZ03, comparison between the return periods of 475 and 2475 years, for prediction models ITA18 and ITA18-NESS2.

When ITA18-NESS is applied to a Thrust-Fault mechanism site, major impacts are found also on the longer periods, probably due to the enrichment of TF mechanism in NESS2 through the introduction of worldwide events, with respect to ITA18 dataset, which is instead dominated by normal style of faulting, in agreement with Sgobba et al. [7]; this evidence is also validated by the uniform hazard spectrum depicted above, computed for the dominant source zone (SZ03). To support the results, the trends of the corrective factor are shown in Figure 4.39, considering a zero distance in Thrust-Fault mechanism, and in Figure 4.40 the influence on the spectral shapes. A complete view of the spectral accelerations trends is provided also in Figure 4.41 with the introduction of various magnitude and then distances.

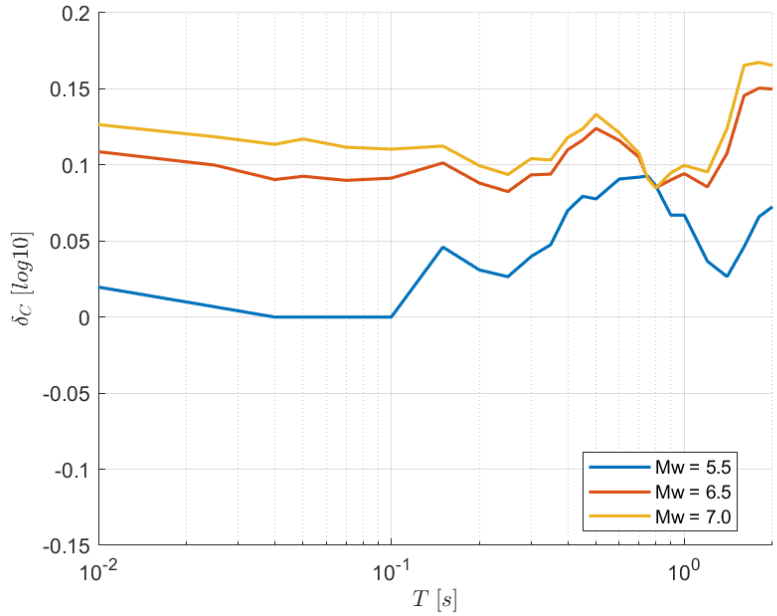

Figure 4.39 Corrective factor in ITA18-NESS, R = 0 km, Mw = 5.5; 6.5; 7.0 with Thrust-Fault mechanism.

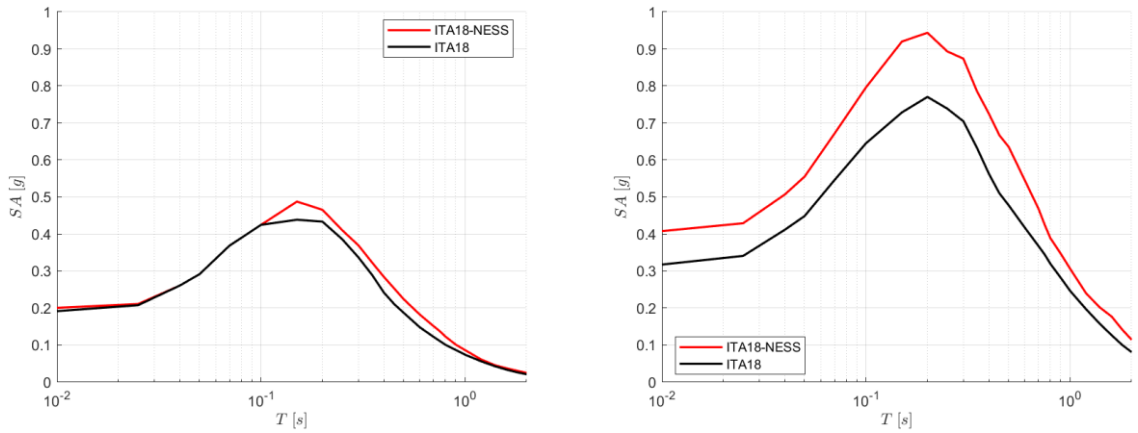

(a) Mw = 5.5 (b) Mw = 6.5

Figure 4.40 Comparison between the horizontal spectral acceleration predictions of ITA18 and ITA18-NESS with Thrust-Fault mechanism, R = 0 km.

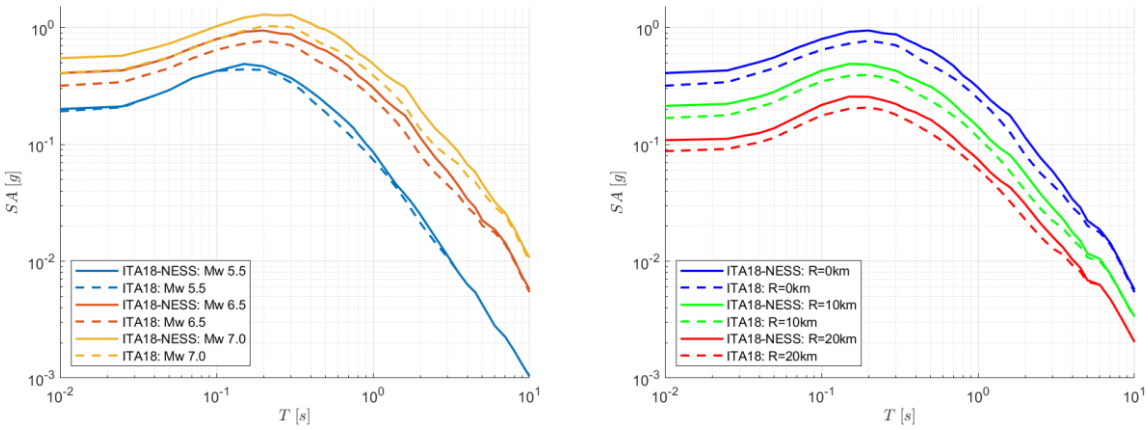

(a) R_{JB} = 0 km, for Mw = 5.5; 6.5; 7.0 (b) Mw = 6.5 for R_{JB} = 0; 10; 20 km

Figure 4.41 Spectral accelerations from ITA18-NESS2 and ITA18, for TF mechanism and rock site conditions (EC8-A), for (a) different magnitude and (b) different distances.

The near-source correction (NESS2) provides a broadband contribution to the spectral amplification with increasing magnitude and decreasing distances (Figure 4.41), in agreement with Sgobba et al. [7], and has significant influence for moment magnitude larger than 5.5, as depicted in Figure 4.40 and evidenced in terms of spectral shapes in Figure 4.40. Moreover, the near-source adjustment is applied also for the vertical component ITA18-V(VH) according to the NESS1 dataset [51], whose results are shown in Figure 4.42 and Figure 4.43, in terms of UHS obtained for the dominant SZ03, by implementing the near-source adjustment for the vertical component ITA18-V(VH) according to the NESS1 dataset [51] and comparing with the hazard estimates produced with the ITA18-V and ITA10-H models (i.e., without correction), and the related spectral acceleration with various magnitude and then distances.

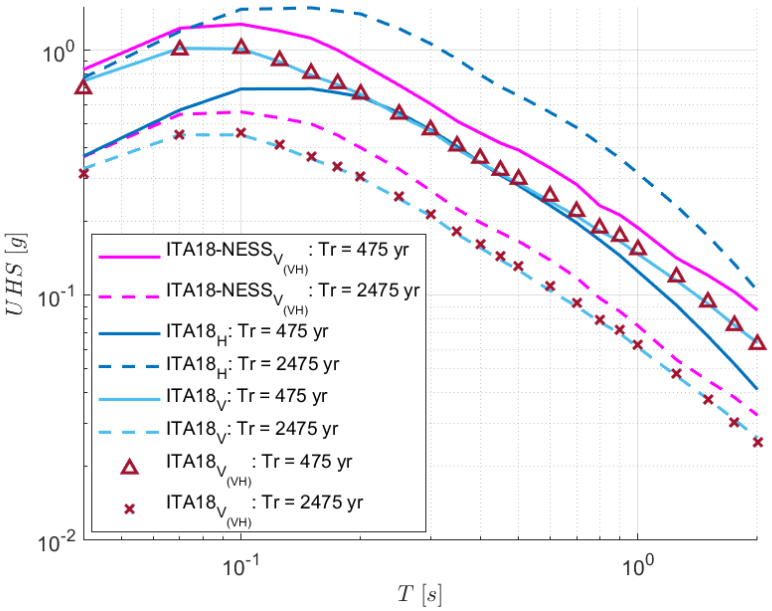

Figure 4.42 UHS for the site of Gemona del Friuli, SZ03, comparison between the return periods of 475 and 2475 years, prediction models ITA18H, ITA18-V, ITA18-V(VH) and ITA18-V(VH)-NESS1.

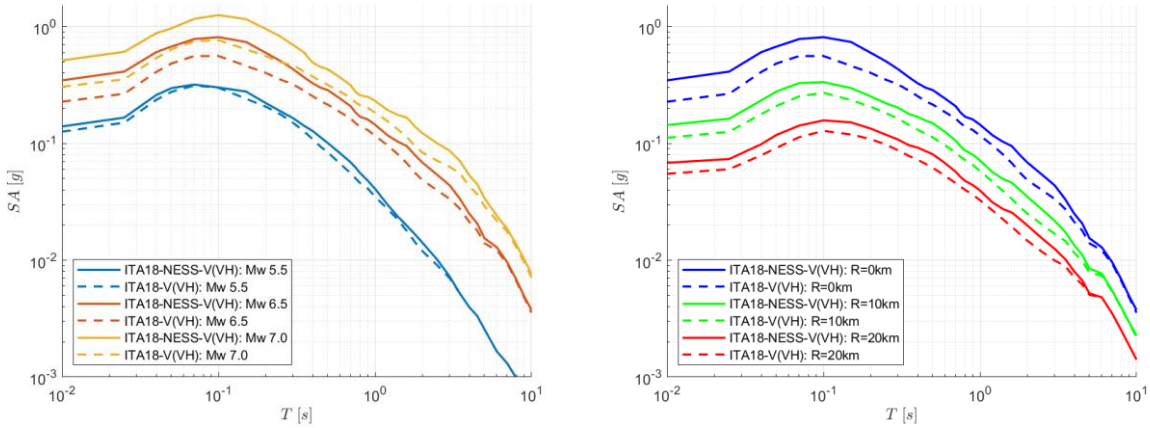

(a) R_{JB} = 0 km, for Mw = 5.5; 6.5; 7.0 (b) Mw = 6.5 for R_{JB} = 0; 10; 20 km

Figure 4.43 Spectral accelerations from ITA18-NESS1 and ITA18 for V(VH) direction, for TF mechanism and rock site conditions (EC8-A), for (a) different magnitude and (b) different distances.

The same observations evidenced until now are obtained: the UHS of Figure 4.42 evidence larger impact at long vibration periods for a Thrust-Fault mechanism site, a broadband contribution is provided with the near-source correction (NESS1) to the spectral amplification in Figure 4.43, with increasing magnitude and decreasing distances. Even though the near-source correction amplifies the spectral acceleration of the vertical component, the horizontal one remains the dominant UHS curve.

V/H spectral ratios computed between the UHS calculated with SZ03 and with the corresponding prediction models (considering the predominant scenario Mw 6.5 and R = 0 km) are shown below by comparing the results obtained from ITA18-V(VH)-NESS/ITA18H and ITA18V/ITA18H in Figure 4.44 and Figure 4.45, respectively for the prediction ratios and UHS ratios, to furtherly highlight the difference between the vertical component with and without near source correction and the horizontal components not corrected.

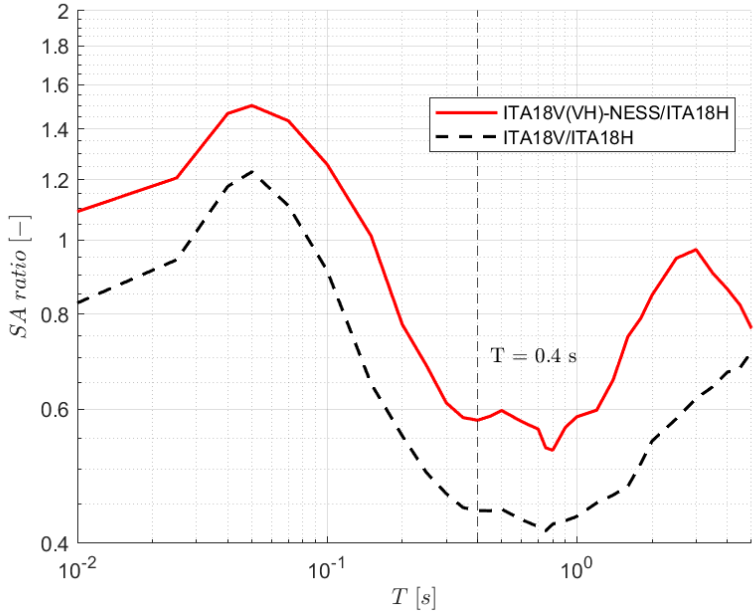

Figure 4.44 Spectral ratio between the prediction models ITA18-V(VH)-NESS and ITA18-H for Mw 6.5, R = 0 km, NF, EC8-A.

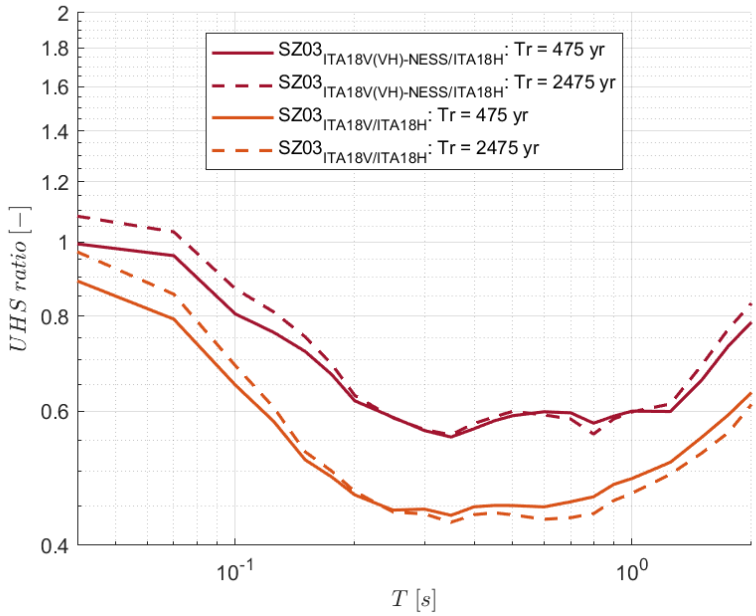

Figure 4.45 UHS ratio in SZ24 for Tr = 475 and Tr = 2475 years from prediction models ITA18-V(VH)-NESS and ITA18-H.

As a general comment, the ratio is sensitive to distance and spectral periods, tending to decrease as the period T increases, as expected. In detail, the ratio of the SA assumes an average unitary value at short periods, in accordance with the UHS trend (for both the return periods, i.e., 475 and 2475 years), meaning that the vertical component shall not be neglected for seismic design purposes; this trend tends to decrease for increasing structural periods, with a minimum of 0.55 at around T = 0.4 s. As expected, as the near-source correction account for broadband adjustment to the amplifications, the ratios evidence a further relevance of the vertical component on different structural periods.

4.3. Zafferana Etnea case study

This case-study is introduced to analyse the effects of considering a volcanic GMM (the LL19 model) instead of an active shallow crustal one (the ITA18 model). Results calculated with R-CRISIS in terms of UHS are therefore compared. The municipality of Zafferana Etnea (Lat: 37.692; Lon: 15.105) is sited in the Italian region of Sicily, and more precisely in the area source #49 (Etna) of ZS16 [4], characterized by a Strike-Slip mechanism. The Mt. Etna region is characterized by earthquakes with hypocentral depth < 10 *km* assigned to the volcanic domain (source zone #49) and by earthquakes with hypocentral depth ≥ 10 *km* assigned to the underlying active crustal area source (#44, #45, #46) [4].

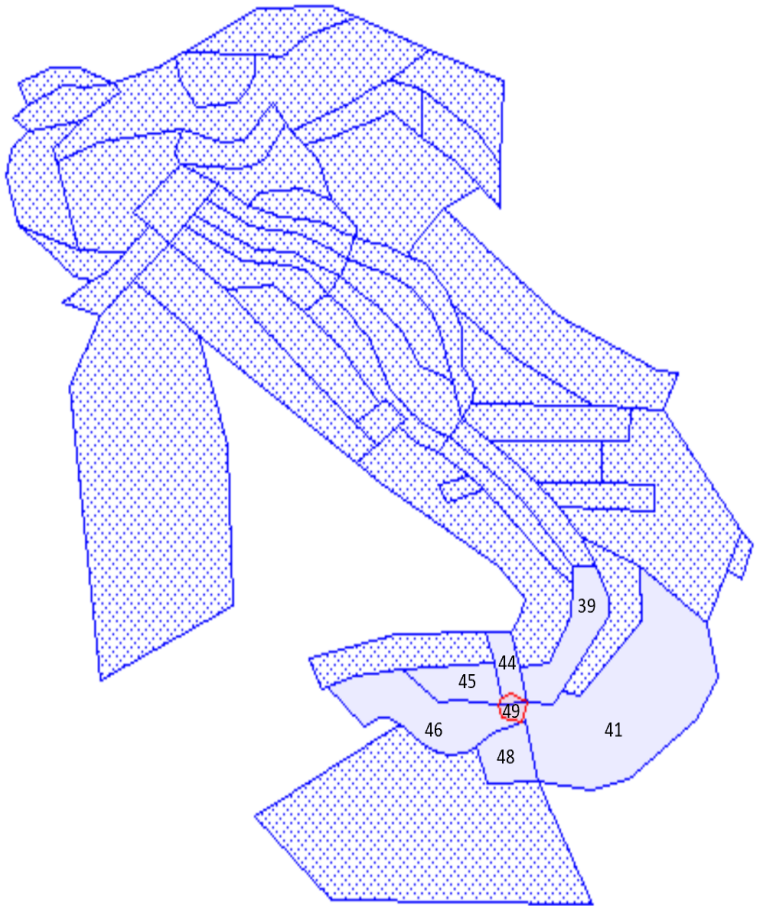

Figure 4.46 Map of Italy - case study of Zafferana Etnea: the SZ considered are those with uniform blue color, the SZ containing the site is evidenced in red, other SZ are in dotted blue and are neglected.

The seismicity of each SZ is described after Visini et al. [4]; the following table show the parameters of the GR relationships adopted.

Table 4.4 Gutenberg-Richter parameters, styles of faulting and depth of SZ adopted in the PSHA study of Zafferana Etnea.

GR	SZ49	SZ39	SZ41	SZ44	SZ45	SZ46	SZ48	Rif.
b	1.29	0.7	1.2	1.11	0.96	1.2	0.7	Suppl. 3
M_0	3.96	3.96	4.42	4.19	4.19	4.42	4.42	Suppl. 3
$\lambda(M_0)$	0.0412	0.2653	0.0532	0.0927	0.0848	0.0897	0.732	Suppl. 3
β	2.97033	1.61181	2.7631	2.55587	2.21048	2.7631	1.61181	$ln(10) \cdot b$
M_{max}	5.6	7.5	6.7	6.7	6.7	6.7	7.6	Suppl. 3
Sof	SS	NF	SS	SS	SS	SS	SS	Visini2022
Hypo1	3	8	-	9	6	10	-	Suppl. 1
Hypo2	-	-	25	-	-	-	22	Suppl. 1
K1	0.011	0.0207	0.011	0.011	0.011	0.011	0.011	W&C

The Italian volcanic seismicity is typically characterized by a faster attenuation with distance than the shallow crustal one, according to macroseismic observations [58] and, more recently to strong and weak motion recordings; besides, large values of peak parameters of records are expected very close to the source [8] [14].

A complete view of the seismic hazard behaviour is reported in Figure 4.47, where the UHS calculated for all the SZ at apply are shown for two values of the probability of exceedance, using the ITA18 attenuation model for sources #39, #41, #44, #45, #46, #48 and the LL19 model considering only shallow events ($depth < 5km$) for the #49 source.

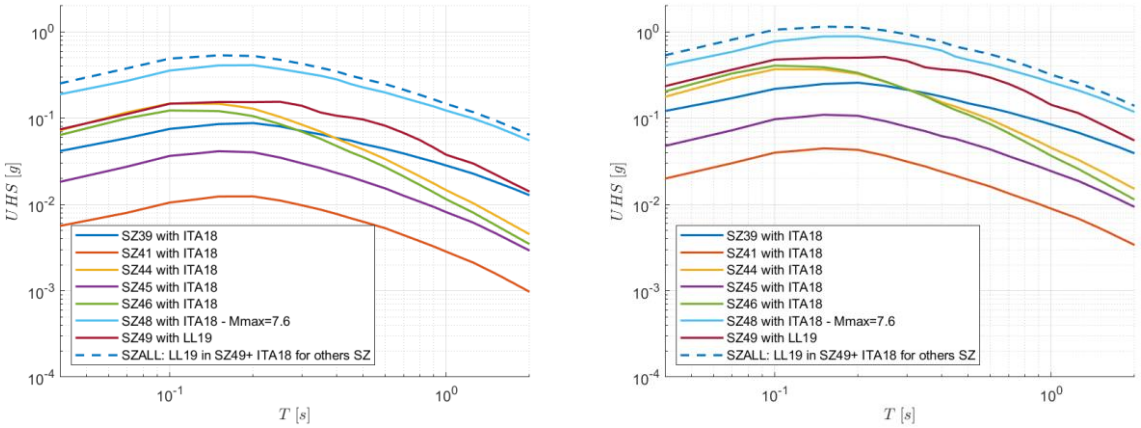

(a) Tr = 475 years (b) Tr = 2475 years

Figure 4.47 UHS for the site of Zafferana Etnea with prediction model ITA18 for SZ39, SZ41, SZ44, SZ45, SZ46, SZ48 and LL19 for SZ49, with the related SZALL.

The strong influence of the maximum magnitude is noticeable with a trend inversion of the spectral shape, leading to an enrichment of the spectral content at long periods: the SZ48 is prevailing on the other seismogenic zones at longer periods, because of the high *Mmax* equal to 7.6, in fact, the SZ48 curve nearly overlaps the SZALL across all periods. Also, the SZ49 is the seismogenic zone with the lower $Mmax$ which is equal to 5.6, leading to a predominance in the short periods, even though, still with lower amplitudes than SZ48.

Beware that here the ITA18 GMM is calibrated according to the rupture distance instead of the Joyner-Boore assumed for the precedent cases study (ITA18 is calibrated for both R_{Rup} and R_{JB} distances); this choice is motivated by a comparable metric distance formulation with respect to the LL19 volcanic model, which is calibrated only with R_{Hypo}, for which the depth of the events is relevant. In fact, the rupture distance is the closest distance to rupture surface and contains information on both the depth and the dip of the faults, whereas the Joyner-Boore distance is the shortest distance from a site to the surface projection of the rupture [33].

To deeper investigate the role of the volcanic model within the hazard assessment of the site, thereafter, a comparison is performed between the two GMM ITA18 and LL19, by focusing the attention on the hazard spectra obtained activating all the SZ, i.e., SZALL: in this case, the volcanic model (modelled with LL19) is related only to the volcanic area source (#49) whereas the other seismogenic zones are modelled with ITA18. It should be noted that although there is overlap between SZ #46 and #49, the events are distinguished by focal depth (surface seismicity of a volcanic nature is made to belong to zone #49 while deeper seismicity of a tectonic nature belongs to zone 46).

As a results, the Figure 4.48 shows: on one hand there are all the SZ modelled with ITA18 and on the other hand all the SZ are modelled with ITA18, except of SZ49 which is alternatively modelled with LL19 (ITA18+ LL19 in SZ49 hereafter).

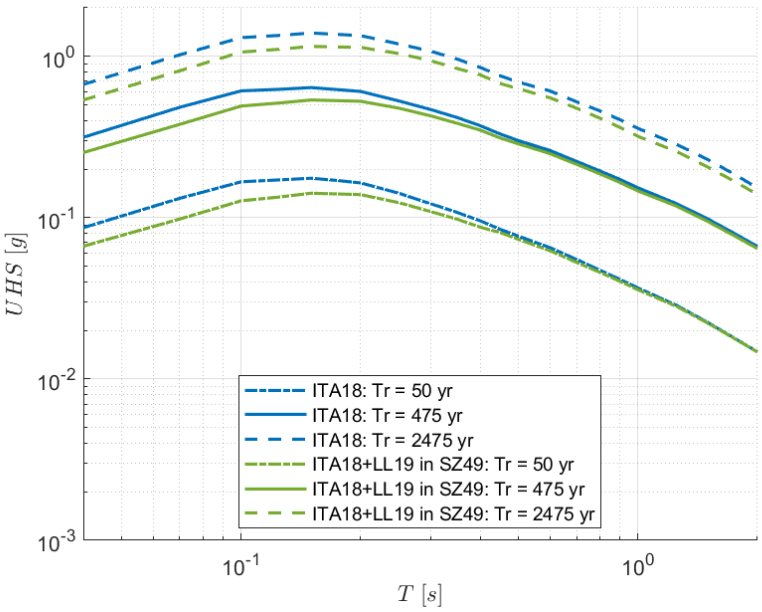

Figure 4.48 UHS for the site of Zafferana Etnea, comparison between the return periods of 475 and 2475 years, seismogenic zone SZALL.

The three sets of UHS curves reported in Figure 4.48 evidence no significant differences, due to the dominance of the tectonic seismicity which is particularly influenced by the SZ48; the volcanic model, while making a very large contribution to the total hazard, does not control the seismic hazard when all seismogenic zones adjacent to the site are considered active; for decreasing return periods, the UHS associated with the use of the two GMMs widens at short vibration periods and gets closer at long periods, however, no trend reversal is observed at return periods of 50 years (or lower).

Validation of results is required and is implemented with the representation of ITA18 and LL19 GMM reported in Figure 4.51, interpreted at the light of the dominant scenario (Mw 4.44-5.33, R_{Rup} = 0-12 km) obtained through the disaggregation analysis tool available in the software (see Figure 4.49 and Figure 4.50), by considering all the

source zones of Zafferana Etnea case study, relating the LL19 model to the volcanic source zone SZ49, and the ITA18 model to the others (SZ39, SZ41, SZ44, SZ45, SZ46, SZ48).

The spectral accelerations related to ITA18 and LL19 are also compared in Figure 4.52, considering various magnitude and then distances.

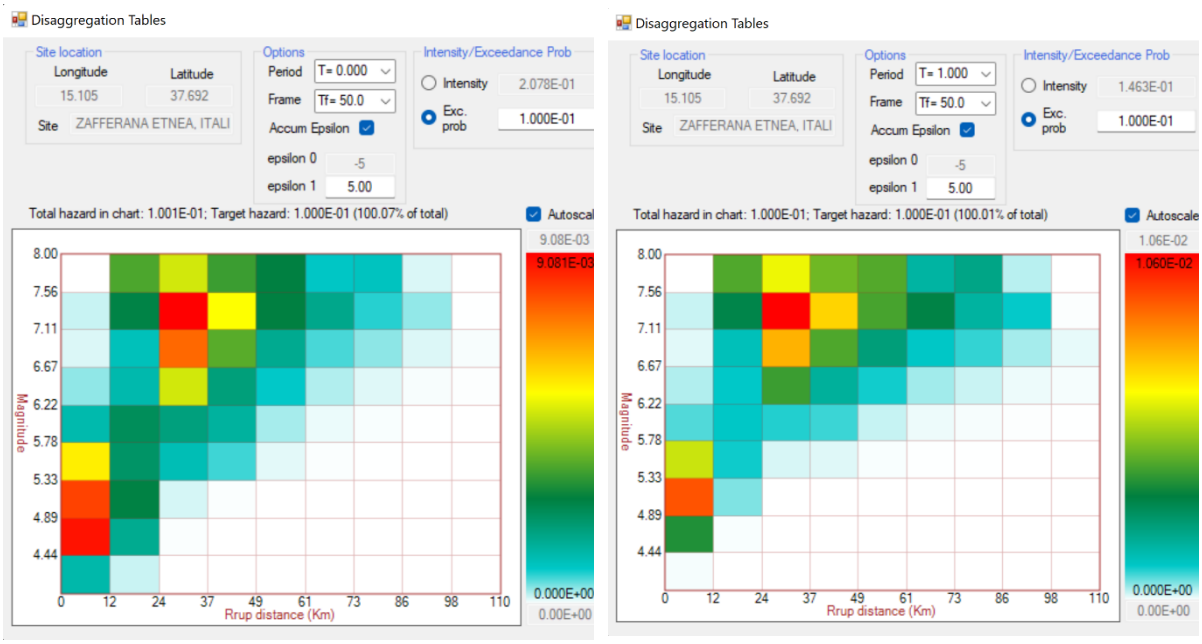

(a) T = 0 s

(b) T = 1 s

Figure 4.49 Plot of disaggregation analysis from R-CRISIS for the site of Zafferana Etnea, with ITA18 GMM and LL19 applied to SZ49, Tr = 2475 years, for (a) PGA and (b) 1 s.

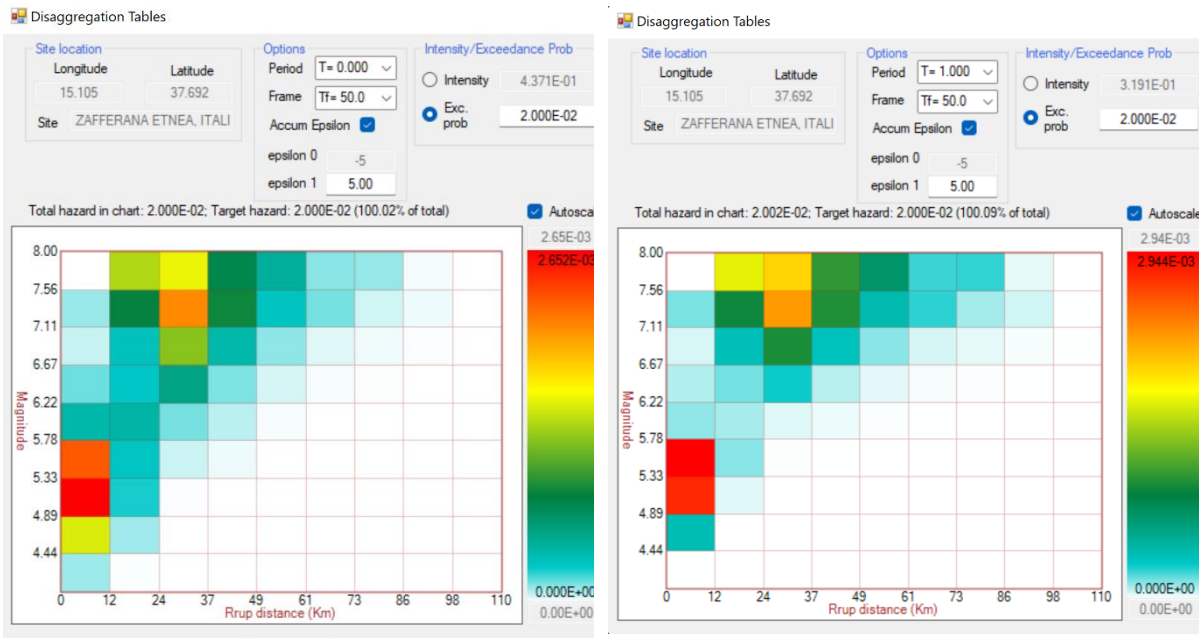

(a) T = 0 s (b) T = 1 s

Figure 4.50 Plot of disaggregation analysis from R-CRISIS for the site of Zafferana Etnea, with ITA18 GMM and LL19 applied to SZ49, Tr = 475 years, for (a) PGA and (b) 1 s.

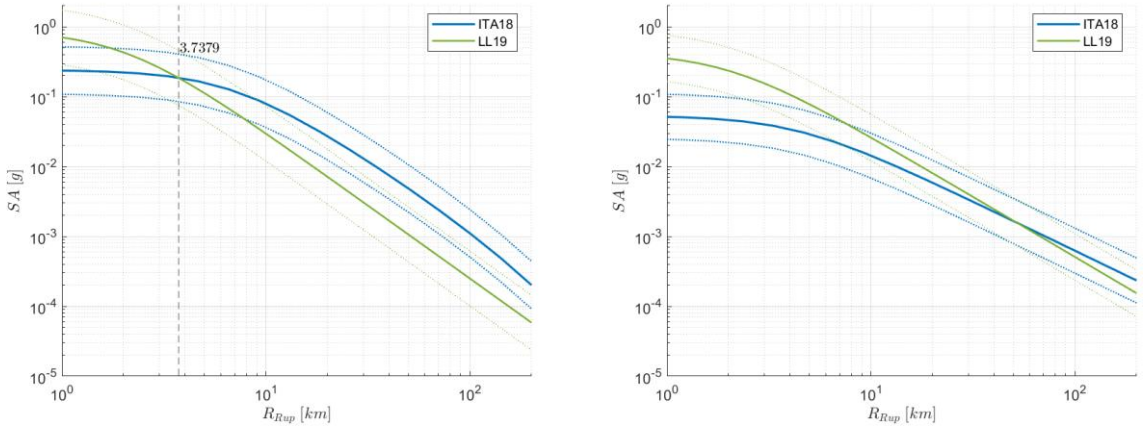

(a) T = 0 s (b) T = 1 s

Figure 4.51 SA predictions according to ITA18 and LL19, for Mw = 4.9, SS mechanism and reference rock site (EC8-A).

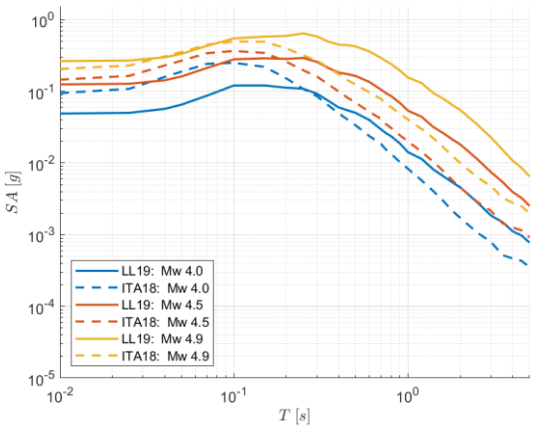

(a) R_{Rup} = 3 km, for Mw = 4.0; 4.5; 4.9

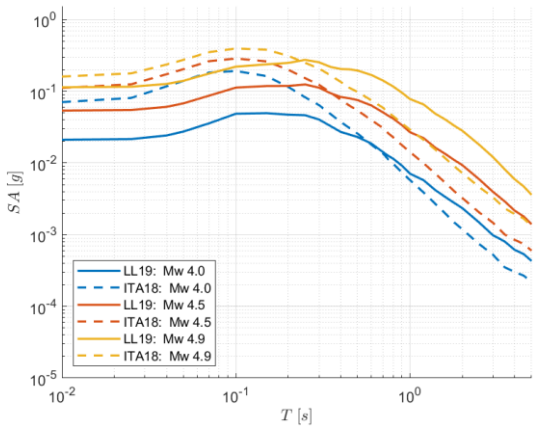

(b) R_{Rup} = 5 km, for Mw = 4.0; 4.5; 4.9

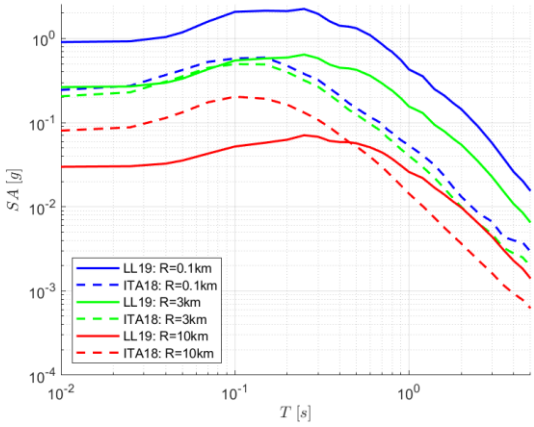

(c) Mw = 4.9 for R_{Rup} = 0.1; 3; 10 km

Figure 4.52 Spectral accelerations from ITA18 and LL19, for SS mechanism and rock site conditions (EC8-A), for (a) different magnitude, R=3km, (b) different magnitude R=5km and (c) different distances.

The behaviour evidenced for the UHS of Figure 4.48 is in line with the trend observed in GMMs predictions obtained according the predominant magnitude-distance scenario (Mw 4.9, R = 5 km), i.e., spectral acceleration increases for increasing magnitude and decreasing distance (see Figure 4.52), and long vibration periods are characterized by higher spectral accelerations when the LL19 prediction model is assumed rather than ITA18; in fact, the volcanic ground motion model is applied herein only with reference to the shallower earthquakes, occurred below a limit depth of 5 km, which are very similar to long period earthquakes, caused by cracks resonating as magma with gases moving toward the surface [14], as a results, long periods are better constrained to a dataset of volcanic shallow events that mostly occur at high frequencies.

While, at short periods, the spectral accelerations have higher values when the tectonic ground motion is assumed, with exception of the first 3.7 km of rupture distances that

are controlled by the volcanic model, in agreement with Figure 4.51; however, in near-source region, ITA18 predictions (blue curves) of Figure 4.51 tend to underestimate the spectral accelerations with respect to LL19 (green curves), particularly at long vibration periods.

4.3.1. Vertical ITA18 and LL19

Thereafter, the seismic hazard is performed also for the vertical ground motion models according the two methods implemented for ITA18 (ITA18-V(VH) and ITA18-V), and the calibration performed on the vertical LL19 (LL19-V) applied only to the volcanic domain (area source #49) for the two different return periods. Hence, Figure 4.53 shows the UHS implemented with the abovementioned models and compared with the related horizontal components for the SZ49; also the spectral accelerations trends are provided in Figure 4.54 and at various magnitudes and distances in Figure 4.55 for ITA18 and Figure 4.56 for LL19 attenuation model.

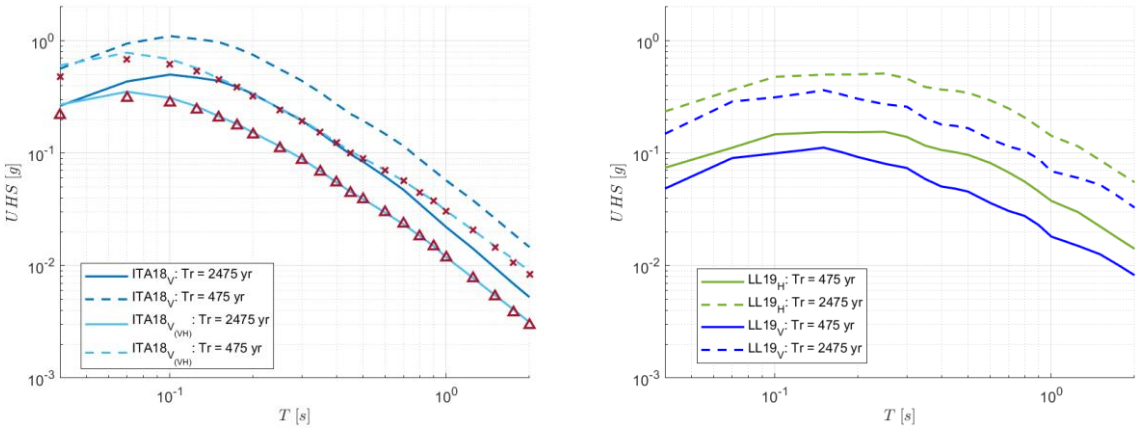

(a) ITA18 (b) LL19

Figure 4.53 UHS for the site of Zafferana Etnea, SZ49, comparison between the return periods of 475 and 2475 years, in horizontal and vertical directions.

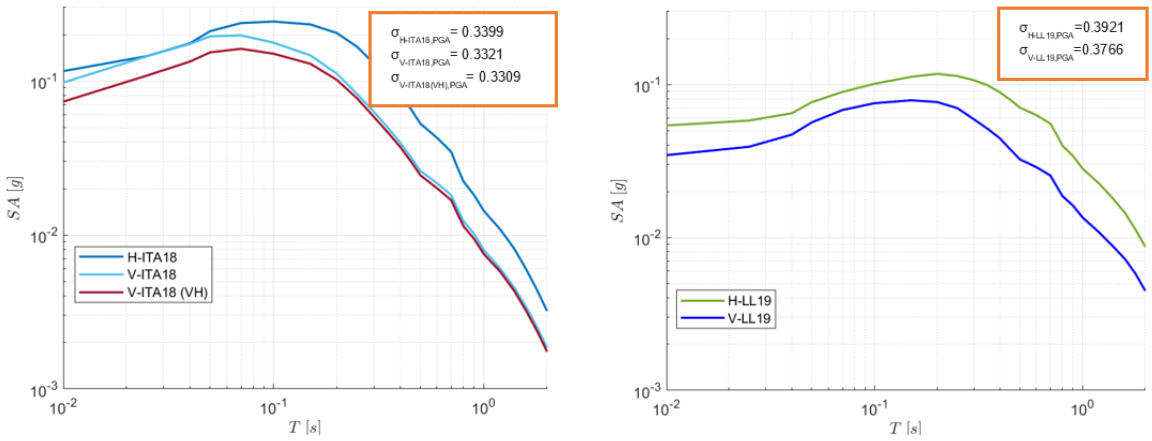

(a) ITA18-H, ITA18-V and ITA18-V(VH) (b) LL19-H, LL19-V

Figure 4.54 Spectral accelerations, R_{Rup} = 5 km, Mw = 4.9, for SS mechanism and reference rock site (EC8-A).

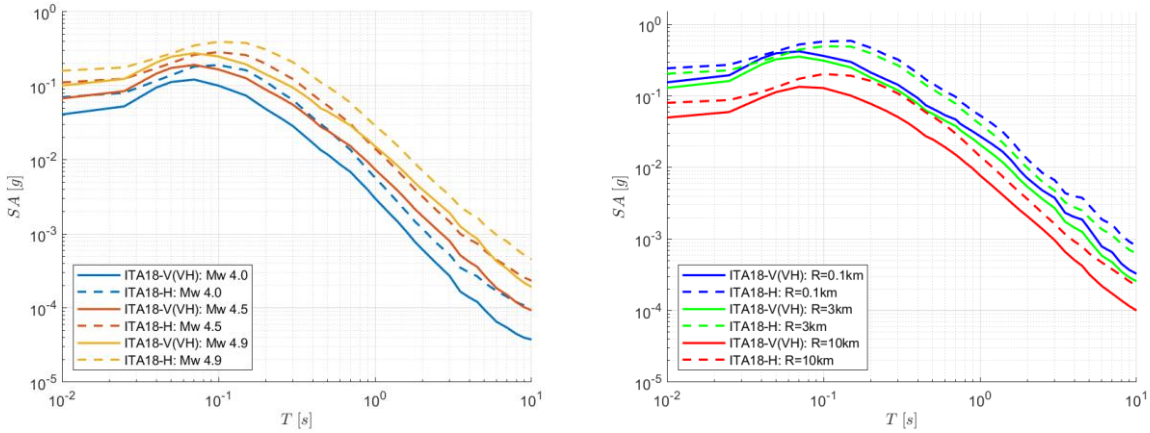

(a) R_{Rup} = 3 km, for Mw = 4.0; 4.5; 4.9 (b) Mw = 4.9 for R_{Rup} = 0.1; 3; 10 km

Figure 4.55 Spectral accelerations from ITA18-V(VH) and ITA18-H, for SS mechanism and rock site conditions (EC8-A), for (a) different magnitude and (b) different distances.

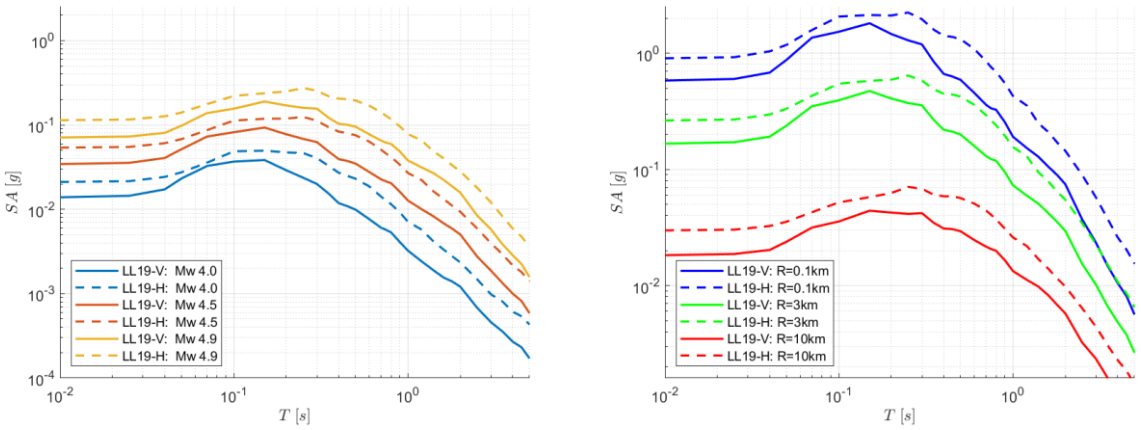

(a) R_{Rup} = 3 km, for Mw = 4.0; 4.5; 4.9 (b) Mw = 4.9 for R_{Rup} = 0.1; 3; 10 km

Figure 4.56 Spectral accelerations from LL19-V and LL19-H, rock site conditions (EC8-A), for (a) different magnitude and (b) different distances.

The first important evidence is that the UHS developed with the two ITA18 vertical models (i.e., ITA18-V(VH) and ITA18-V) are again coincident with one another and the same observation provided for L'Aquila and Gemona del Friuli are also evidenced in this case study of Zafferana Etnea, developped according both ITA18 and LL19 models (see figures above): the spectral acceleration increases for increasing magnitude and decreasing distance; the vertical spectral acceleration has always lower or at least the same amplitude with respect to the horizontal one also in proximity of the source, with a rapid attenuation [13]. The increase in variability may reflect the peculiarity of volcanic events, since the location and magnitude estimation have larger uncertainties than in case of tectonic events (see Figure 4.54).

V/H spectral ratios computed between the UHS calculated with SZ49 and with the corresponding prediction models (ITA18V/ITA18H and LL19V/LL19H for the dominant scenario) are shown in Figure 4.57 and Figure 4.58, respectively for the prediction ratios and UHS ratios, to furtherly highlight the difference between the vertical and the horizontal components according a tectonic and a volcanic model.

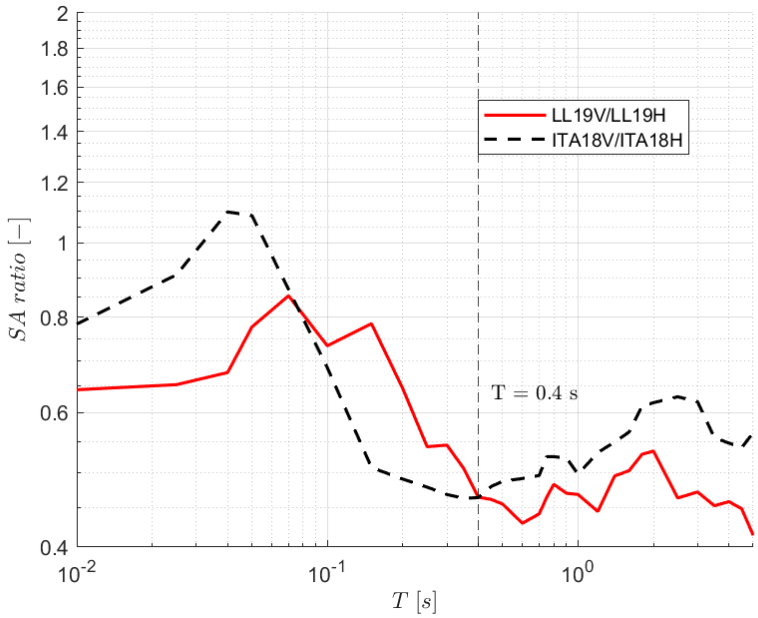

Figure 4.57 Spectral ratio between the prediction models ITA18-V/ ITA18-H and LL19V/LL19H for Mw 4.9, R = 5 km, SS, EC8-A.

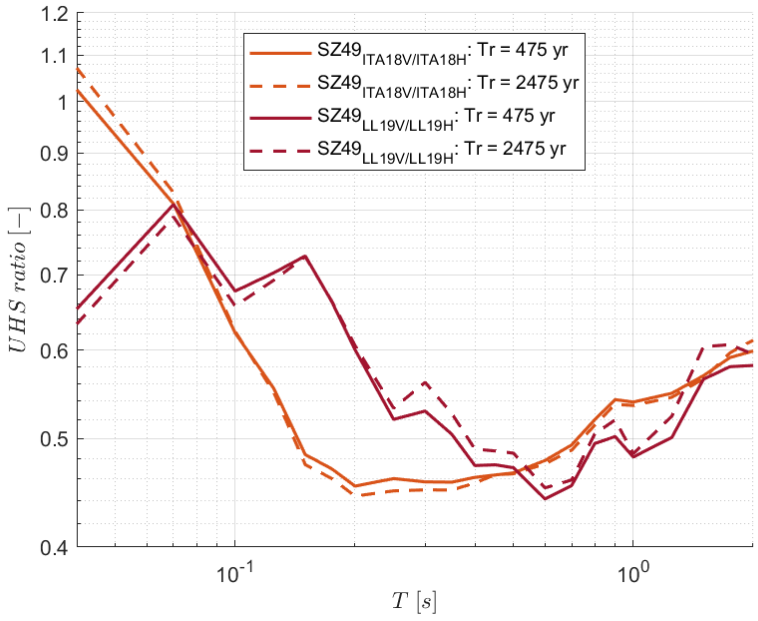

Figure 4.58 UHS ratio in SZ49 for Tr = 475 and Tr = 2475 years from prediction models ITA18-V/ITA18-H and LL19V/LL19H.

As a general comment, the ratio is sensitive to distance and spectral periods, tending to decrease as the period T increases, as expected. In detail, the ratio of the SA-ITA18 assumes an average unitary value at short periods, in accordance to the UHS trend for both the return periods, i.e., 475 and 2475 years, meaning that the vertical component shall not be neglected for seismic design purposes; this trend tends to decrease for

increasing structural periods, with a minimum of 0.45 at around T = 0.4 s, in agreement with the UHS ratios obtained at Tr = 475 years and at Tr = 2475 years. On the other hand, the SA-LL19 assume values lower than units across all the periods, even though it is characterized by moderate ratio values around 0.7 at short periods, in accordance with the results obtained for the UHS ratios obtained at Tr = 475 and at Tr = 2475 years.

Conclusion

This work aimed to focus on the impact, within the seismic hazard calculation, of new GMMs (ITA18 and LL19) specifically calibrated for the Italian context for shallow crustal earthquakes [6] and for volcanic areas [14], as well as on the empirically derived correction factors used to adjust the median predictions of these GMMs to take into account the effects of near-source [7].

The case studies examined for the thesis were L'Aquila (Abruzzo) and Gemona (Friuli), sited in high seismic regions, characterized by Normal-Fault and Reverse-fault mechanisms, respectively, and Zafferana Etnea (Sicily), located in a volcanic zone, dominated by Strike-Slip mechanism. The main results are reported in the table below, with quantitative percentages in terms of differences on the UHS for each sensitivity analysis performed.

For the case study of L'Aquila, the UHS obtained from the comparison between ITA18 and ITA10 models highlighted that, ITA18 predicts higher values than ITA10 at short periods (around 30%, see

Table 0.1), probably because of a better constraint of ITA18 to lower magnitudes (the calibration dataset is based on a higher number of small earthquakes); instead, at intermediate-long periods, the overprediction of UHS related to ITA10 came to light, particularly for higher return period (Tr = 2475 years for which the increment is of 30 %) and could be justified with a higher related sigma value with respect to ITA18 attenuation model, which are for instance, according to the dominant scenario (Mw 6.5, R = 0km) and for a period $T = 1s$: $\sigma_{ITA10,T=1s} = 0.3600$, $\sigma_{ITA18,T=1s} = 0.3235$.

Substantial differences between the two GMMs came to light for higher distances and as the vibration periods increase, in fact, the mean trend evidenced that for long-periods, ITA18 predicted almost half of ITA10 spectral acceleration.

Then, a specific attention was paid to the ITA18 ground motion variability [6], with the introduction of the ITA18 heteroscedastic modelling of the site-to-site and event- and site-corrected variability. Effective reduction of the estimated hazard could be evidenced only at very long return periods (even though this reduction was quite limited), while, at ordinary return periods, any significant differences were evidenced in terms of seismic hazard between the two models (maximum of 8% as shown in

Table 0.1), meaning that the heteroscedastic model could be neglected. A strong emphasis was also laid on the two approaches introduced to evaluate the impact of the vertical component of ITA18 model on PSHA [13]: the two methods produce results that are almost coincident with one another and had a lower impact on the seismic hazard with respect to the horizontal component. In fact, even though the UHS vertical component became more significant at shorter periods and almost comparable with the horizontal one, particularly at longer return periods, it had always lower amplitude (13% of differences as shown in

Table 0.1) amplitude with respect to the horizontal one, also in proximity of the source and was generally of higher frequency (shifted to the short periods), with a sudden attenuation [13].

Finally, the near-source adjustment was accounted to ITA18 model with the introduction of NESS correction [7] on the UHS which was mainly evidenced at short periods (until periods of about 0.45 s), for a Normal-Fault site mechanism, as the case of L'Aquila, for the area source #24. The increment at short periods is equivalent to 20%, while for longer periods just about 5% (see

Table 0.1) Although the main near-source features were expected to produce larger effects at longer periods, this behaviour could be accounted for by presence of a bias in the residuals between ITA18 and the NESS observations at Mw 6.5 (dominant magnitude of L'Aquila case study), in agreement with Paolucci et al. [57]. In fact, the NESS correction was modelled on the total residuals and therefore incorporates global near-source effects, also related to inter-event biases caused by a different average stress-drop and different tectonic environments of NESS events with respect to Italian events. Also, even though the introduction of NESS led to higher values on the UHS, when this is applied to the vertical component through ITA18-V(VH), the impact is lower with respect to the UHS obtained with the horizontal ITA18 ground motion model without correction, particularly at intermediate-long periods which are characterized by 30-40% lower amplitudes, as shown in

Table 0.1.

Thereafter, when the NESS correction [7] was applied to a Thrust-Fault mechanism site, as the case of Gemona del Friuli, for the area source #03, major impacts were found also on the longer periods (with an increment of 20%, as shown in

Table 0.1). This was probably related to the enrichment of TF mechanism in NESS dataset through the introduction of worldwide events, with respect to the ITA18 one, which was instead dominated by normal style of faulting, in agreement with Sgobba et al. [7]. Hence, ITA18-NESS provided a more significant contribution to the spectral amplification with respect to the uncorrected ITA18, mainly at short-medium periods for NF mechanisms, while a broadband increment is observed on TF ones.

The correction effect was not meaningful at all scenarios and periods, likely because the near-source features contained in NESS2 arose as smeared and counterbalanced effects in the correction, resulting in a slight average amplification. As expected, the near-source correction was higher when considering a Thrust-Fault mechanism, consequence of the fact that ITA18 was mainly characterized by NF, while ITA18-NESS dataset was enriched with TF mechanisms through worldwide earthquakes. Also, for this case study, the impact of the near source applied to the vertical component led to lower UHS amplitudes with respect to the horizontal non corrected spectral accelerations (30-40% of decrement as shown in

Table 0.1).

Finally, the contribution of a volcanic model (LL19; [14]) to the total hazard was accounted for Zafferana Etnea site, for the volcanic zone SZ49, evidencing the dominance of the tectonic seismicity applied to the adjacent considered source zones, particularly by the SZ48. The behaviour evidenced for the UHS of Zafferna Etnea was in line with the trend observed in ITA18 and LL19 predictions models: long vibration periods were characterized by higher spectral accelerations when the LL19 prediction model was assumed rather than ITA18 (with an increment of 130% and 226% for Tr = 475 and Tr = 2475 years, respectively as shown in

Table 0.1); in fact, the volcanic ground motion model was applied herein only with reference to the shallower earthquakes (i.e., with focal depth less than 5 km), which behave similarly to long period earthquakes as a result of the earthquake process, which is due to cracks resonating as magma with gases moving toward the surface [14]. In contrast, at short periods, the spectral accelerations had higher values when

the tectonic ground motion was assumed (239% more), even though, in near-source region, ITA18 predictions tend to underestimate the spectral accelerations with respect to LL19, particularly at long vibration periods. The same evidence is also founded for the vertical component, with higher impact of LL19 on the long periods (with an increment of 121% and 226% for Tr = 475 and Tr = 2475 years, respectively as shown in Table 0.1).

Table 0.1 Results in terms of differences in percentages on the UHS for each of the sensitivity analyses performed on the different case studies: L'Aquila, Gemona del Friuli and Zafferana Etnea.

Sensitivity analyses	Period T s	Return period *Tr* years	L'Aquila (SZ24) %	Gemona del Friuli (SZ03) %	Zafferana Etnea (SZ49) %
ITA18 w.r.t. ITA10 (H)	0 – 0.1	475	28	-8.6	-
		2475	33	-5	-
	0.1 – 1	475	0	-21	-
		2475	-7	-26	-
	1 – 2	475	-16	-14	-
		2475	-24	-24	-
ITA18 hetero w.r.t. homo (H)	0 – 0.1	475	3	-	-
		2475	0	-	-
	0.1 – 1	475	-3	-	-
		2475	-7	-	-
	1 – 2	475	-4	-	-
		2475	-8	-	-
ITA18-V w.r.t. ITA18-H	0 – 0.1	475	-20	-	-18
		2475	-13	-	-16
	0.1 – 1	475	-49	-	-51
		2475	-50	-	-51
	1 – 2	475	-38	-	-43
		2475	-40	-	-43
ITA18-NESS w.r.t. ITA18-H	0 – 0.1	475	22	19	-
		2475	18	18	-

	0.1 – 1	475 2475	9 9	22 24	- -
	1 – 2	475 2475	2 5	20 27	- -
ITA18-V(VH)-NESS w.r.t ITA18-H	0 – 0.1	475 2475	-10 -5	-10 -3	- -
	0.1 – 1	475 2475	-42 -41	-40 -40	- -
	1 – 2	475 2475	-34 -34	-33 -30	- -
LL19 w.r.t. ITA18 (H)	0 – 0.1	475 2475	- -	- -	-70 -55
	0.1 – 1	475 2475	- -	- -	14 70
	1 – 2	475 2475	- -	- -	130 226
LL19 w.r.t. ITA18 (V)	0 – 0.1	475 2475	- -	- -	-74 -63
	0.1 – 1	475 2475	- -	- -	12 73
	1 – 2	475 2475	- -	- -	121 226

Future developments

The accuracy of the predicted ground-motion amplitude is a fundamental issue for both the probabilistic and deterministic approaches, especially when the analysed site and the seismic source are very close one another [1]. In such a case, the ground-motion median and standard deviation evaluated from any GMM are usually poorly constrained, due to the general lack of strong-motion records in near-source conditions, and the assessment of ground-motion variability associated to a single fault is even more difficult due to the paucity of multiple records generated by the same fault.

Near-source effects on the ground motion are multiple and include phenomena such as directivity, fault hanging-wall or footwall, radiation-pattern, and slip distribution. Directivity effects have the largest impact on the ground-motion variability at low and intermediate frequencies, causing amplification at sites in the forward direction of the rupture [1]

The correction proposed with NESS for hazard estimations does not aim to model each near-source peculiar phenomenon, such as directivity, pulse-like, and so on, although it incorporates all these effects in the model variability. Instead, it should be intended as a posteriori empirical adjustment to be used for increasing the median predictions of specific GMMs that are affected by a bias due to paucity of large-magnitude and short-distance records in their calibration dataset. In such cases, the correction enables to improve the predictive power of the biased attenuation model through a conservative increment that covers the global near-source effects recognized in NESS2 [7]. A valid alternative to overcome the limitations of the proposed GMMs of this work, can be represented by finite-fault simulations, that are able to model all these near-source effects in the low and intermediate frequency range.

Although the use of numerical simulations require a very high-performance computational resources, it is increasingly widespread to improve the ground-motion description; in fact, several initiatives worldwide are promoting their application for hazard assessment purposes [59] [60], as for instance, the Southern California Earthquake Center [59] which promotes the CyberShake Project. The aforementioned project extensively utilizes 3D numerical simulations coupled with kinematic source models to compute low-frequency ground motions (up to 0.5 Hz) and assess both deterministic and probabilistic seismic hazard in southern California, whose related hazard maps differ from the classical ones (based on empirical GMPEs) by including long-period effects (e.g., basin and directivity effects).

More in general, hybrid approaches that combine empirical data and simulations may improve the accuracy of shaking estimates for seismic hazard in near source region, providing, for example, physic-based constraints to empirical GMMs in the proximity of the faults.

More in general, a possible strategy to improve the accuracy of shaking estimates for seismic hazard is to develop hybrid approaches (combining empiric data and simulations) to provide physic-based constraints to empirical GMMs in the proximity of the faults.

Although the use of numerical simulations require a very high-performance computational resources, it is increasingly widespread to improve the ground-motion description; in fact, several initiatives worldwide are promoting their application for hazard assessment purposes [59] [60], as for instance, the Southern California Earthquake Center [59] which promotes the *CyberShake Project*. The aforementioned project extensively utilizes 3D numerical simulations coupled with kinematic source models to compute low-frequency ground motions (up to 0.5 Hz) and assess both deterministic and probabilistic seismic hazard in southern California, whose related hazard maps differ from the classical ones (based on empirical GMPEs) by including long-period effects (e.g., basin and directivity effects).

A possible strategy to inject simulated ground motion into PSHA is by means of the computation of generalized attenuation functions (GAFs), which replace the empirical predictions with large sets of numerical simulations from which the first two moments of the ground-motion parameters probability distributions are derived [61] [62] [63]. The GAFs can be generated with different simulation codes (purely deterministic, stochastic, hybrid), depending on the target of the hazard analysis, and validated beforehand by the comparison with observed records [64]. For instance, a high-frequency deterministic technique is used by [61] for the prediction of the ground motion in a characteristic earthquake and showed the effect of the source radiation pattern and directivity at several sites around the fault. Also, Villani et al. [63] used 3D numerical simulations to demonstrate how near-source high-resolution representation of hazard, which accounts for combined 3D effects (site effects, basin effects, and topographic features), is more realistic than those purely based on traditional GMPEs.

Deterministic–stochastic methods of ground motion simulation (DSM [65]) can be explored to predict the ground motion close to the source, assess its variability, and calibrate synthetic attenuation models, including directivity effects, to be incorporated into PSHA.

Future developments in PSHA in the proximity of a single fault will focus on different ways of integrating observed data and simulations, which could be particularly suited to capture the characteristics of seismic shaking at regional scale, thus including simulation results which, conversely, reproduce well the multiple source effects that occur during medium-strong earthquakes.

Bibliography

[1] Maria D'Amico, Mara Monica Tiberti, Emiliano Russo, Francesca Pacor, and Roberto Basili, "Ground-Motion Variability for Single Site and Single Source through Deterministic Stochastic Method Simulations: Implications for PSHA," *Bulletin of the Seismological Society of America,* 2017.

[2] R. K. McGuire, "Probabilistic seismic hazard analysis: Early history," *Risk Engineering,* 2007.

[3] Stucchi, M., Meletti, C., Montaldo, V., Crowley, H., Calvi, G.M., and Boschi, E., "Seismic hazard assessment (2003-2009) for the Italian building code," *Bulletin of the Seismological Society of America,* vol. 101, 2011.

[4] Francesco Visini, Carlo Meletti, Andrea Rovida, Vera D'Amico, Bruno Pace, Silvia Pondrelli, "Updated area-source seismogenic model for seismic hazard of Italy," *Natural Hazards and Earth System Sciences,* 2022.

[5] Carlo Meletti, Warner Marzocchi, Vera D'Amico, Giovanni Lanzano, Lucia Luzi, Francesco Martinelli, Bruno Pace, Andrea Rovida, Matteo Taroni, Francesco Visini & the MPS19 Working Group, "The new Italian Seismic Hazard Model (MPS19)," *Annals of Geophysics,* 2021.

[6] Giovanni Lanzano, Lucia Luzi, Francesca Pacor, Chiara Felicetta, Rodolfo Puglia, Sara Sgobba, and Maria D'Amico, "A Revised Ground-Motion Prediction Model," *Bulletin of the Seismological Society of America,* vol. 109, 2019.

[7] Sara Sgobba, Chiara Felicetta, Giovanni Lanzano, Fadel Ramadan, Maria D'Amico, and Francesca Pacor, "NESS2.0: An Updated Version of the Worldwide Dataset for Calibrating and Adjusting Ground-Motion Models in Near Source," *Bulletin of the Seismological Society of America,* 2021.

[8] I. I, "Il moto al suolo nel terremoto di Viagrande (CT).," *Progettazione Sismica,* 2019.

[9] Meletti, C., Galadini, F., Valensise, G., Stucchi, M., Basili, R., Barba, S., Vannucci, G., and Boschi, E., "A seismic source model for the seismic hazard assessment of the Italian territory," *Tectonophysics,* vol. 450, 2008.

[10] Silvia Pondrelli, Francesco Visini, Andrea Rovida, Vera D'Amico, Bruno Pace, and Carlo Meletti, "Style of faulting of expected earthquakes in Italy as an input for seismic hazard modeling," *Natural Hazard and Earth System Sciences,* 2020.

[11] Ordaz M. and Salgado-Gálvez M.A., "R-CRISIS v20 Validation and Verification Document," ERN Technical Report., Mexico City, Mexico., 2020.

[12] D. Bindi, F. Pacor, L. Luzi, R. Puglia, M. Massa, G. Ameri, R. Paolucci, "Ground motion prediction equations derived from the Italian strong motion database," *Bulletin of Earthquake Engineering,* 2011.

[13] Ramadan F, Smerzini C, Lanzano G, Pacor F, "An empirical model for the vertical-to-horizontal spectral ratios for Italy," *Earthquake Engineering Structural Dynamics,* 2021.

[14] Giovanni Lanzano, Lucia Luzi, "A ground motion model for volcanic areas in Italy," *Bulletin of Earthquake Engineering,* 2020.

[15] J. W. Baker, "An Introduction to Probabilistic Seismic Hazard Analysis (PSHA)," 2008. [Online]. Available: https://citeseerx.ist.psu.edu/viewdoc/download?doi=10.1.1.575.7494&rep=rep1&type=pdf.

[16] C. C.A., "Engineering seismic risk analysis," *Bulletin of the Seismological Society of America,* 1968.

[17] B. Gutenberg and C. F. Richter, "Frequency of Earthquakes in California," *Bulletin of the Seismological Society of America,* 1944.

[18] Francesco Visini et al., "Earthquake Rupture Forecasts for the MPS19 Seismic Hazard Model of Italy," *Annals of Geophysics,* vol. 64, 2021.

[19] Rovida, A., Locati, M., Camassi, R., Lolli, B., and Gasperini, P., "CPTI15, the 2015 version of the Parametric Catalogueue of Italian Earthquakes," Istituto Nazionale di Geofisica e Vulcanologia, 2016.

[20] Rovida, A., Locati, M., Camassi, R., Lolli, B., and Gasperini, P., "The Italian earthquake catalogueue CPTI15," *Bulletin of Earthquake Engineering,* vol. 18, 2020.

[21] Gasperini P., B. Lolli, G. Vannucci, "Catalogue of Mw magnitudes for the Italian area, 1981-2015," MPS16 Project Internal report, 2016.

[22] Basili, R., Valensise, G., Vannoli, P., Burrato, P., Fracassi, U., Mariano, S., and Tiberti M.M., "The Database of Individual Seismogenic Sources (DISS), version 3: summarizing 20 years of research on Italy's earthquake geology," *Tectonophysics,* 2008.

[23] Devoti R., N. D'Agostino, E. Serpelloni, G. Pietrantonio, F. Riguzzi, A. Avallone, A. Cavaliere, C. Cheloni, C. Cecere, C. D'Ambrosio, L. Franco, G. Selvaggi, M. Metois, A. Esposito, V. Sepe A. Galvani, M. Anzidei, "A Combined Velocity Field of the Mediterranean Region," *Annals of Geophysics,* 2017.

[24] Gardner, J.K., and Knopoff L., "Is the sequence of earthquakes in Southern California, with aftershocks removed, Poissonian?," *Bulletin of the Seismological Society of America,* 1974.

[25] Stucchi, M., Albini, P., Mirto, C., Rebez, A., "Assessing the completeness of Italian historical earthquake data.," *Annual of Geophysics,* 2004.

[26] Albarello D., Camassi R., and Rebez A., "Detection of space and time heterogeneity in the completeness of a seismic catalogue by a statistical approach: an application to the Italian area," *Bulletin of the Seismological Society of America,* 2001.

[27] Meletti C., Patacca E., Scandone P., "Construction of a seismotectonic model: the case of Italy," 2000a.

[28] Mariucci, M.T., and Montone, P., "Database of Italian present-day stress indicators," *IPSI,* 2020.

[29] Solarino S., and Cassinis R., "Seismicity of the upper lithosphere and its relationships with the crust in the Italian region," *Bollettino di Geofisica teorica ed applicata,* vol. 48, 2007.

[30] Di Stefano, R., Bianchi, I., Ciaccio,M.G., Carrara,G., and Kissling, E., "Three-dimensional Moho topography in Italy: new constraints from receiver functions and controlled source seismology," *Geochem. Geophy. Geosyst,* vol. 12, 2011.

[31] D. Weichert, "Estimation of the earthquake recurrence parameters for unequal observation periods for different magnitudes," *Bulletin of the Seismological Society of America,* vol. 70, 1980.

[32] Linda Al Atik, Norman Abrahamson, Julian J. Bommer, Frank Scherbaum, Fabrice Cotton, and Nicolas Kuehn, "The Variability of Ground-Motion Prediction Models and Its Components," *Seismological Research Letters,* 2010.

[33] J. Douglas, "Earthquake ground motion estimation using strong-motion records: a review of equations for the estimation of peak ground acceleration and response spectral ordinates," *Earth-Science Reviews,* vol. 61, 2003.

[34] Russo E, Felicetta C, D Amico M, Sgobba S, Lanzano G, Mascandola C, Pacor F, Luzi L, "Italian Accelerometric Archive v3.2," Istituto Nazionale di Geofisica e Vulcanologia, Dipartimento della Protezione Civile Nazionale, 2022. [Online]. Available: http://itaca.mi.ingv.it.

[35] Abrahamson NA, Youngs RR, "A stable algorithm for regression analyses using the random effects model," *Bulletin of the Seismological Society of America,* 1992.

[36] Boore DM, Atkinson GM, "Ground-Motion prediction equations for the average horizontal component of PGA, PGV, and 5%-damped PSA at spectral periods between 0.01 s and 100 s," *Earthq Spectra,* 2008.

[37] Joyner, W. B., and D. M. Boore, "Peak horizontal acceleration and velocity from strong-motion records including records from the 1979 Imperial Valley, California earthquake," *Bull. Seismol. Soc. Am,* 1981.

[38] D. M. Boore, "Orientation-independent, nongeometric-mean measures of seismic intensity from two horizontal components of motion," *Bulletin of the Seismological Society of America,* 2010.

[39] Paolucci, R., F. Pacor, R. Puglia, G. Ameri, C. Cauzzi, and M. Massa, "Record processing in ITACA, the new Italian strong-motion database, in Earthquake Data in Engineering Seismology," *Geotechnical, Geological and Earthquake Engineering Series,* vol. 14, 2011.

[40] Boore, D. M., J. P. Stewart, E. Seyhan, and G. M. Atkinson, "NGA-West2 equations for predicting PGA, PGV, and 5% damped PSA for shallow crustal earthquakes," *Earthq. Spectra,* vol. 30, 2014.

[41] Bates D, Mächler M, Bolker B,Walker S., "Fitting linear mixed-effects models using," *Jf Stat Softw,* 2015.

[42] De Natale G, Faccioli E, Zollo A, "Scaling of peak ground motions from digital recordings of small earthquakes at Campi Flegrei, southern Italy," *Pure appl Geophys,* vol. 126, 1988.

[43] Montaldo V, Faccioli E, Zonno G, Akinci A, Malagnini L, "Treatment of ground-motion predictive relationships for the reference seismic hazard map of Italy," *J Seismol,* vol. 9, 2005.

[44] Faccioli E, Bianchini A, Villani M, "New ground motion prediction equations for T > 1 s and their influence on seismic hazard assessment," in *Proceedings of the University of Tokyo symposium on long-period ground motion and urban disaster mitigation*, 2010.

[45] Woessner J, Laurentiu D, Giardini D, Crowley H, Cotton F, Grünthal G, Valensise G, Arvidsson R, Basili R, Arvidsson R, Basili R,, "The 2013 European seismic hazard model: key components and results," *Bull Earthq Eng,* vol. 13, 2005.

[46] Munson CG, Thurber CH, "Analysis of the attenuation of strong ground motion on the island of Hawaii," *Bull Seismol Soc Am,* vol. 87, 1997.

[47] McVerry GH, Zhao JX, Abrahamson NA, Somerville PG, "Crustal and subduction zone attenuation relations for New Zealand earthquakes," *Bull New Zeal Soc Earthq Eng,* vol. 39, 2006.

[48] G. M. Atkinson, "Ground-motion prediction equations for Hawaii from a referenced empirical approach," *Bulletin of the Seismological Society of America,* 2010.

[49] Boore DM, Atkinson GM, "Ground-motion prediction equations for the average horizontal component of PGA, PGV, and 5%-damped PSA at spectral periods between 0.01 s and 10.0 s," *Earthq Spectra,* vol. 24, 2008.

[50] Tusa G, Langer H, "Prediction of ground motion parameters for the volcanic area of Mount Etna," *J Seismol,* vol. 20, 2015.

[51] Francesca Pacor, Chiara Felicetta, Giovanni Lanzano, Sara Sgobba, Rodolfo Puglia, Maria D'Amico, Emiliano Russo, Georgios Baltzopoulos, and Iunio Iervolino, "NESS1: A Worldwide Collection of Strong-Motion Data to Investigate Near-Source Effects," *Seismological Research Letters,* vol. 89, 2018.

[52] G. Atkinson, "Alternative ground-motion prediction equations for eastern North America from a referenced empirical approach: Implications for epistemic uncertainty," *Bulletin of the Seismological Society of America,* 2008.

[53] Pacor, F., C. Felicetta, G. Lanzano, S. Sgobba, R. Puglia, M. D'Amico, and L. Luzi, "NEar-Source Strong-Motion Flatfile (NESS), Version 1.0, Data Set," Istituto Nazionale di Geofisica e Vulcanologia (INGV), Rome, 2018.

[54] Wells D.L. and Coppersmith K.J., "New empirical relationships among magnitude, rupture length, rupture width, rupture area and surface displacement," *Bulletin of the Seismological Society of America,* vol. 84, 1994.

[55] Ross Stein and Volkan Sevilgen, "A L'Aquila trigger, seismic gaps and poor construction: WHat we've learned from the August earthquake in Italy," *The Science Behind the Headlines,* 2016.

[56] I. Iervolino, G. Manfredi, M. Polese, A. Prota, G.M. Verderame, "Chapter 10 - L'Aquila Earthquake: : A Wake-Up Call For European Research and Codes," in *Performance-Based Seismic Engineering: Vision for an Earthquake Resilient Society*, Springer Science+Business Media Dordrecht, 2014.

[57] Roberto Paolucci, Angela Chiecchio, Manuela Vanini, "The older the better? The strange case of empirical ground motion models in the near-source of moderate-to-large magnitude earthquakes," *Bulletin of Earthquake Engineering,* 2021.

[58] Azzaro R, Barbano MS, D'Amico S, Tuvè T, "The attenuation of seismic intensity on the Etna region and comparison with other Italian volcanic districts," *Ann Geophys,* vol. 49, 2006.

[59] Graves, R., T. H. Jordan, S. Callaghan, E. Deelman, E. Field, G. Juve, C. Kesselman, P. Maechling, G. Mehta, K. Milner, et al., "Cyber Shake: A physics-based seismic hazard model for southern California," *Pure Appl. Geophys,* vol. 168, 2010.

[60] Dreger, D. S., and T. H. Jordan, "Introduction to the Focus Section on validation of the SCEC broadband platform V14.3 simulation methods," *Seismol. Res. Lett.*, vol. 86, 2015.

[61] V. Convertito, "Seismic-hazard assessment for a characteristic earthquake scenario: An integrated probabilistic–deterministic method," *Bull. Seismol. Soc. Am,* vol. 96, 2006.

[62] F. E., "Recent evolution and challenges in the seismic hazard analysis of the Po Plain region, northern Italy," *Bull. Earthq. Eng.,* vol. 11, 2013.

[63] Villani, M., E. Faccioli, M. Ordaz, and M. Stupazzini, "High resolution seismic hazard analysis in a complex geological configuration: The case of the Sulmona basin in central Italy," *Earthq. Spectra,* vol. 30, 2014.

[64] Goulet, C. A., N. A. Abrahamson, P. G. Somerville, and K. E. Wooddell, "The SCEC broadband platform validation exercise: Methodology for code validation in the context of seismic-hazard analyses," *Seismol. Res. Lett.,* vol. 86, 2015.

[65] Pacor, F., G. Cultrera, A. Mendez, and M. Cocco, "Finite fault modeling of strong ground motions using a hybrid deterministic–stochastic approach," *Bull. Seismol. Soc. Am.,* vol. 95, 2005.

[66] Lolli B., D. Randazzo, G. Vannucci, P. Gasperini, "The Homogenized Instrumental Seismic Catalog (HORUS) of Italy from 1960 to Present," 2020.

[67] Pondrelli, S., Ekström, G., and Morelli, A., "Seismotectonic reevaluation of the 1976 Friuli, Italy, seismic sequence," *J. Seismol.,* 2001.

[68] J. J. Bommer, "Deterministic vs. probabilistic seismic hazard assessment: An exaggerated and obstructive dichotomy," *J. Earthq. Eng,* 2002.

[69] Slejko D., Peruzza L., Rebez A. , "Seismic hazard maps of Italy," *Annals of Geophysics,* 1998.

[70] Martinelli, F., and C.Meletti, "AWebGIS application for rendering seismic hazard data in Italy," *Seismol. Res. Lett.,* vol. 79, 2008.

[71] Eugenio Chioccarelli and Iunio Iervolino, "Near-source seismic hazard and design scenarios," *Earthquake Engng Struct. Dyn,* vol. 42, 2013.

[72] Sara Sgobba, Giovanni Lanzano, Francesca Pacor and Chiara Felicetta, "An Empirical Model to Account for Spectral Amplification of Pulse-Like Ground Motion Records," *geosciences,* 2021.

[73] M. C. Gerstenberger , W. Marzocchi , T. Allen , M. Pagani , J. Adams, L. Danciu, E. H. Field , H. Fujiwara, N. Luco, K.-F. Ma, C. Meletti, and M. D. Petersen, "Probabilistic Seismic Hazard Analysis at Regional and National Scales: State of the Art and Future Challenges," *Reviews of Geophysics,* vol. 58.

A Appendix A

A.1. Gemona del Friuli case study: ITA10 vs ITA18

As done for L'Aquila, a global view of the seismic hazard at the site of Gemona del Friuli has been implemented as well, by analysing the impact on the UHS obtained with the most recent model ITA18 is compared with the previous ITA10 and focusing the attention on the most dangerous area source, which dominates the seismic hazard due to a higher spectral acceleration amplitude and probability of exceedance. In the next figures, the UHS calculated for the site of Gemona del Friuli are shown, considering the use of the area sources, individually (i.e., SZ1, SZ2, SZ3, SZ4, SZ13) and together (i.e., SZALL), once with a return period of 475 years and then of 2475 years; the comparison between the UHS modelled with two different model (i.e., ITA10 and ITA18) follows.

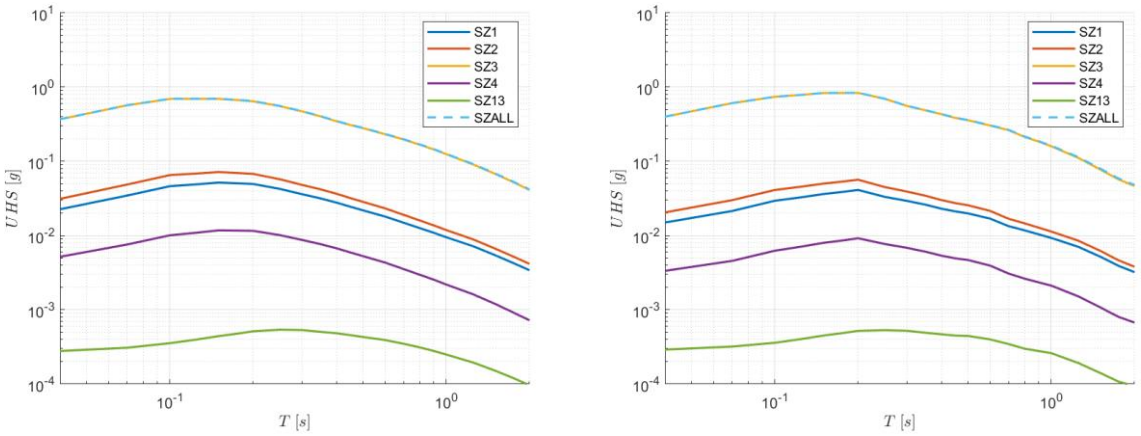

(a) ITA18 (b) ITA10

Figure A.1 Uniform hazard spectra for the site of Gemona del Friuli, return periods 475 years, calculated using (a) ITA18 model and (b) ITA10 one. In the figures, the contributions to the total hazard (SZALL) from the different SZ are also shown.

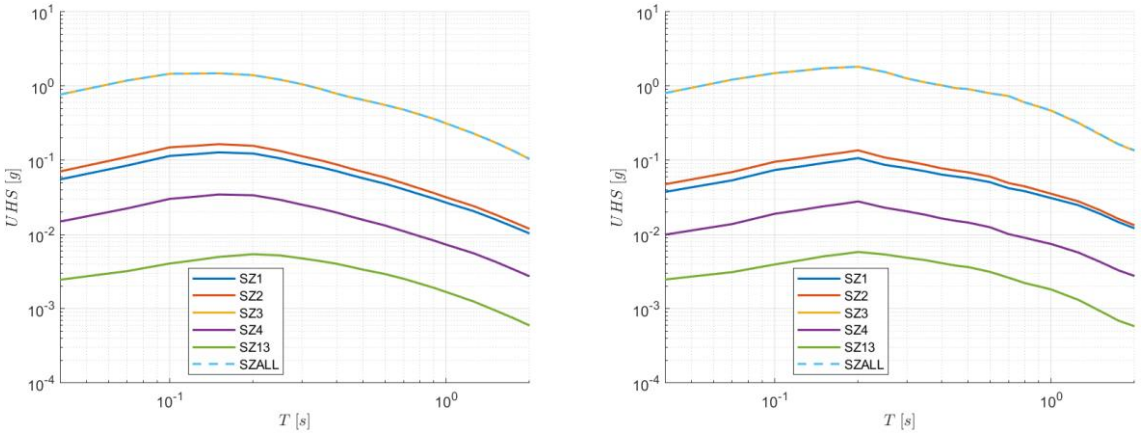

(a) ITA18 (b) ITA10

Figure A.2 Uniform hazard spectra for the site of Gemona del Friuli, return periods 2475 years, calculated using the (a) ITA18 model and the (b) ITA10 one. In the figures, the contributions to the total hazard (SZALL) from the different SZ are also shown.

As expected, the dominating seismogenic zone is the one where the site of Gemona del Friuli is located (SZ03), as highlighted in Figure A.1 and Figure A.2, and overlap the SZALL curve across all vibration periods, for both the return periods, 475 and 2475 years, respectively. As the source areas are characterized by very similar maximum magnitude *Mwmax* (see Table 4.3), no evidence comes to light in the trend, which are indeed uniform one another.

A disaggregation hazard analysis is also implemented and reported in Figure A.3 and Figure A.4, for a return periods of 475 and 2475 years, respectively by considering all the source zones of Gemona del Friuli case study, relating the ITA18 model to the source zones SZ1, SZ2, SZ3, SZ4, SZ13); the value at each cell corresponds to the probability that the selected intensity level is exceeded in 50 years, considering magnitude and distances within the accounted range [11].

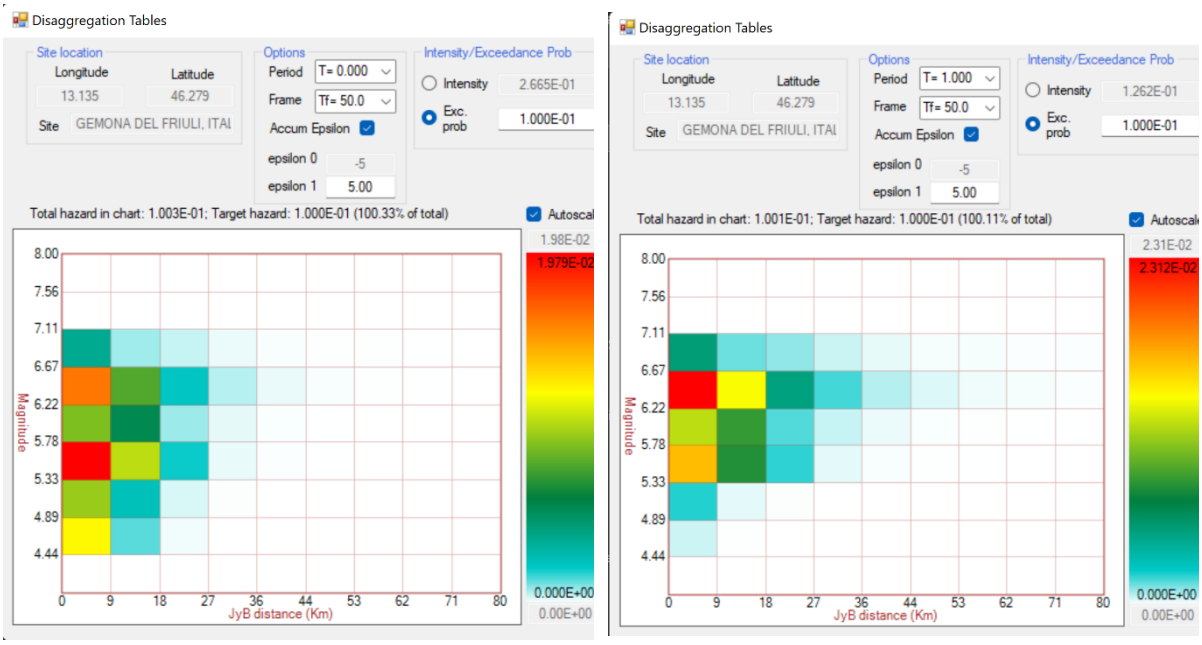

(a) T = 0 s (b) T = 1 s

Figure A.3 Plots of disaggregation analysis from R-CRISIS, for the site of Gemona del Friuli, with ITA18 GMM, Tr = 475 years, for (a) PGA and (b) 1s.

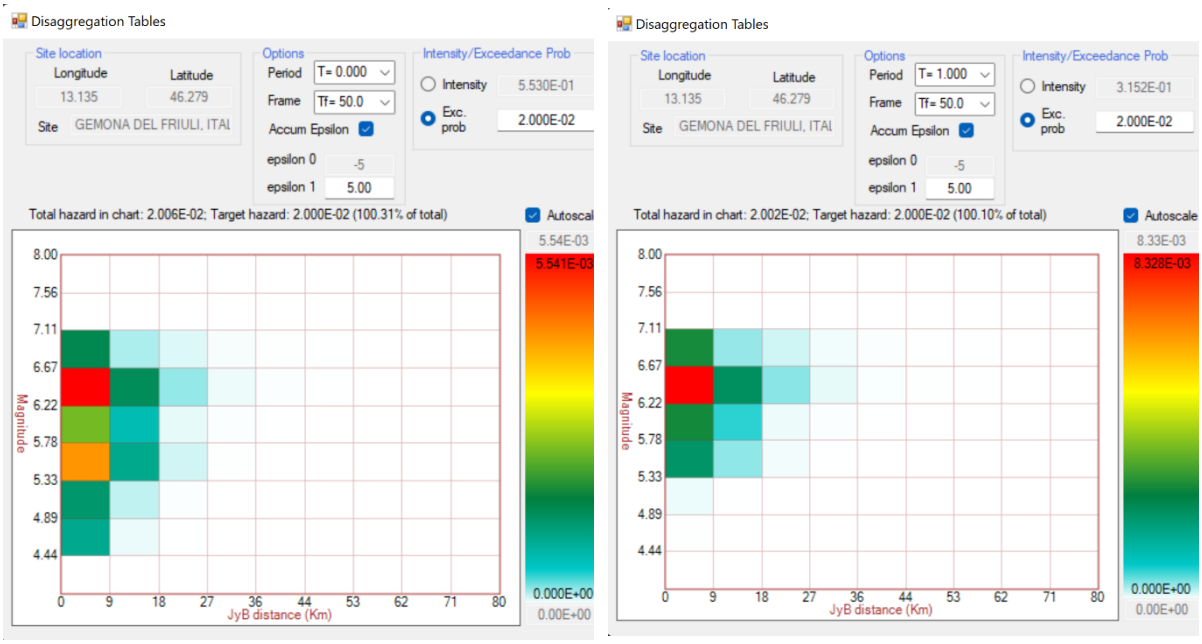

(a) T = 0 s (b) T = 1 s

Figure A.4 Plots of disaggregation analysis from R-CRISIS, for the site of Gemona del Friuli, with ITA18 GMM, Tr = 2475 years, for (a) PGA and (b) 1 s.

The predominant scenario obtained from the disaggregation analysis is identified in the red bin of figures above and ranges in magnitude Mw 6-22-6.67 and distances 0-9 km.

The comparison implemented above between the UHS obtained adopting the two attenuation models (i.e., ITA18 and ITA10) is done again in Figure A.5, focusing the attention on the SZ03 curve, to capture as best as possible the peculiarities of the models; the results are supported by the illustration of the spectral acceleration of ground motion models of Figure 4.7, interpreted at the light of the disaggregation analyses reported above, according to the most relevant scenario (Mw 6.22-6.67 and R = 0-9 km).

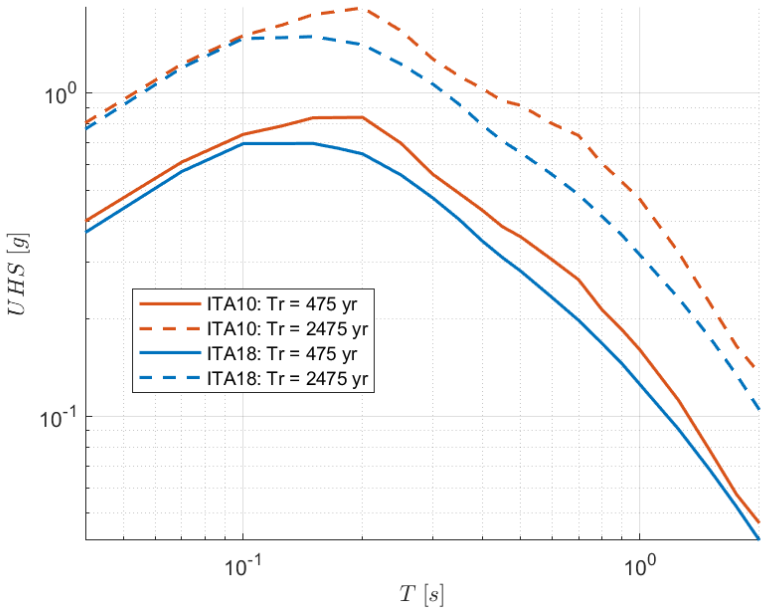

Figure A.5 Uniform hazard spectra for the site of L'Aquila, with the single SZ24, comparison between the return periods of 475 and 2475 years, prediction models ITA10 and ITA18.

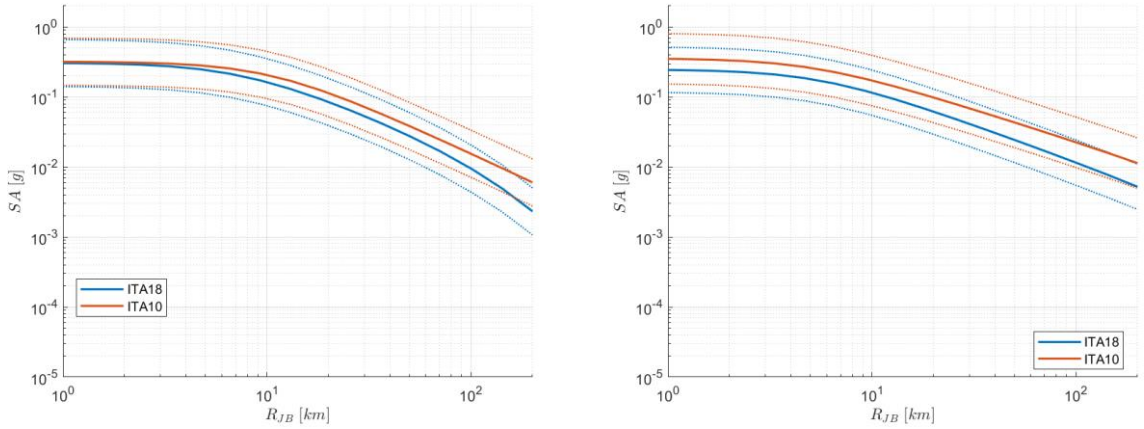

(a) T = 0 s (b) T = 1 s

Figure A.6 SA predictions according to ITA10 and ITA18, for Mw = 6.5, TF mechanism and reference rock site (EC8-A) for (a) PGA and (b) 1 s.

Figure A.6 shows a predominance of the ITA10 prediction; in particular, at long vibration periods and for longer distances; in particular, the two models are strongly

influenced by the median predictions, accordingly ITA10 predicts higher values than ITA18 (see Figure 4.7). Instead, at intermediate-long periods, the overprediction of ITA10 comes to light; this is evidenced particularly for higher return period (Tr = 2475 years).

The numerical differences between the spectral accelerations implemented with the two models are better represented in the Figure 4.8 and Figure 4.9, by implementing the spectral ratios between the two SA (ITA18/ITA10 for the dominant scenario: Mw 6.5, R = 0 km) and UHS (ITA18/ITA10 for the SZ03), respectively. Also, the spectral acceleration ratios are also shown as function of distance, both at short and long periods in Figure 4.10.

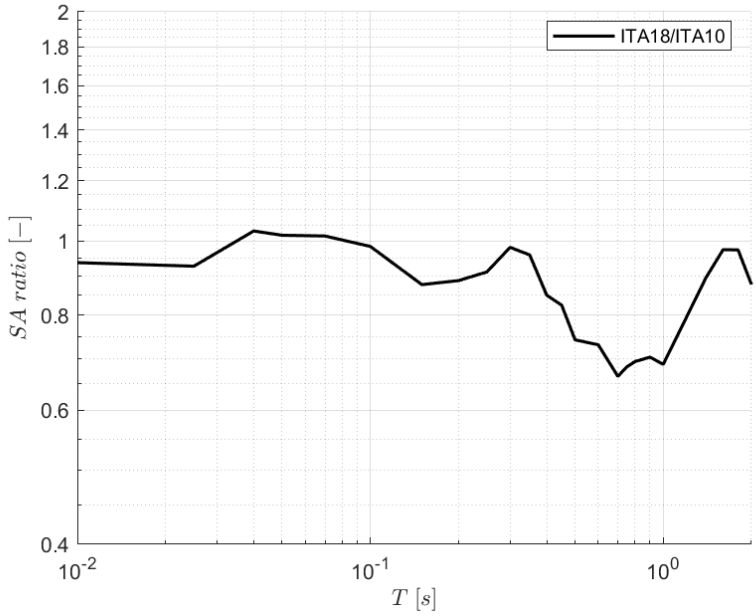

Figure A.7 Spectral ratio between the prediction models ITA18 and ITA10 for Mw 6.5, R = 0 km, TF, EC8-A.

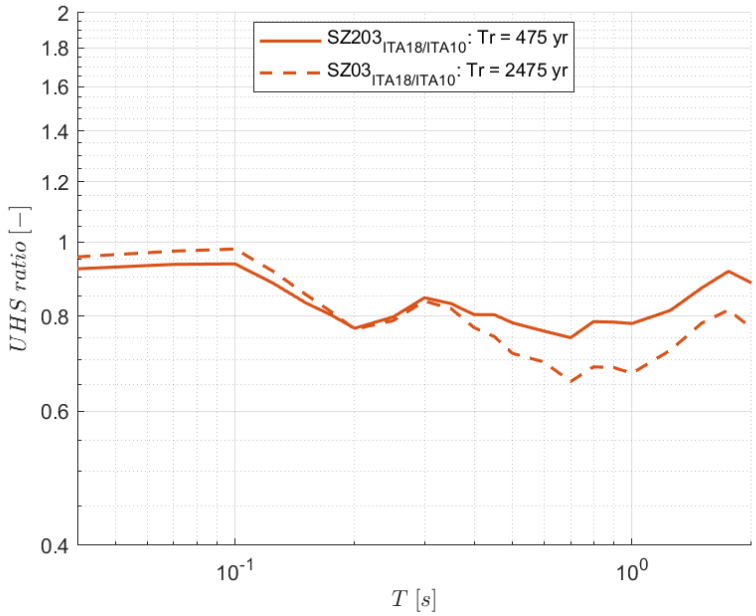

Figure A.8 UHS ratio in SZ03 for Tr = 475 and Tr = 2475 years from prediction models ITA18 and ITA10.

The spectral acceleration ratio represented in Figure A.7 is characterized by an unitary average ratio when we are close to the source (R = 0 km) and until a vibration periods T = 0.2 s, meaning that the ITA18 spectral acceleration is almost equal to ITA10, while for higher periods, the differences between the two models are quite higher (average ratio equal to 0.85). On the other hand, the average spectral ratios of UHS of Figure A.8 evidence the same trend as SA prediction ratios, both at Tr = 475 years and at Tr = 2475 years.

List of Figures

List if Tables

List of symbols

Variable	Description	SI unit
λ_m	Rate of earthquake	-
$\boldsymbol{a}$	Overall rate of earthquake in a region	-
$\boldsymbol{b}$	Relative ration of small and large magnitudes	-
$\boldsymbol{M}$	Magnitude	-
f_M	PDF for magnitude	-
f_R	PDF for distance	-
f_E	PDF for error	-
F_M	Magnitude scaling function	-
F_D	Distance function	-
F_S	Site amplification function	-
F_{Sof}	Style of faulting correction function	-
PGA	Peak Ground Acceleration	m/s^2
PGV	Peak Ground Velocity	m/s
PGD	Peak Ground Displacement	m
SA	Spectral Acceleration	m/s^2
V_{S30}	Shear wave velocity over 30 m	m/s
$\Lambda(M)$	Cumulative number of earthquakes per unit time	?
M_0	Magnitude threshold	-
M_u	Maximum magnitude	-
β	Gutenberg-Richter slope	?
Λ_0	Cumulative threshold number of earthquakes per unit time	?
M_w	Moment magnitude	-
R_{Ref}	Reference distance	km
R_{JB}	Joyner-Boore distance	km

R_{Rup}	Rupture distance	km
R_{hyp}	Hypocentral distance	km
ε	Error	-
M_h	Hinge magnitude	-
M_{ref}	Reference magnitude	-
M_j	Corner magnitude	-
c_j	Path coefficient	-
C_j	Site class	-
f_j	Fault coefficient	-
E_j - SoF_j	Fault class	-
h	Pseudo depth	km
σ	Total standard deviation	-
τ	Between-event variability	-
ϕ_{S2S}	Site-to-site variability	-
ϕ_0	Residual aleatory variability	-
V_j	Corner velocity	m/s
δB_e	Between-event residual	-
$\delta S2S_S$	Site-to-site residual	-
δW_{es}	Site- and event-corrected residual	-
dW_0	Remaining aleatory residual	-
δ_c	Correction factor	-

Acknowledgments

Inizio con il ringraziare il prof. Paolucci per avermi offerto questa splendida opportunità di crescita sia accademica che personale; lo ringrazio per la forte passione trasmessa, che mi ha affascinato sin dalla prima lezione e che ha portato a voler accrescere la mia conoscenza nella sismologia applicata.

La stesura di questa tesi non sarebbe stata possibile senza il contributo di Sara che mi ha guidata passo dopo passo e ha creduto sin da subito nelle mie capacità; la ringrazio per i preziosi insegnamenti trasmessi e per la dedizione nei miei confronti.

Ringrazio la prof.ssa Vanini per avermi aiutata nell'elaborazione di questo lavoro e aver sempre chiarito ogni mio dubbio.

Ringrazio anche Francesca e Giovanni per aver stimolato le mie curiosità e che insieme a tutto il gruppo di INGV mi hanno accolta e supportata in questi mesi di lavoro e di stesura della tesi, per le pause caffè e le chiacchierate insieme che hanno alleviato il peso della giornata.

Ringrazio mamma e papà che hanno condiviso insieme a me il raggiungimento di questo traguardo per niente semplice, per le loro soddisfazioni che sono anche le mie.

Ringrazio mio fratello Michele per avermi sempre detto ciò di cui avevo bisogno nei momenti di sconforto e per avermi spronata a fare sempre del mio meglio.

Ringrazio Chiara e Alessia, le amiche di una vita, e tutte le persone che mi hanno incoraggiata e che mi sono state vicine nel percorso seguito in questi anni.